MODIFIED DIRECT TORQUE AND PREDICTIVE TORQUE CONTROL STRATEGIES FOR INDUCTION MOTOR DRIVE

Submitted in partial fulfilment of the requirements

for the award of the degree of

DOCTOR OF PHILOSOPHY

By

K.M. Ravi Eswar

(Roll No. 701606)

Supervisor:

Dr. T. Vinay Kumar

Assistant Professor

DEPARTMENT OF ELECTRICAL ENGINEERING

NATIONAL INSTITUTE OF TECHNOLOGY

WARANGAL – 506004, TELANGANA STATE, INDIA

AUGUST-2020

APPROVAL SHEET

This Thesis entitled "**Modified Direct Torque and Predictive Torque Control Strategies for Induction Motor Drive**" by **K.M. Ravi Eswar** is approved for the degree of Doctor of Philosophy

Examiners

_____

_____

_____

Supervisor
Dr. T. Vinay Kumar
Assistant Professor
EED, NIT Warangal

Chairman
Dr. S. Srinivasa Rao
Professor & Head,
EED, NIT Warangal

Date: _____

DEPARTMENT OF ELECTRICAL ENGINEERING
NATIONAL INSTITUTE OF TECHNOLOGY
WARANGAL – 506 004

DEPARTMENT OF ELECTRICAL ENGINEERING
NATIONAL INSTITUTE OF TECHNOLOGY WARANGAL

CERTIFICATE

This is to certify that the thesis entitled **"Modified Direct Torque and Predictive Torque Control Strategies for Induction Motor Drive"**, which is being submitted by **Mr. K.M. Ravi Eswar** (Roll No. 701606), is a bonafide work submitted to National Institute of Technology, Warangal in partial fulfilment of the requirement for the award of the degree of **Doctor of Philosophy** in Department of Electrical Engineering. To the best of my knowledge, the work incorporated in this thesis has not been submitted elsewhere for the award of any degree.

Dr. T. Vinay Kumar
(Supervisor)
Assistant Professor
Department of Electrical Engineering
National Institute of Technology
Warangal – 506004

Date:

Place: Warangal

DECLARATION

This is to certify that the work presented in the thesis entitled "**Modified Direct Torque and Predictive Torque Control Strategies for Induction Motor Drive"** is a bonafide work done by me under the supervision of **Dr. T. Vinay Kumar**, Department of Electrical Engineering, National Institute of Technology, Warangal, India and was not submitted elsewhere for the award of any degree.

I declare that this written submission represents my ideas in my own words and where others ideas or words have been included; I have adequately cited and referenced the original sources. I also declare that I have adhered to all principles of academic honesty and integrity and have not misrepresented or fabricated or falsified any idea/data/fact/source in my submission. I understand that any violation of the above will be a cause for disciplinary action by the institute and can also evoke penal action from the sources which have thus not been properly cited or from whom proper permission has not been taken when needed.

K.M. Ravi Eswar
(Roll. No: 701606)

Date:
Place: Warangal

ACKNOWLEDGEMENTS

It gives me immense pleasure to express my deep sense of gratitude and thanks to my supervisor **Dr. T. Vinay Kumar,** Assistant Professor, Department of Electrical Engineering, National Institute of Technology Warangal, for his invaluable guidance, support, and suggestions. His knowledge, suggestions, and discussions helped me to become a capable researcher. He has shown me the interesting side of this wonderful and potential research area. His encouragement helped me to overcome the difficulties encountered in my research as well in my life.

I am very much thankful to **Prof. S. Srinivasa Rao**, Head, Department of Electrical Engineering for his constant encouragement, support and cooperation.

I take this privilege to thank all my Doctoral Scrutiny Committee members, **Dr. Chintham Venkaiah**, Associate Professor, Department of Electrical Engineering, **Dr. G. Siva Kumar,** Assistant Professor, Department of Electrical Engineering and **Dr. U.S.N. Raju,** Assistant Professor, Department of Computer Science and Engineering for their detailed review, constructive suggestions and excellent advice during the progress of this research work.

I also appreciate the encouragement from teaching, non-teaching members, and fraternity of Department of Electrical Engineering of NIT Warangal. They have always been encouraging and supportive.

I wish to express my sincere thanks to **Prof. N.V. Ramana Rao**, Director, NIT Warangal for his official support and encouragement.

I convey my special thanks to contemporary Research Scholars Dr. K.V. Praveen Kumar, Mr. K. Eshwar, Mr. Sagar Petkar, Mr. T. Abhilash, Dr. S. Venu, Dr. Suresh Lakhimsetty, Dr. M. Hareesh, Mr. A. Pranay Kumar, Mr. S. Ram Kumar, Mr. B. Kiran Babu, Mr. Patnana Hema Kumar, Mr. K. Hema Sundar and Mr. K. Narender Reddy.

I acknowledge my gratitude to all my teachers and colleagues at various places for supporting and co-operating me to complete the work.

I express my deep sense of gratitude and reverence to my beloved Father Sri. **K.M. Rama Prasad**, Mother Smt. **K.M. Lakshmi**, Wife Smt. **K.M. Priyanka**, paternal grandmother

Smt. **K.M. Amba Bai**, maternal grandmother Smt. **K. Subamma** for their sincere prayers, blessings, constant encouragement, shouldering the responsibilities and moral support rendered to me throughout my life, without which my research work would not have been possible. I would like to express my greatest admiration to all my family members for their positive encouragement that they showered on me throughout this research work. Without my family's sacrifice and support, this research work would not have been possible. It is a great pleasure for me to acknowledge and express my appreciation to all my well-wishers for their understanding, relentless supports and encouragement during my research work. Last but not the least, I wish to express my sincere thanks to all those who helped me directly or indirectly at various stages of this work.

This section would remain incomplete without remembering my paternal grandfather Sri. **K.M. Eswara Rao** and maternal grandfather Sri. **K. Veeranna,** who left their soul. I would like to express my love and respect for their everlasting affection and support.

Above all, I express my deepest regards and gratitude to "**ALMIGHTY**" whose divine light and warmth showered upon me the perseverance, inspiration, faith and enough strength to keep the momentum of work high even at tough moments of research work.

K.M. Ravi Eswar

ABSTRACT

In industrial applications, the necessity of high performance electric drive becomes compulsory. Among various AC motors, the Induction Motor (IM) is identified for its ruggedness. However, for the operation of IM in the area of electric drives, various control schemes are essential which improve IM dynamic nature. In literature, it is established that the application of Direct Torque Control (DTC) strategy accomplishes high dynamic performance for motor drives. The operation of DTC and its final Voltage Vector (VV) outcome is based on stator flux sector, stator flux and torque hysteresis controller outputs provided to the heuristic lookup tables. Therefore, the final VV selection from lookup table has direct influence on flux and torque control. The DTC execution at high sampling frequency is required to work hysteresis controllers in an accurate manner. Besides this, possibility of reverse VV selection from existing lookup tables causes high ripple in torque and also raise in switching frequency. The DTC operation with basic lookup table lags in flux controlling during start up process i.e. at zero speed. This leads to inrush current at the moment during start up. To answer all these issues linked with basic DTC, this thesis presents a modified look-up table based DTC scheme for three-level inverter drive. The DTC operations are performed for Open-Ended Winding IM (OEWIM) drive supplied from three-level dual Voltage Source Inverter (VSI). The basic look-up tables are formed based on the effective 19 VVs of three-level dual VSI for the application of flux and torque control. The above mentioned problems are identified with these basic look-up tables of DTC operation for three-level inverter drive. These basic look-up tables are replaced with proposed look-up tables, where the VVs placement aims to solve the issues such as high ripple in torque, high switching frequency and flux instability at zero speed. Therefore, an improved DTC scheme is proposed for the operation of three-level dual VSI supplied OEWIM drive, where the DC link voltages to the dual two level VSIs are in proportion of 1:1 (i.e. equal values of DC supplies provided to VSI-1 and VSI-2). This can be verified through various test results for existing and proposed DTC schemes when performed for three-level inverter drive.

The other control scheme for motor drive which is developing nowadays is Finite Control Set Predictive Torque Control (FCS-PTC). Its notable gains are structural simplicity, intuitive and multi objective control. Its functioning involves in the sequence of measurement and estimation, prediction of control variables and cost function optimization. The cost function formation involves multiple objectives with weighting factors. These weighting factors choice plays a crucial role, since the PTC operation for VV selection is based on cost

function evaluation. Therefore, the weighting factor tuning is a major aspect owing to its direct influence over control operation and thereby final VV selection. However, the choice of weighting factors using manual process is complex and time taking task. The other constraint with PTC is complex operation owing to increase in computational burden, when it is implemented for multi-level VSI fed IM drives. The increase in prediction VVs raise the computations at prediction and cost function evaluation stages. In this thesis, a modified PTC schemes are presented. The two level VSI supplied IM drive is functioned with proposed PTC scheme, where the weighting factor is auto tuned based on flux control objective. Thus, cost function having auto tuned weighting factor is evaluated to achieve optimal control response of torque and flux. The subsequent works in PTC are extended for OEWIM drive which is one among numerous multi-level IM drives and provides major benefits compared to other multi-level IM drives. In OEWIM drive, the dual two level VSI's DC link voltages are supplied with the proportion of 2:1 (i.e. DC supply input to VSI-1 is two times of DC supply input to VSI-2), through which four-level OEWIM drive operation is gained. To operate PTC without weighting factor assignment, a combined flux space vector objective and ranking analysis is employed which provides better torque, flux and switching frequency control. Using stator flux error, the prediction VVs are restricted to 20 out of 37. This helps in reducing computations in PTC of four-level OEWIM drive. Another PTC scheme is proposed for the same four-level OEWIM drive operation which is simpler than former PTC scheme. To perform PTC operation relieving from weighting factor, cost function is modified with same units while implementing reactive torque control as a substitute for flux control. Thus, achieving optimal response in terms of torque and flux. Furthermore, based on nearest VV selection, the prediction VVs are limited to 12 from the possible 37 for simplified PTC operation, which also helps in switching frequency reduction. In final stage of the work, an improved PTC operation for four-level OEWIM drive is presented. The prediction VVs are effectively reduced to maximum of 4 from the possible 37 using reference VV location, which leads in significant reduction in computational burden. The flux space vector objective is used to implement weighting factor independent operation and thereby optimal flux and torque control. Considering redundant switching combinations of VVs, the switching frequency reduction is gained. These modified PTC schemes are verified through various tests in comparison with existing PTC.

For all the above discussed control schemes, experimentations are performed using dSPACE-1104 control platform. Therefore, it can be stated that the thesis presents and verifies the modified direct torque and predictive torque control strategies for IM drive application.

Table of Contents

List of Figures

List of Tables

Abbreviations

AC	Alternating Current
ADC	Analog to Digital Converter
AI	Artificial Intelligence
ASDs	Adjustable Speed Drives
BNC	Bayonet Neill–Concelman
CCS	Continuous Control Set
CF	Cost Function
CHB	Cascaded H-Bridge
CMV	Common Mode Voltage
DC	Direct Current
DCM	Duty Cycle Modulation
dSPACE	Digital Signal Processing and Control Engineering
DTC	Direct Torque Control
EV	Electric Vehicle
FCS	Finite Control Set
FOC	Field Oriented Control
FC	Flying Capacitor
GA	Genetic Algorithm
IGBT	Insulated Gate Bipolar Transistor
IM	Induction Motor
MATLAB	MATrix LABoratory
MRAS	Model Reference Adaptive System
MLI	Multi-Level Inverter

MPC	Model Predictive Control
MC	Matrix Converter
NPC	Neutral Point Clamped
OEWIM	Open-End Winding Induction Motor
PI	Proportional Integral
PMSM	Permanent Magnet Synchronous Motor
PTC	Predictive Torque Control
PCC	Predictive Current Control
PWM	Pulse Width Modulation
RTI	Real Time Interface
RPM	Revolutions Per Minute
SMC	Sliding Mode Control
SFSV	Stator Flux Space Vector
SVM	Space Vector Modulation
THD	Total Harmonic Distortion
VSI	Voltage Source Inverter
VV	Voltage Vector

List of Symbols

c_1,c_2, c_3	Motor constants
i_f	Field current
i_a	Armature current
V_{dc} or E_{dc}	DC-link voltage
T or T_m or T_{motor}	Electromagnetic torque
T_r	Reactive torque
C_1	Constant- 2/3
C_2	Constant- 1/3
S_a, S_b and S_c	Switching pulses applied to Inverter
R_s	Stator resistance
R_r	Rotor resistance
L_s	Stator inductance
L_r	Rotor inductance
L_m	Mutual inductance
i_s	Stator current space vector in stationary reference frame
V_s or E_s	Voltage space vector in stationary reference frame
i_r	Rotor current space vector in stationary reference frame
ψ_s or λ_s	Stator flux space vector in stationary reference frame
ψ_r or λ_r	Rotor flux space vector in stationary reference frame
P	Number of poles
J	Moment of inertia
T_l	Load torque
ω_m	Rotor speed in rad/s (Mechanical system)

ω_r	Rotor speed in rad/s (Electrical system)
i_a, i_b and i_c	Phase currents of IM drive
abc-αβ	Clarke's transformation
n or *j*	Voltage space vector number
T_s	Sampling time
N	Null voltage state
S_{opt}	Optimal switching states to inverter
S_n	Stator flux sector location
W	Weighting factor
G	Cost function
H_T	Output of torque hysteresis controller
H_ψ	Output of flux hysteresis controller

Chapter 1

Introduction

Chapter 1
Introduction

1.1 Background

The energy utilization from the conventional resources such as coal, natural gas etc., has to be reduced to safeguard them for future generation and for risk free environment. To achieve this, one of the key solution is effective energy utilization at load end. The electric motors are pronounced as one of the most utilizing loads in daily applications [1], [2] which converts electrical energy to mechanical energy, via flux medium. Some of the well-known electric motor applications are: electric propulsion, pumps, fans, conveyors and compressors [3]. In all these applications, to regulate output (for example, air or water discharge) and for effective energy utilization, the power electronics plays a pivotal role. Power electronics is defined as the operation of power semiconductor devices for efficient control and conversion of electric power [4]. Nowadays, power electronics has become the life blood of new technologies in electrical branch, thanks for the developments in power electronic semiconductors [5] and digital platform. The application of power electronics in effective energy utilization and output control in electric motors is called an Adjustable Speed Drives (ASD) [3]. It is designed to convert energy from electrical to mechanical, providing control over electrical energy. In all the industrial process applications, where the wide range of speed control is necessary, the ASDs are inevitable and integral. Recently, in the field of Electric Vehicles (EVs) the ASD application is pronounceable and plays a major role [6]. The basic block representation of electric drive structure is presented in Figure 1.1. Thus, it is equipped with electric power source, converter, motor-load and controller. A power source can be AC or DC based on the availability. The power source is provided as input to the power converter. The power converter has a function to supply regulated AC or DC output which is required by motor-load application. To achieve this regulation, controller is placed to consider necessary actions based on inputs provided to it. The controller inputs may be from power source and motor. Thus, the control signals acquired from controller are supplied to power electronic converter switches for attaining regulated AC or DC output as required by motor load. Based on motor types, electric drives are categorized into two: 1. DC motor drives and 2. AC motor drives.

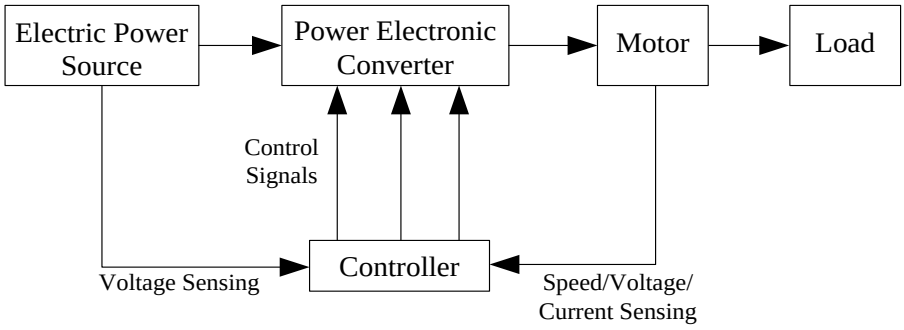

Figure 1.1 Block diagram of electric drive

1.1.1 DC motor drives

In these kind of electric drives, in order to provide regulated DC supply input to the DC motor, the power electronic converter may be a DC-DC (or) AC-DC depending on main electrical supply. DC motors whose armature and field windings are excited with separate DC source are named as separately excited DC motors, which are become very popular for speed control applications from past years [7], [8]. Its torque (T) equation is given by (1.1). From this simple equation, it can be observed that the torque can be controlled by armature and field current. Here, both the armature and field current are orthogonal and independently controlled via their separate DC excitations connected to armature and field windings. Thus, by maintaining field current constant and controlling armature current, simple and fast control of torque and speed is accomplished. The DC motor drive with inner current control and outer speed control gains more popularity for its faster dynamic response. Its block diagram is shown in Figure 1.2. Owing to this faster dynamic nature, this kind of electric drives are extensively used in industrial applications such as textile, paper, steel mill drives, etc.

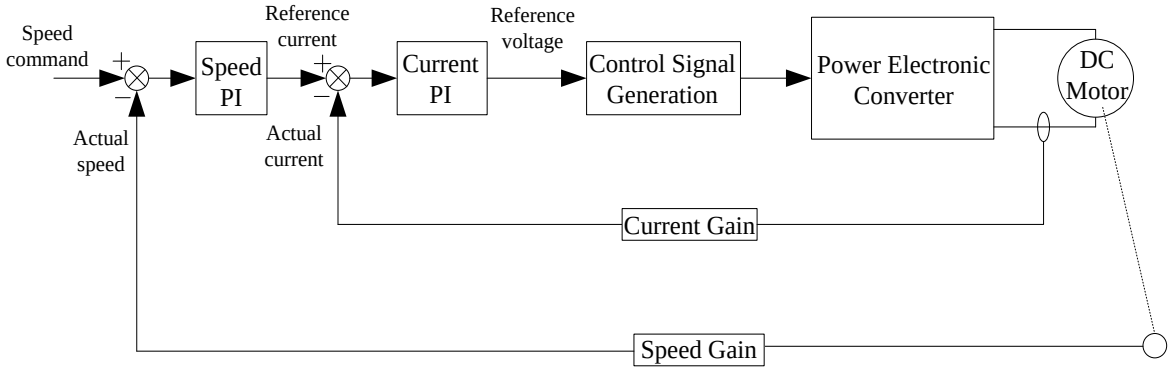

Figure 1.2 Block diagram of DC motor drive

$$T = c_1 i_f i_a \tag{1.1}$$

In (1.1), 'c_1' is constant, 'i_a' and 'i_f' are the armature and field currents, respectively.

However, DC motor drives face major flaws with the presence of commutator and brushes. The deterrents are the following: 1. Requires periodic care, 2. Not applicable for high speed and voltage range, 3. Its application is not suitable in explosive and corrosive locations.

1.1.2 AC motor drives

In AC motor drives, based on main electrical supply input, power electronic converters may be DC-AC (or) AC-AC, while providing regulated AC supply input to the electrical motor. The different configurations of AC motors are [7]: 1. Asynchronous and 2. Synchronous motors. Squirrel cage and slip ring induction motors fall under Asynchronous configuration, where the rotor speed is less than synchronous speed. Whereas, in the case of synchronous motor, the rotor speed matches with the supply synchronous speed. In all the three phase AC motors, stator is provided with three phase windings which are displaced by 120^0 electrically. But the rotor structure varies based on configuration. In squirrel cage induction motor, the rotor slots are provided with copper bars whose ends are permanently short circuited. In slip ring induction motor configuration, the rotor three phase windings are accessible out. In synchronous motor, rotor filed winding is excited with DC supply. Permanent Magnet Synchronous Motors (PMSM) comes under special category, where the rotor is assembled with permanent magnets instead of windings. Among these various AC motor configurations, the squirrel cage induction motors become more popular. They are also named as workhorse of industry. The reasons for its popularity include: 1. Rugged structure, 2. High speed operation, 3. Low inertia, 4. Improved power to weight ratio and 5. Minimal maintenance. However, in past years, even though having such a significant benefits for induction motors, the DC motors are only widely used in electric drive applications owing to its fast dynamic response [9]. At the present time, modern control methods are accessible for induction motor drives to improve dynamic response equally with DC motor drives, thanks for the development in control processors. With this possibility, at present induction motor drives are finding equal importance and occupying the position of DC motor drives in many industrial applications [10].

The different speed control platforms for induction motor drives are presented in Figure 1.3. The following are classical speed control methods for induction motor drives [11]: (a). Voltage control, (b). Frequency control and (c). Voltage per Frequency control.

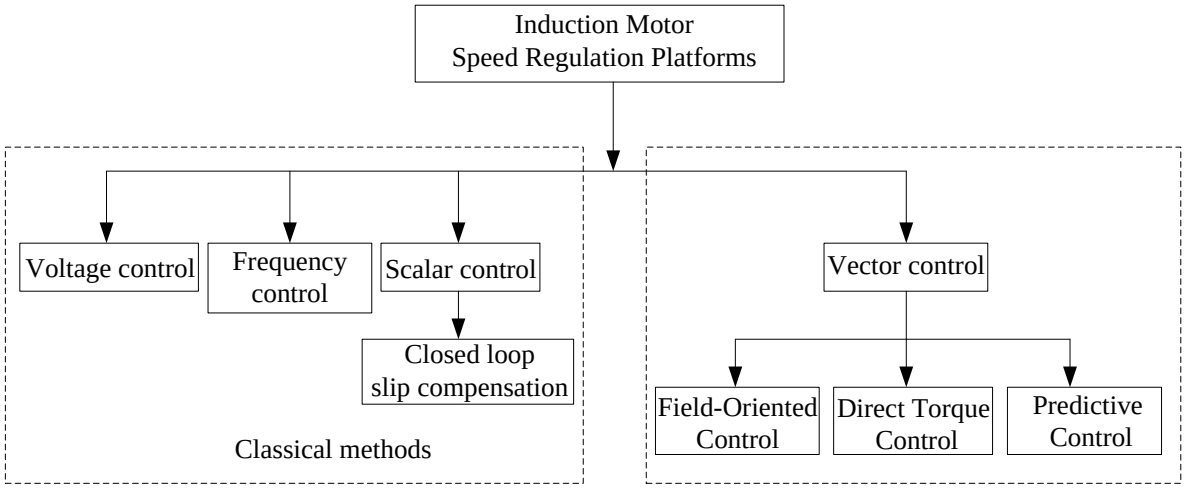

Figure 1.3 Block representation of various control schemes for induction motor

(a) Voltage control

In this control scheme, supply frequency is maintained as constant, whereas the supply voltage input to the induction motor is regulated until its rated value to attain desired speed control till the rated speed. In this control, the maximum motor torque capability depends on supply voltage. This kind of control scheme can be used sometimes for fan load applications, where the load torque (T_l) decreases with decrease in motor speed (ω), exhibiting the relation $T_l \propto \omega^2$.

(b) Frequency control

Here, the supply input frequency is regulated for speed control of induction motor, while maintaining the supply voltage constant. Generally, this control scheme is preferred for above rated speeds of motor with reduced load torque, as the motor torque capability reduces with increase in speeds above rated.

(c) Voltage per Frequency control

It is also named as scalar control. In this, both the motor input supply voltage and frequency are regulated, while maintaining constant ratio between them. Thus, constant rated flux (*V/F*) in machine is attained at all the regulated conditions of motor speed. For attaining regulated voltage and frequency supply input to the motor, Voltage Source Inverter configuration is widely used in AC motor drive applications. The scalar control scheme provides two key contributions: 1. Ability of motor drive to operate at any load torque till its rated over wide speed range. This indicates the motor drive control without losing maximum torque capability. 2. Advantage of gaining high starting torque at low supply frequencies.

The closed loop scalar control [12] for induction motor drive is accomplished by slip compensation technique. Its block diagram is presented in Figure 1.4.

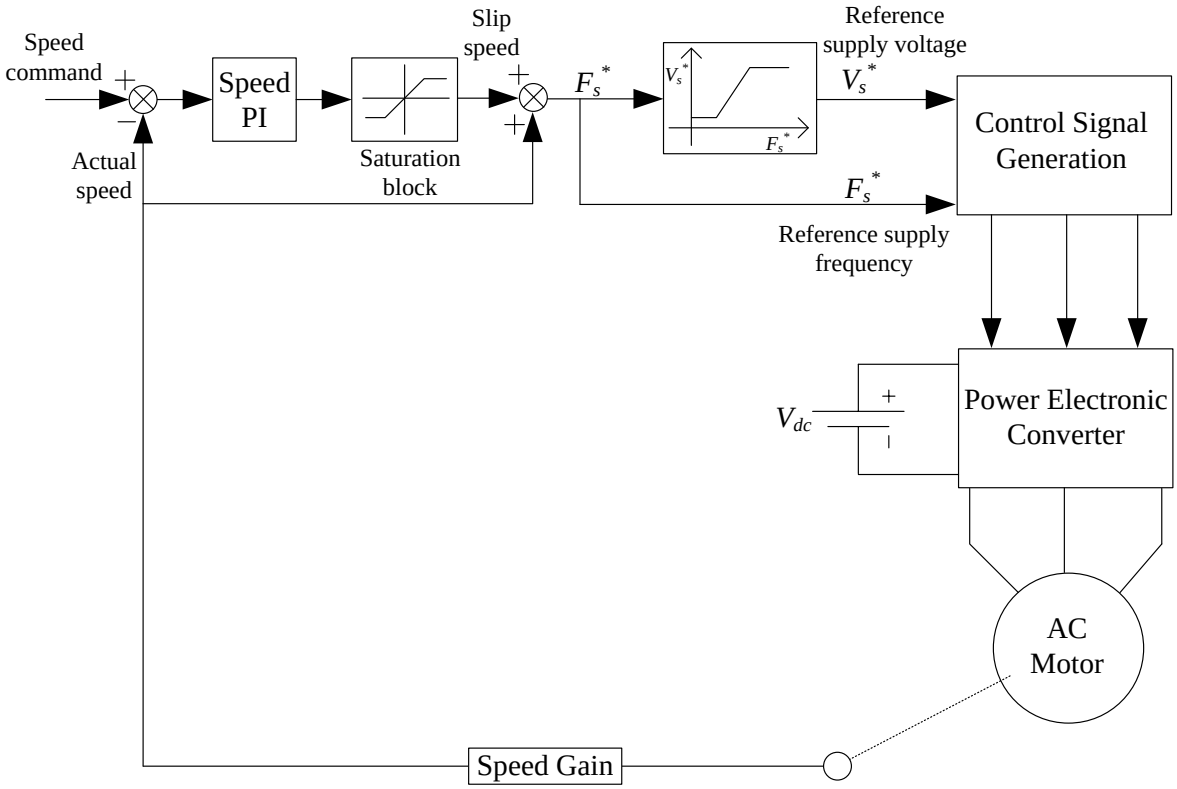

Figure 1.4 Block diagram of induction motor drive using slip compensation

The above discussed classical speed control schemes for induction motor drive are mainly built on motor steady state conditions, and are not good enough for the applications where quick dynamic response is must. To accomplish this, motor dynamic model based advanced control methods are required [12]. This motivates introduction for vector control scheme based induction motor drives [13], [14].

1.2 Existing vector control schemes and principles

The above mentioned control schemes for AC motor drive does not guarantee high dynamic performance, but with good steady state performance. The reason behind this is that the above classical control schemes alters only magnitude and frequency of AC supply excitation. Due to the presence of only one physical winding through which excitation is provided for induction motor, the flux and torque control is coupled each other. During machine dynamics, the flux linkages vary in magnitude, frequency and phase also. The scalar control scheme fails to address phasor control of excitation. This consequences oscillations in flux linkages, which eventuates undesirable motor torque oscillations. Moreover, this effect

results in heavy stator currents which demands the requirement of high rating and costly inverters [3].

In case of DC motor drives, field flux is maintained constant by fixing field excitation and by altering armature excitation independently, there by simple and high dynamic control response is attained. This decoupled feature in torque and flux can be possible in AC motor drives with the introduction of vector control techniques. With the support of enormous growth in microprocessors, the various vector control techniques have emerged for AC motor drives and satisfactorily replaced the DC motor drives in various high dynamic performance applications [15]. The vector control techniques for AC motor drives are as follows: 1. Field-Oriented Control (FOC), 2. Input-Output linearization control, 3. Direct Torque Control (DTC) and 4. Predictive Control. In [16], Input-Output linearization control is introduced as substitute for FOC of induction motor drive implementation. The independent speed and flux regulation is achieved by transforming state variables to new coordinate system. However, the control scheme is complex and requires full state variable measurements for motor drive operation [17]. The following subsection gives brief discussion about the key vector control schemes for induction motor drive as given below.

1.2.1 Field-Oriented Control (FOC)

The FOC implementation represents Induction Motor (IM) drive as same as DC motor drive in terms of dynamic behaviour. It was introduced in the year 1968 [18], [19] by suitable modelling of IM using the concept of space vector theory [13]. To accomplish high dynamic performance as analogous to DC motor drive, the following control actions are performed in FOC of IM drive [15]:

(a) Shifting stator currents (i_a, i_b and i_c) to a new synchronous rotating frame of reference (i_d and i_q). This action results in AC components to be appear as DC components, similar to the currents in DC machine.

(b) Alignment of flux-linkage space vector with d-axis reference frame. This action ensures orthogonality of flux and torque controlling currents (i_d and i_q) which are decoupled, similar to that of field and armature currents in DC motor. Here, the flux linkage space vector can be a stator or rotor or magnetizing component [15].

The FOC block diagram for IM drive is presented in Figure 1.5. With these control actions, the motor torque is modelled as a function of flux and torque producing currents which are independent to each other. Thus, the torque equation is framed as (1.2). By

maintaining flux component of current constant and altering torque component of current, high dynamic performance is achieved for IM drive as similar to DC motor drive. However, FOC implementation has certain limitations: 1. The control action is fully relying on flux linkage angle (ρ) determination, which is essentially needed for coordinate frame transformation. The inaccuracy of this, degrades both steady state and dynamic response [20]. 2. The requirement of extra current PI regulators, flux observer for angle measurement and coordinate frame transformations shaped FOC scheme clumsy for motor drive operation.

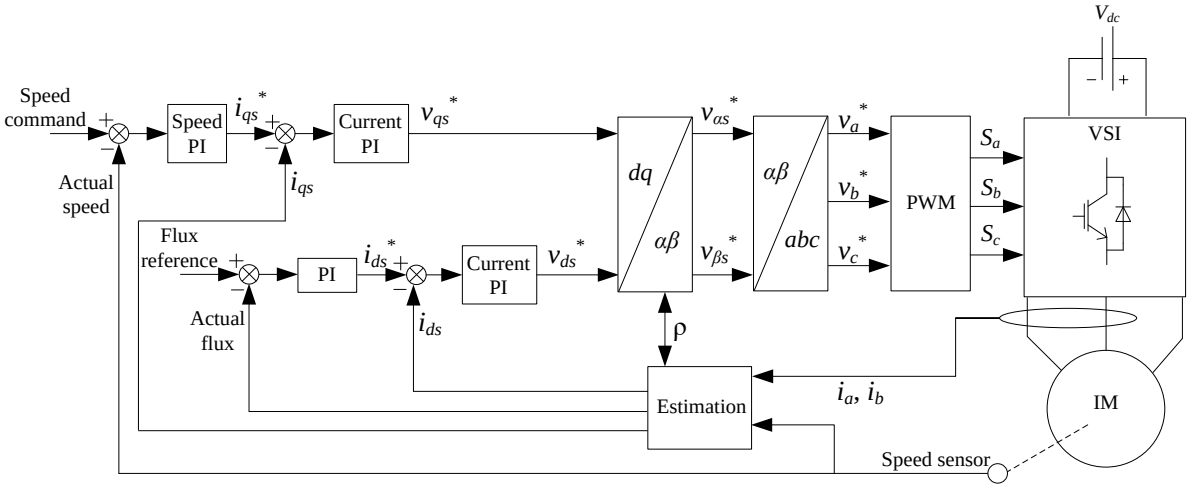

Figure 1.5 Block diagram of induction motor drive using FOC

$$T = c_2 i_{mr} i_{qs} \tag{1.2}$$

In (1.2), 'c_2' is constant, 'i_{mr}' is rotor flux magnetizing current and 'i_{qs}' is q-axis stator current, which is preferred for torque control.

1.2.2 Direct Torque Control (DTC)

In the year 1986, DTC scheme is realized [20] for high dynamic performance of IM drives, which gained significant role in industry within a short duration when related to FOC. Unlike FOC, DTC is independent from coordinate frame transformations and current PI regulators [21]. Thus, DTC is known for its simplicity for motor drive operation. Besides this, control operation is less sensitive to parameter variations. The DTC block diagram for IM drive is presented in Figure 1.6. Depending on the information of stator flux ($d\lambda$) and torque (dT_m) errors and stator flux sector (S_n), predefined look-up table is prepared for suitable voltage vector (VV) selection. Thus, achieving benefit of direct control over flux and torque. The features of DTC implementation are as follows [13], [15]: 1. Control execution in stationary reference frame, 2. Torque and flux control in direct manner. With the application of appropriate VV (V_s), the change in stator flux and torque (1.3)- (1.4) are achieved, 3. The

control operation requires torque estimation and only the sector information of stator flux space vector but not its exact angle value, 4. Absence of modulation stage, 5. The individual torque and flux control loops elects desired voltage space vector for control operation, 6. Simple control structure.

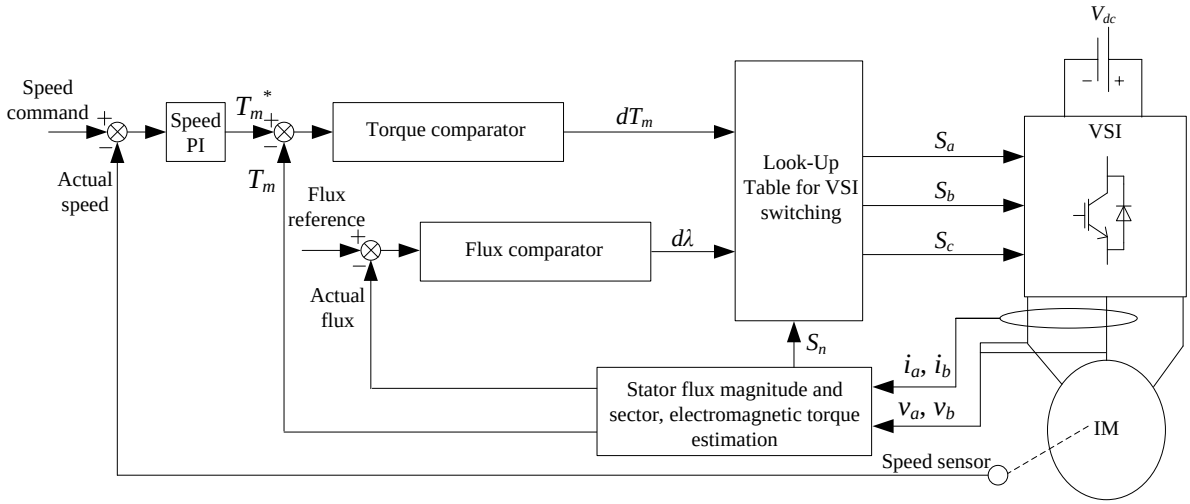

Figure 1.6 Block diagram of induction motor drive using DTC

$$\Delta\lambda_s = V_s T_s - R_s i_s T_s \tag{1.3}$$

$$\Delta T_m = c_3 \left|\lambda_s + \Delta\lambda_s\right| \left|\lambda_r\right| \sin\Delta\delta \tag{1.4}$$

(1.3) and (1.4) signifies the possibility of change in flux and torque variables with the application of voltage space vector. The term δ indicates the angle between stator flux (λ_s) and rotor flux (λ_r) phasors. It is also called as the torque angle. The terms, 'i_s' is stator current phasor, 'R_s' is stator resistance, 'c_3' is constant- $L_m/(L_sL_r - L_m^2)$. Thus, by maintaining stator flux constant and changing δ with the application of suitable 'V_s' in a sample instant 'T_s', fast dynamic response is attained.

However, the various limitations in DTC implementation are [21]- [23]: 1. The existence of hysteresis controllers imposes high sampling frequency in digital platform, 2. Variable switching frequency, 3. Large ripples in flux, current and torque response, 4. Poor flux regulation at low speeds. The active research is going on in the field of DTC to cope with its limitations.

1.2.3 Predictive Control

The history of Model Predictive Control (MPC) scheme started in the year 1960, where it was applied in chemical domain applications successfully [24], [25]. The MPC

requires longer time for its operation and same nature is supported for chemical domain, where the time constants are high. At the beginning, MPC is not applied in power electronics domain, where the faster control actions are necessary. However, the growth of powerful and fast microprocessors gives fillip for MPC utilization in power electronics application from the past decade. The control scheme attains several gains [26]: 1. Control concept is intuitive and simple, 2. Easy regulation of multiple objectives, 3. Various systems in power electronics can be employed with the control scheme and 4. Non-linearities of system can be included easily.

The control scheme considers entire system discrete dynamic mathematical model for its operation. Hence, it is termed as model based method. The system control variables are predicted for future behaviour with all the possible inputs. The optimization problem i.e. cost function (CF) minimization is formulated, which is function of future and reference variables. The possible input solving the optimization problem is selected as desired control action. Taking the advantage of powerful microprocessors, MPC scheme started as emerging in power electronics field from 1980s. The various categorizations in MPC are [26]: Continuous Control Set (CCS) and Finite Control Set (FCS). In CCS scheme, the reference modulating signal is produced during its operation and undergoes Pulse Width Modulating (PWM) generation for applying control pulses to inverter switches. Thus, CCS scheme requires modulating stage which facilitates fixed switching frequency operation. On the other side, FCS scheme does not require any PWM stage and the control operation directly outputs discrete switching states of inverter which is established from cost function optimization. The elementary model of FCS operated IM drive is presented in Figure 1.7. The prediction model is framed by using discrete equations of IM. From this, the prediction outputs are determined with the information of future inputs, present outputs from system and past input. The cost function comprises of number of constraints with suitable weights. The constraints are function of their references and prediction outputs. The future input is considered for which minimum cost function is pertained and applied to IM drive.

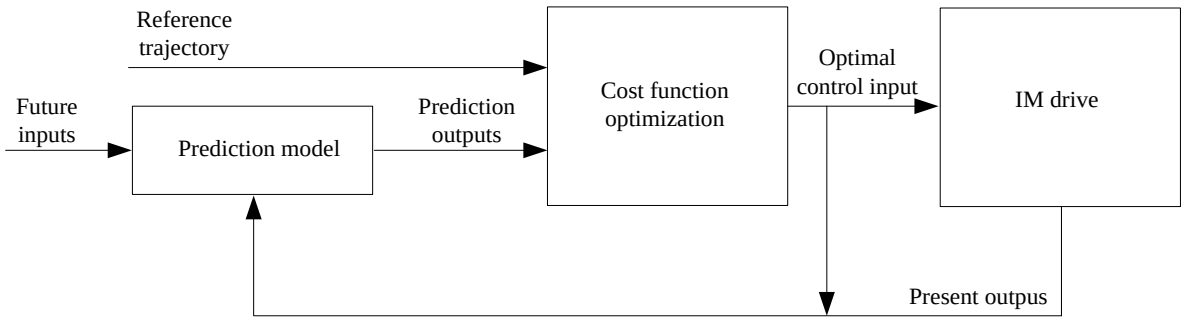

Figure 1.7 Basic block diagram of FCS-MPC for IM drive

The FCS scheme is subcategorized as Predictive Current Control (PCC) and Predictive Torque Control (PTC). In PCC, the CF is combination of reference and future currents. Thus, torque and flux variables are indirectly controlled by regulating currents. Whereas, in PTC the torque and flux variables are directly involved in CF having their reference and future values. Thus, direct control over flux and torque is possible. Both PCC and PTC attains the benefits of MPC. However, the notable differences in between them are: High dynamic performance and less torque ripples for PTC. Therefore, the PTC scheme is given as main preference in the field of high performance electric drives. Still, the limitations are: CF design with proper weighting factors, high computational time, variable switching frequency and parameter sensitivity.

The brief outlook over the discussed vector control schemes for IM drives is presented in Table 1.1 by doing comparisons with various terms among them. The principal focus of this thesis is on research of DTC and PTC schemes to handle the issues associated with them for motor drive application.

Table 1.1 Assessment of key control schemes for motor drive [26], [27]

Terms	FOC	DTC	PTC
Coordinate frame (dq) Transformation	Yes	No	No
Accurate flux position necessity	Yes	No	No
Modulator requirement	Yes	No	No
Physical Complexity	High	Low	Low
Parameter sensitivity	High	Low	High
Flux and torque ripple	Low	High	Low
Insertion of constraints	Difficult	Difficult	Simple
Weighting factor requirement	No	No	Yes
Computational burden	Low	Low	High

1.3 Multi-level VSI supplied AC motor drives

At the beginning, the discussed vector control schemes are applied to motor drives when supplied from two-level Voltage Source Inverter (VSI) only. However, in the applications of medium and high power range, the use of Multi-Level VSIs (MLIs) are preferable [28]- [32]. The following are benefits of it: 1. Reduced switching stress (dv/dt), 2. Realizing improved voltage shape with reduced Total Harmonic Distortion (THD) and 3. low switching frequency. Presently, MLIs are occupying in many applications [33] of AC

motor drive systems such as ship propulsion, hybrid electric vehicles and rolling mills. The most recognized various MLI structures [28]- [32] are: 1. Cascaded H-Bridge (CHB), 2. Neutral Point Clamp (NPC) and 3. Flying Capacitor (FC). In MLI fed motor drives operation, the increase in voltage space vector number allows for its better control. Newly, the dual inverter structure is paying more attention in the field of MLIs for motor drives [33]. The structure of Open-Ended Winding Induction Motor (OEWIM) supplied from dual-inverter is presented in Figure 1.8. The open-ended winding for AC motor is formed by disjoining the star connected windings neutral point. Both sides of windings are connected to individual two-level VSI phase legs. The two VSIs DC link voltage ratio can be supplied either equal or unequal [34] manner. The following are motives [35] behind this structure of AC motor drive: 1. Simple structure comprising only two basic two-level VSIs offering multi levels, 2. Clamping diodes are excluded (as related to NPC), 3. Fewer capacitors (as related to FC), 4. Fewer DC sources (as related to CHB), 5. Fault-tolerance capacity, 6. Voltage space vectors having more redundancy. Owing to the above stated benefits, the dual inverter supplied open-ended winding AC motors are emerging in multi-level drive applications [35].

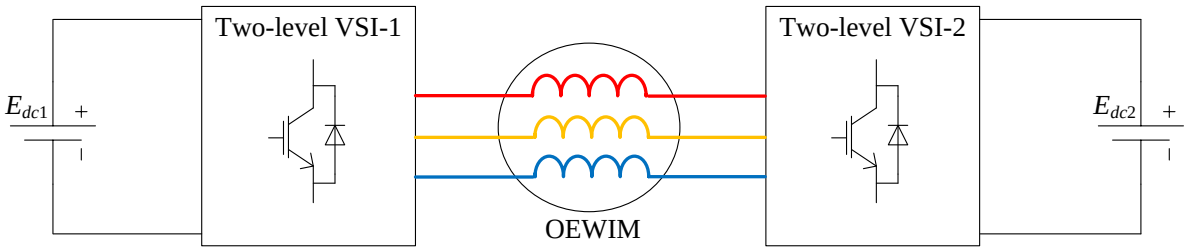

Figure 1.8 Block diagram of dual VSI supplied OEWIM

1.4 Literature survey on DTC schemes

As it is said previously that DTC scheme took very short period of time to attract industries when related to FOC scheme, however it has the limitations [36]. The research on DTC is still active to cope with their limitations. DTC scheme is started from 1986 onwards where it was first applied to IM drive supplied from two-level VSI [20]. Later, it is extended to PMSM drive [37] also. In [36], performance comparison is made for FOC and DTC schemes which are applied to IM. The various measures are incorporated to modify the classical DTC to improve its response for motor drive, which are discussed in this section.

In [38]- [45], Space Vector Modulation (SVM) is used in DTC scheme to attain constant switching frequency with less torque ripples. The calculated reference voltage vector for motor drive operation is given to SVM, which generates control pulses to VSI switches.

However, control implementation complexity grows when related to classical DTC scheme. In [46]- [48] Duty Cycle Modulation (DCM) is introduced in DTC operation of AC motor drive, where the selected active and zero VVs are applied for particular calculated durations in a sample period to minimize torque error. In [49], PI controllers in DTC-SVM are substituted with type-2 fuzzy controllers for improving dynamic performance.

In [50], [51], constant switching frequency in DTC operation is achieved by varying the hysteresis bandwidths based on operating speeds. In [52], DTC of IM drive having self-tuned neuro-fuzzy control for improving dynamic performance and variable hysteresis torque controller for improving steady state response is introduced. In [53], [54], acoustic noise, flux and torque errors are reduced in DTC operation using dithering approach. The low period triangular signal is injected to the flux and torque errors. This method enlarges switching frequency in DTC operation, however it is not fixed and still depends on operating conditions. In [55], torque error is minimized and constrained within the band by calculating suitable time duration of VV in DTC operation of IM drive. In [56], low cost IM drive with DTC operation is proposed where the motor phase currents are restructured without sensing its actual values. In [57], a new DTC for IM drive to reduce Common Mode Voltage (CMV) is introduced, where the active VVs are only considered which are grouped to even and odd. However, large ripples in torque are noticeable. In [58], classical PI controllers in DTC-SVM are replaced with Sliding Mode Controller (SMC). The IM drive performance is tested with both the controllers, where the advantages of SMC is highlighted.

In [59], [60], constant switching frequency torque controller is incorporated in DTC scheme to address the poor flux regulation at very low speeds and torque ripples. However, the operation affects dynamic performance as compared to conventional DTC [61]. Alternatively, dynamic hysteresis torque band is performed in DTC operation [62] on IM drive to preclude the flux regulation problem associated with conventional DTC at low speeds. In [62], torque hysteresis bands are altered based on conditions of speed and flux error. In [63], [64], the current DTC schemes applied for motor drives are given.

The research on DTC scheme is extended while applying to MLI supplied AC motor drives. The NPC inverter supplied to IM drive using DTC scheme is implemented in [65]-[67], where the care on capacitor voltage balance is achieved during its control operation. In [68], PI and fuzzy based DTC-SVM are developed for diode clamped inverter, where the motor drive performance comparisons between them are made. In [69], [70], CHB inverter supplied IM drive is operated by means of DTC scheme. In [69], performance wise

comparison is implemented for three and five level CHB inverter, concluding better torque performance for five level CHB inverter. The five-level CHB is considered in [71], where artificial intelligence (AI) is used along with DTC-SVM for IM drive operation. In [72], FC MLI is used for supplying IM drive with DTC scheme and compared its performance with two-level DTC, where the FC MLI performance is superior. Besides this, the improved DTC schemes are extended to Matrix Converter (MC) supplied AC motor drives to gain better performance as in [73]- [75].

Recently, DTC schemes are implemented for Open-Ended Winding Induction Motor (OEW-IM) drives as reported in [76]- [82]. In [76]- [82] OEW-IM drive with DTC scheme is implemented, where the predefined lookup table is considered for VV selection during control operation. However, the problems associated with the classical look-up table based DTC are: high ripple in torque, poor flux regulation at low speeds and variable switching frequency. In [83]- [86] DTC-SVM is implemented for OEW-IM drive which confirms improved performance compared to two-level inverter supplied motor drive scheme. In [87], Five level OEW-IM drive is operated with DTC-SVM scheme fed by two individual three level VSIs. The SVM scheme ensures constant switching frequency with improved motor drive performance in DTC operation. However, control complexity grows when compared to conventional DTC scheme.

1.5 Literature survey on predictive control schemes

As stated in early discussion, among various mentioned control schemes, PTC indicates present good alternative for motor drive applications. In [88], [89], two family members of MPC scheme such as CCS and FCS are assessed for electric drive system. The advantage of faster dynamic response in FCS is identified, since it is a sample based control. The ongoing research in FCS MPC scheme and its applications are pointed out in [90]. In [27], FCS MPC structure and implementation are compared with FOC and DTC schemes, where the FCS MPC demonstrates better comparative results. In [91], performance of PTC scheme for motor drive is tested in relation with DTC scheme. The benefits of simplicity in control structure and low torque ripples in PTC over DTC scheme are highlighted. The PCC and PTC which are subdivisions of FCS scheme are evaluated in [92], [93]. In [92], FCS scheme performance comparison is provided with DTC scheme. Lower torque ripples and fast dynamic response is observed in PTC implementation for motor drive. From these initial

literature survey, it can be stated that PTC could become a viable in high performance electric drives.

The PTC implementation for motor drive with various power converter topologies are presented as follows: In [94]- [96], two-level VSI supplied IM drive is operated with PTC scheme. The various converter fed IM drives with PTC implementation are reported in [97], [98]. As it is said previously the importance of multi-level VSIs in high power range, PTC started its application for MLI supplied motor drives also. The three-level VSI supplied motor drive is operated using PTC scheme in [99]- [102]. Besides this, MC supplied IM drives also operated with PTC scheme as in [103]- [105]. Owing to the attractive features of dual inverter structure in MLI family, PTC strategy taking place its application for the operation of dual inverter supplied motor drive. In [106], the dual inverter DC link voltages are maintained same for three level operation and the OEW-IM drive is implemented with PTC scheme, where the zero sequence currents are suppressed. In [107], PTC for four level dual inverter supplied OEW-IM drive is introduced, where the unequal DC link voltages which are in 2:1 proportion are set for dual inverter.

Similar to DTC [46]- [48], PTC is extended with duty ratio control for further improvement of motor drive performance in its operation [108], [109]. In [110] an improved duty cycle PTC is presented, where both VV selection and duty ratio are optimized simultaneously. In [111], Generalized PTC (GPTC) is introduced to modify duty ratio control and provides relaxation in VV selection unlike [108]- [110], where only two VVs such as active and null are selected. However, the process complicates PTC operation.

In [94]- [111] PTC operation is conducted with manual regulation of weighting factors in cost function. However, proper adjustment of weighting factors should be ensured during control operation to attain better performance of motor drive. This is due to the direct influence of weighting factor value on final VV selection from cost function optimization. Therefore, the proper choice of weighting factor using tedious manual process is considered as one of the impediments in PTC implementation for motor drives. In [112], guidelines are mentioned to formulate the cost function for various applications and weighting factor choice in cost function. However, the manual adjustment of weighting value utilizes more time and said to be tedious than PI controller parameters tuning [90]. In [108], [113], optimized weight value is placed in cost function for PTC of IM drive. This method of weight determination is limited to two control objectives only and requires comprehensive mathematical analysis having greater involvement of system parameters. In [114], [115], TOPSIS and VIKOR

methods which are part of multi-criteria decision making algorithms are presented in the application of PTC for two-level VSI supplied IM drive. However, the provided solutions create complexity for PTC operation. Using multi objective Genetic Algorithm (GA) method, optimized weighting values are chosen in MPC [116] operation. In [117], desired group of weighting factors are chosen using GA method in PTC operation for IM drive. Through empirical search procedures, the range of optimal weighting values to be placed in cost function are identified in PTC [105]. However, these [105], [116] offline methods for determining weighting values always takes longer time and tedious. In [118]- [120], fuzzy methodology is presented in PTC operation for IM drive to address the problem in choosing weighting values. The membership functions are allocated with priority coefficients in [118], [120] should be adjusted for optimal IM drive response. However, these fuzzy methodologies [118]- [120] in PTC operation consequences extra burden. In PTC [121], [122] for IM drive, the control objectives of torque and flux are individually optimized one after the other. With this strategy of individual assessment of control objectives, the weighting factor is eliminated in PTC operation. However, the combined control optimization for torque and flux is lost. Using SVM strategy in predictive control operation [123], the weighting factors are obviated. However, the need for modulation stage vanish the uniqueness of PTC operation. In [124], [125], the two control objectives of torque and flux in cost function are modified with a single alternative flux space vector objective which facilitate combined control. Hence, PTC operation of IM drive is free from flux weighting factor. However, the method still requires weighting factor selection for extra control objectives such as switching frequency when it is included in cost function. Besides this, all the VVs of two level VSI are utilized in PTC operation and computational burden need to be addressed.

Apart from the issue of weighting factors choice, the complex operation involved in MPC is to be addressed. In MPC operation, the two stages such as prediction and cost function optimization are operated with all the possible VVs of VSI. These VVs are specifically named as prediction VVs which are involved in PTC operation. When MPC is used for multi-level VSIs, the complexity of operation becomes more significant. Currently, sensorless motor drives operation is started implementing with predictive control schemes, where speed is estimated. Several speed observes are introduced for estimating speed such as: Full and reduced order observers [126], Extended Kalman Filters [127]. These observers require high computational time for its execution. Hence, the controller alone must be efficient computationally to incorporate speed estimation in it. This insists for simplicity in predictive

control operation. To cope with this complexity of operation issue in MPC, the VVs involved in MPC operation should be restrained. In [128], Predictive Current Control (PCC) is performed for three level OEWIM drive aiming to reduce computational burden by considering individual phase currents in PCC operation. In [96], [129], prediction VVs are clustered to limited numbers which facilitate reduced computational burden in PTC operation of two-level VSI. However, this limitation is mainly to ensure minimum switching frequency of VSI in PTC operation which consequences increase in ripple content of torque and flux. Some of the listed techniques used to limit prediction VVs in predictive control operation of converters are: graphical approach [130], one-time prediction [131] and Lyapunov approach [132]. The predictive control schemes become simple with prediction of control variables at one step horizon. However, it is prone for sample delay issues. To overcome this, the multi-step prediction horizon is implemented, which is named as delay compensation method. The two step prediction horizon requires more computations. Considering the case of two-level VSI having seven VVs, it requires (7×7) times of calculations. By limiting the number of VVs to four, the required calculations are limited to (4×4) in [96] for extended prediction horizon. A modified predictive control schemes with simple two step prediction horizon are introduced in [133]- [135].

1.6 Motivation

From the extensive literature survey, it is noticed that DTC and PTC schemes possess high dynamic performance for electric drives. These schemes are needed to be suitable with MLI operation also, owing to the importance of MLIs in medium and high power drive applications. From the literature of MLI supplied motor drives, dual inverter configuration gains numerous advantages. This motivates the application of DTC and PTC schemes for dual inverter supplied OEWIM drive.

In basic DTC operation, selection of the final VV is from the look-up tables. The look-up table formation is based on stator flux sector, hysteresis stator flux and torque errors. Unlike FOC, it is less sensitive to parameter variations and low complexity. When basic DTC operation is concerned, it has the issues of higher ripple in torque, variable switching frequency and poor flux regulation at low speeds. To get rid of these problems, several improvements have been used in DTC operation as cited in literature. This motivates drawing attention over the problems of basic DTC operation. In this thesis, the modified DTC is proposed for OEWIM drive supplied from three-level dual inverter. The proposed DTC

scheme is based on effective look-up table design to improve the performance of DTC operation for OEWIM drive.

On the other hand, PTC is coming into existence as an advanced control scheme in the domain of electric drives. The PTC operation is model based and associated with three key steps as seen in literature. The motivation behind PTC implementation is due to its attractive features such as: intuitive, simple and inclusion of multiple objectives for control. However, the major concerns of PTC operation are: choice of weighting factor values in cost function, complex computations which is more significant for MLI drive operation, variable switching frequency and complete parameter dependency. This thesis works out on the issues of weighting factor choice in cost-function, complex computations and switching frequency control, to improve the PTC operation for motor drives.

To study these DTC and PTC schemes, the mathematical modelling is derived for IM drives. The mathematical modelling of two-level VSI followed by dual inverter structure in three and four levels are derived. The dynamic modelling of IM is derived in stationary frame of reference in which DTC and PTC operations are performed.

1.7 Thesis objectives

The concentration of this thesis work is to adopt modified DTC and PTC strategies for IM drives. The following objectives are provided below:

1. To implement simple and effective modified DTC scheme for three-level dual inverter supplied OEWIM drive operation, which addresses the problems involved in conventional DTC such as high torque ripples and switching frequency, and flux instability at zero speed. For this, effective modified look-up tables are incorporated which allows proper voltage vector switching for low and high speeds in proposed DTC operation of OEWIM drive.

2. The implementation of PTC scheme is discussed for IM drives. The manual adjustment of weighting factor in cost function for PTC operation of IM drives is addressed using auto-tuning process.

3. To circumvent the cumbersome process involved in choice of weighting factors, the weighting factor elimination methods are introduced for the PTC operation of OEWIM drive.

4. To simplify and reduce computational burden for PTC operated OEWIM drive, prediction voltage vector limitation schemes are introduced.
5. Minimizing the switching frequency of dual inverter in PTC operation of OEWIM drive.

1.8 Thesis organization

The organization of thesis work on modified DTC and PTC strategies for IM drives is made into overall eight chapters and each chapter's brief outlook is provided below:

Chapter 1 describes the complete view of topic which includes background of Electric drives, literature survey on existing control schemes for motor drives, multilevel VSIs and priority of dual VSI supplied OEWIM drive. The motivation of research work on DTC and PTC schemes for motor drives and thesis objectives are presented.

Chapter 2 presents the mathematical modelling of two-level VSI, dual VSI in three and four level operation. Besides this, dynamic modelling of IM is presented in stationary reference frame for the analysis of DTC and PTC schemes.

Chapter 3 describes the basic DTC operation and its implementation for three-level dual inverter supplied OEWIM drive. The modified look-up tables involved in proposed DTC operation are presented. The proposed DTC is verified by performing simulation and experimentation, comparing the attained response with the conventional DTC for three-level dual inverter supplied OEWIM drive.

Chapter 4 presents operation of PTC scheme for two-level VSI supplied IM drive. An auto-tuning technique is introduced in proposed PTC operation for online selection of desired weighting factor. The attained results for conventional and proposed PTC are compared to verify the proposed PTC for two-level VSI supplied IM drive.

Chapter 5 presents PTC operation of four-level dual inverter supplied OEWIM drive, where the weighting factor elimination strategy such as combined stator flux space vector based objective and ranking analysis is introduced to avoid the cumbersome process involved in choice of weighting factors. The number of prediction VVs involved in four-level dual inverter operation are limited to 20 using stator flux error scheme to circumvent the complexity of PTC operation. The simulation and experimental results validates the proposed

PTC in comparison with conventional PTC for four-level dual inverter supplied OEWIM drive.

Chapter 6 introduces simplified PTC operation of four-level dual inverter supplied OEWIM drive, where the cost function is modified with the same units of control objectives and thus eliminating weighting factor. Besides this, nearest voltage vector selection strategy is presented in proposed PTC to limit the number of prediction VVs of four-level dual inverter. Hence, the reduction in computational burden is achieved in proposed PTC operation. The comparison of attained results of proposed PTC for four-level dual inverter supplied OEWIM drive with conventional PTC is presented for verification.

Chapter 7 proposes an improved weighting factor less PTC scheme for four-level dual inverter supplied OEWIM drive. The significant reduction in prediction VVs number is realized for proposed PTC operation based on reference VV generation and its location in voltage space vector plane. Using redundant switching combinations of dual VSI, the reduction in switching frequency is gained. Through various OEWIM drive tests, the proposed PTC is verified.

At the end, **Chapter 8** concludes the overall key achievements accomplished in this thesis along with the future scope of work.

Chapter 2

Mathematical Modelling of System

Chapter 2
Mathematical Modelling of System

2.1 Introduction

The operation of vector control schemes necessitates system mathematical modelling. Especially when PTC operation is concerned, the complete discretized mathematical model of system should be known. In this thesis, system includes a three-phase IM supplied from inverter. Here, two inverter configurations are considered for motor drive operation. The following are: 1. Two-level VSI and 2. Dual VSI. Therefore, this chapter deals with mathematical modelling of two-level VSI and dual VSI, along with dynamic modelling of IM.

The chapter organization is framed as: Section 2.2 and section 2.3 describes the mathematical modelling of two-level VSI and dual VSI respectively. In section 2.4, co-ordinate frame transformation and space vector representation are discussed. In section 2.5, IM's dynamical mathematical modelling is derived. Finally, in section 2.6, the overall summary about mathematical modelling of system is made.

2.2 Mathematical modelling of two-level VSI

The schematic view of two-level VSI supplied from DC link voltage E_{dc} is presented in Figure 2.1. Each leg is facilitated with two power electronic switches. The switching combinations for top and bottom switches of the three legs are represented as (S_a^+, S_b^+, S_c^+) and (S_a^-, S_b^-, S_c^-) respectively. The two switches in a leg are provided with complementary pulses. The pole voltage of each leg are indicated by E_{ao}, E_{bo} and E_{co} which are displaced by 120^0 apart. By switching on top switch of each leg, the pole voltage of $+E_{dc}$ or by switching on bottom switch, the pole voltage of 0 is attained. Therefore, two switching states are possible for each leg, thus occurring overall 2^3 switching combinations for two-level VSI operation. The mathematical equation of pole voltages with respect to switching states are given by (2.1).

$$\begin{pmatrix} E_{ao} \\ E_{bo} \\ E_{co} \end{pmatrix} = \begin{pmatrix} S_a^+ \\ S_b^+ \\ S_c^+ \end{pmatrix} E_{dc} \tag{2.1}$$

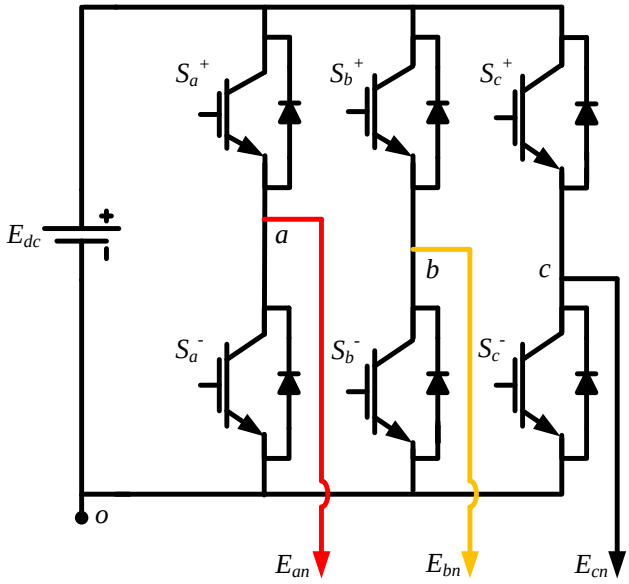

Figure 2.1 Schematic view of two-level VSI

In (2.1), the condition of switching states S_a^+, S_b^+, S_c^+ may be '1' or '0' based upon switching turn-on or off.

The net voltage space vector (E_s) production is denoted as (2.2). From this generalized representation, the possible voltage space vectors for different conditions of switching combinations in two-level VSI operation are listed in Table 2.1 and their position in α-β voltage space vector plane is indicated in Figure 2.2. Therefore, among the overall 2^3 voltage vectors, six of them belong to active voltage vector group and remaining two are null voltage vectors.

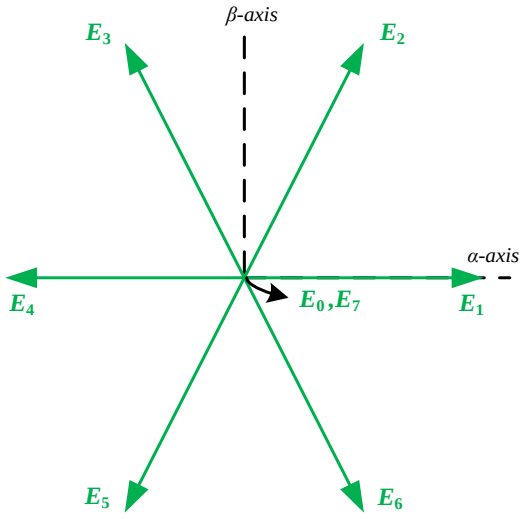

Figure 2.2 Voltage space vectors of two-level VSI operation

$$E_s = \left(S_a^+ + S_b^+ e^{j(2\pi/3)} + S_c^+ e^{j(4\pi/3)}\right)\left(\frac{2}{3}\right)E_{dc} \tag{2.2}$$

Table 2.1 Possible VVs for two-level VSI operation

Switching combinations of VSI			Net VV	$E_{s\alpha}$	$E_{s\beta}$
S_a^+	S_b^+	S_c^+	E_s		
1	0	0	E_1	$2E_{dc}/3$	0
1	1	0	E_2	$E_{dc}/3$	$E_{dc}/1.732$
0	1	0	E_3	$-E_{dc}/3$	$E_{dc}/1.732$
0	1	1	E_4	0	$-2E_{dc}/3$
0	0	1	E_5	$-E_{dc}/3$	$-E_{dc}/1.732$
1	0	1	E_6	$E_{dc}/3$	$-E_{dc}/1.732$
1	1	1	E_7	0	0
0	0	0	E_0	0	0

The phase voltages as a function of pole and common mode voltage are represented by (2.3) and (2.4).

$$\begin{pmatrix} E_{an} \\ E_{bn} \\ E_{cn} \end{pmatrix} = \begin{pmatrix} E_{ao} \\ E_{bo} \\ E_{co} \end{pmatrix} - \begin{pmatrix} E_z \\ E_z \\ E_z \end{pmatrix} \tag{2.3}$$

$$\begin{pmatrix} E_{an} \\ E_{bn} \\ E_{cn} \end{pmatrix} = \begin{pmatrix} 2/3 & -1/3 & -1/3 \\ -1/3 & 2/3 & -1/3 \\ -1/3 & -1/3 & 2/3 \end{pmatrix} \begin{pmatrix} E_{ao} \\ E_{bo} \\ E_{co} \end{pmatrix} \tag{2.4}$$

where, common mode voltage E_z (2.5) is derived by summing all the pole voltages (2.3) for a balanced 3-phase load.

$$E_z = \frac{E_{ao} + E_{bo} + E_{co}}{3} \tag{2.5}$$

From the above analysis, mathematical modelling of two-level VSI is drawn for IM drive operation.

2.3 Mathematical modelling of dual VSI

The schematic view of dual VSI configuration is presented in Figure 2.3. It is structured with two conventional two-level VSIs. The two individual DC voltage sources E_{dc1} and E_{dc2} are supplied on either side of dual VSI. The switching combinations of top and bottom switches of total six legs are indicated as (S_{a1}^+, S_{b1}^+, S_{c1}^+, S_{a2}^+, S_{b2}^+, S_{c2}^+) and (S_{a1}^-, S_{b1}^-, S_{c1}^-, S_{a2}^-, S_{b2}^-, S_{c2}^-) respectively. As similar to two-level VSI, the two switches in a leg of dual VSI are provided with complementary pulses. As each individual two-level VSI can generate 2^3 switching combinations, there are total 2^6 switching combinations possible for dual VSI operation. By maintaining DC link voltages in the proportion of 1:1 such as $E_{dc1} = E_{dc2} = E_{dc}/2$, the three level dual VSI operation is gained. The pole voltages of VSI-1

and VSI-2 are indicated as (E_{ao}, E_{bo}, E_{co}) and ($E_{a'o'}$, $E_{b'o'}$, $E_{c'o'}$) respectively. They are given by (2.6) and (2.7). From these, the resultant pole voltages are given by (2.8). The combination of resultant pole voltages and zero sequence voltage provides phase voltages as (2.9), where the zero sequence voltage is (2.10).

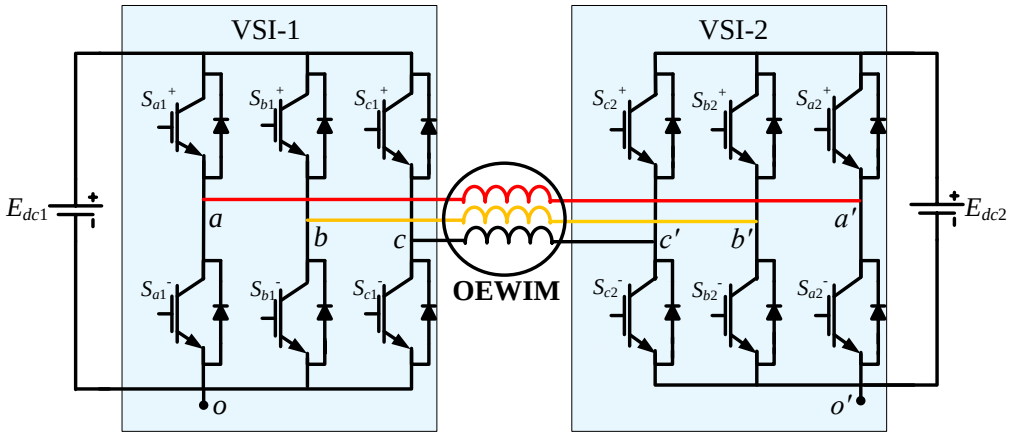

Figure 2.3 Schematic view of dual VSI

$$\begin{pmatrix} E_{ao} \\ E_{bo} \\ E_{co} \end{pmatrix} = \begin{pmatrix} S_{a1}^{+} \\ S_{b1}^{+} \\ S_{c1}^{+} \end{pmatrix} \frac{E_{dc}}{2} \tag{2.6}$$

$$\begin{pmatrix} E_{a'o'} \\ E_{b'o'} \\ E_{c'o'} \end{pmatrix} = \begin{pmatrix} S_{a2}^{+} \\ S_{b2}^{+} \\ S_{c2}^{+} \end{pmatrix} \frac{E_{dc}}{2} \tag{2.7}$$

$$\begin{pmatrix} \Delta E_{aa'} \\ \Delta E_{bb'} \\ \Delta E_{cc'} \end{pmatrix} = \begin{pmatrix} E_{ao} \\ E_{bo} \\ E_{co} \end{pmatrix} - \begin{pmatrix} E_{a'o'} \\ E_{b'o'} \\ E_{c'o'} \end{pmatrix} \tag{2.8}$$

$$\begin{pmatrix} E_{aa'} \\ E_{bb'} \\ E_{cc'} \end{pmatrix} = \begin{pmatrix} \Delta E_{aa'} \\ \Delta E_{bb'} \\ \Delta E_{cc'} \end{pmatrix} - \begin{pmatrix} E_z \\ E_z \\ E_z \end{pmatrix} \quad \text{(or)} \quad \begin{pmatrix} E_{aa'} \\ E_{bb'} \\ E_{cc'} \end{pmatrix} = \begin{pmatrix} \frac{2}{3} & -\frac{1}{3} & -\frac{1}{3} \\ -\frac{1}{3} & \frac{2}{3} & -\frac{1}{3} \\ -\frac{1}{3} & -\frac{1}{3} & \frac{2}{3} \end{pmatrix} \begin{pmatrix} \Delta E_{aa'} \\ \Delta E_{bb'} \\ \Delta E_{cc'} \end{pmatrix} \tag{2.9}$$

$$E_z = \frac{\Delta E_{aa'} + \Delta E_{bb'} + \Delta E_{cc'}}{3} \tag{2.10}$$

The zero sequence voltage (2.10) is derived by summing all the resultant pole voltages (2.9) for a balanced 3-phase load. The individual voltage space vectors such as E_{s1} and E_{s2} of dual VSI are given by (2.11) and (2.12). From these, the resultant voltage space vector E_s of dual VSI operation is attained by (2.13).

$$E_{s1} = \left(S_{a1}^{+} + S_{b1}^{+} e^{j(2\pi/3)} + S_{c1}^{+} e^{j(4\pi/3)}\right)\left(\frac{2}{3}\right) E_{dc1} \tag{2.11}$$

$$E_{s2} = \left(S_{a2}^{+} + S_{b2}^{+} e^{j(2\pi/3)} + S_{c2}^{+} e^{j(4\pi/3)}\right)\left(\frac{2}{3}\right) E_{dc2} \tag{2.12}$$

In (2.6), (2.7), the condition of switching states (S_{a1}^{+}, S_{b1}^{+}, S_{c1}^{+}, S_{a2}^{+}, S_{b2}^{+}, S_{c2}^{+}) may be '1' or '0' based upon switching turn-on or off.

$$E_s = E_{s1} - E_{s2} \tag{2.13}$$

In dual VSI operating mode with $E_{dc1} = E_{dc2} = E_{dc}/2$, the three levels are observed in resultant pole voltages as given in Table 2.2. This is known as three-level dual VSI operation. With the generalized representation (2.11)- (2.13), the possible resultant voltage space vectors for different conditions of switching combinations in three-level dual VSI operation are listed in Table 2.3. From the possible 2^6 switching combinations, the total 19 unique voltage space vectors are acquired. Among these 19 VVs, 18 VVs belongs to active VVs group and one is null VV (*N*). Their phasor representation is indicated in Figure 2.4.

Table 2.2 Pole voltage levels of dual VSI for DC link voltages of 1:1 proportion

VSI-1 possible pole voltage	VSI-2 possible pole voltage	Resultant pole voltage
0	0	0
0	$+E_{dc}/2$	$-E_{dc}/2$
$+E_{dc}/2$	0	$E_{dc}/2$
$+E_{dc}/2$	$+E_{dc}/2$	0

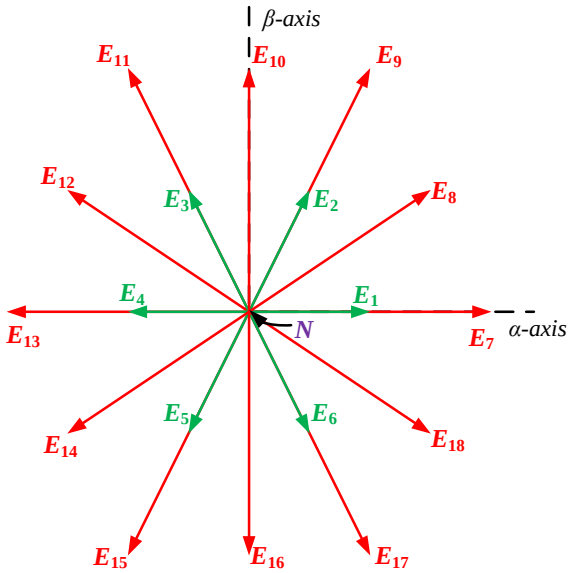

Figure 2.4 Voltage space vectors of three-level dual VSI operation

Table 2.3 Possible switching combinations and effective VVs for dual VSI in three-level operation

Switching combinations of Dual VSI						Net VV (E_s)	$E_{s\alpha}$	$E_{s\beta}$
S_{a1}^{+}	S_{b1}^{+}	S_{c1}^{+}	S_{a2}^{+}	S_{b2}^{+}	S_{c2}^{+}			
0	0	0	0	0	0	*N*	0	0
1	1	1	1	1	1			
0	0	0	1	1	1			

1	1	1	0	0	0			
1	0	0	1	0	0			
1	1	0	1	1	0			
0	1	0	0	1	0			
0	1	1	0	1	1			
0	0	1	0	0	1			
1	0	1	1	0	1			
0	0	0	0	1	1	E_1	$E_{dc}/3$	0
1	0	0	0	0	0			
1	0	0	1	1	1			
1	1	0	0	1	0			
1	0	1	0	0	1			
1	1	1	0	1	1			
0	0	0	0	0	1	E_2	$E_{dc}/6$	$1.732E_{dc}/6$
1	0	0	1	0	1			
1	1	0	0	0	0			
1	1	0	1	1	1			
0	1	0	0	1	1			
1	1	1	0	0	1			
0	0	0	1	0	1	E_3	$-E_{dc}/6$	$1.732E_{dc}/6$
1	1	0	1	0	0			
0	1	0	0	0	0			
0	1	0	1	1	1			
0	1	1	0	0	1			
1	1	1	1	0	1			
0	0	0	1	0	0	E_4	$-E_{dc}/3$	0
0	1	0	1	1	0			
0	1	1	0	0	0			
0	1	1	1	1	1			
0	0	1	1	0	1			
1	1	1	1	0	0			
0	0	0	1	1	0	E_5	$-E_{dc}/6$	$-1.732E_{dc}/6$
0	1	1	0	1	0			
0	0	1	0	0	0			
0	0	1	1	1	1			
1	0	1	1	0	0			
1	1	1	1	1	0			
0	0	0	0	1	0	E_6	$E_{dc}/6$	$-1.732E_{dc}/6$
1	0	0	1	1	0			
0	0	1	0	1	1			
1	0	1	0	0	0			
1	0	1	1	1	1			
1	1	1	0	1	0			
1	0	0	0	1	1	E_7	$2E_{dc}/3$	0
1	0	0	0	0	1	E_8	$E_{dc}/2$	$1.732E_{dc}/6$
1	1	0	0	1	1			
1	1	0	0	0	1	E_9	$E_{dc}/3$	$1.732E_{dc}/3$
1	1	0	1	0	1	E_{10}	0	$1.732E_{dc}/3$
0	1	0	0	0	1			

0	1	0	1	0	1	E_{11}	$-E_{dc}/3$	$1.732E_{dc}/3$
0	1	0	1	0	0	E_{12}	$-E_{dc}/2$	$1.732E_{dc}/6$
0	1	1	1	0	1			
0	1	1	1	0	0	E_{13}	$-2E_{dc}/3$	0
0	1	1	1	1	0	E_{14}	$-E_{dc}/2$	$-1.732E_{dc}/6$
0	0	1	1	0	0			
0	0	1	1	1	0	E_{15}	$-E_{dc}/3$	$-1.732E_{dc}/3$
0	0	1	0	1	0	E_{16}	0	$-1.732E_{dc}/3$
1	0	1	1	1	0			
1	0	1	0	1	0	E_{17}	$E_{dc}/3$	$-1.732E_{dc}/3$
1	0	0	0	1	0	E_{18}	$E_{dc}/2$	$-1.732E_{dc}/6$
1	0	1	0	1	1			

When DC link voltages are maintained in proportion of 2:1 such as $E_{dc1} = 2E_{dc}/3$ and $E_{dc2} = E_{dc}/3$, the four levels are observed in resultant pole voltages as given in Table 2.4. This is known as four-level dual VSI operation. With the generalized representation (2.11)- (2.13), the possible resultant voltage space vectors for different conditions of switching combinations in four-level dual VSI operation are listed in Table 2.5. From the possible 2^6 switching combinations, the total 37 unique voltage space vectors are acquired. Among these 37 VVs, the 36 VVs belongs to active VVs group and one is null VV (*N*). Their phasor representation is indicated in Figure 2.5.

Table 2.4 Pole voltage levels of dual VSI for DC link voltages of 2:1 proportion

VSI-1 possible pole voltage	VSI-2 possible pole voltage	Resultant pole voltage
0	0	0
0	$+E_{dc}/3$	$-E_{dc}/3$
$+2E_{dc}/3$	0	$2E_{dc}/3$
$+2E_{dc}/3$	$+E_{dc}/3$	$E_{dc}/3$

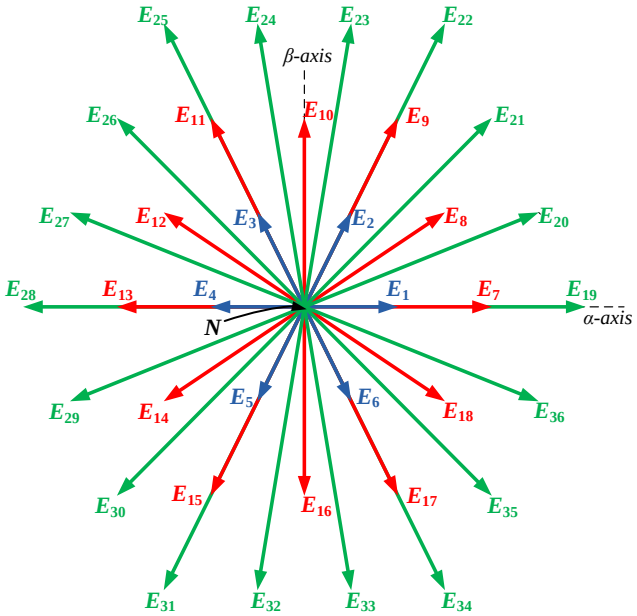

Figure 2.5 Voltage space vectors of four-level dual VSI operation

Table 2.5 Possible switching combinations and effective VVs for dual VSI in four-level operation

Switching combinations of Dual VSI						**Net VV (E_s)**	$E_{s\alpha}$	$E_{s\beta}$
S_{a1}^+	S_{b1}^+	S_{c1}^+	S_{a2}^+	S_{b2}^+	S_{c2}^+			
0	0	0	0	0	0	E_0	0	0
1	1	1	1	1	1			
0	0	0	1	1	1			
1	1	1	0	0	0			
1	0	0	1	0	0	E_1	$2E_{dc}/9$	0
0	0	0	0	1	1			
1	1	1	0	1	1			
1	1	0	1	1	0	E_2	$E_{dc}/9$	$1.732E_{dc}/9$
1	1	1	0	0	1			
0	0	0	0	0	1			
0	1	0	0	1	0	E_3	$-E_{dc}/9$	$1.732E_{dc}/9$
0	0	0	1	0	1			
1	1	1	1	0	1			
0	1	1	0	1	1	E_4	$-2E_{dc}/9$	0
1	1	1	1	0	0			
0	0	0	1	0	0			
0	0	1	0	0	1	E_5	$-E_{dc}/9$	$-1.732E_{dc}/9$
1	1	1	1	1	0			
0	0	0	1	1	0			
1	0	1	1	0	1	E_6	$E_{dc}/9$	$-1.732E_{dc}/9$
1	1	1	0	1	0			
0	0	0	0	1	0			
1	0	0	1	1	1	E_7	$4E_{dc}/9$	0
1	0	0	0	0	0			
1	0	0	1	0	1	E_8	$E_{dc}/3$	$1.732E_{dc}/9$
1	1	0	0	1	0			
1	1	0	1	1	1	E_9	$2E_{dc}/9$	$3.464E_{dc}/9$
1	1	0	0	0	0			
0	1	0	0	1	1	E_{10}	0	$3.464E_{dc}/9$
1	1	0	1	0	0			
0	1	0	1	1	1	E_{11}	$-2E_{dc}/9$	$3.464E_{dc}/9$
0	1	0	0	0	0			
0	1	0	1	1	0	E_{12}	$-E_{dc}/3$	$1.732E_{dc}/9$
0	1	1	0	0	1			
0	1	1	1	1	1	E_{13}	$-4E_{dc}/9$	0
0	1	1	0	0	0			
0	0	1	1	0	1	E_{14}	$-E_{dc}/3$	$-1.732E_{dc}/9$
0	1	1	0	1	0			
0	0	1	1	1	1	E_{15}	$-2E_{dc}/9$	$-3.464E_{dc}/9$
0	0	1	0	0	0			
0	0	1	0	1	1	E_{16}	0	$-3.464E_{dc}/9$
1	0	1	1	0	0			
1	0	1	1	1	1	E_{17}	$2E_{dc}/9$	$-3.464E_{dc}/9$
1	0	1	0	0	0			
1	0	0	1	1	0	E_{18}	$E_{dc}/3$	$-1.732E_{dc}/9$
1	0	1	0	0	1			

1	0	0	0	1	1	E_{19}	$2E_{dc}/3$	0
1	0	0	0	0	1	E_{20}	$5E_{dc}/9$	$1.732E_{dc}/9$
1	1	0	0	1	1	E_{21}	$4E_{dc}/9$	$3.464E_{dc}/9$
1	1	0	0	0	1	E_{22}	$E_{dc}/3$	$1.732E_{dc}/3$
1	1	0	1	0	1	E_{23}	$E_{dc}/9$	$1.732E_{dc}/3$
0	1	0	0	0	1	E_{24}	$-E_{dc}/9$	$1.732E_{dc}/3$
0	1	0	1	0	1	E_{25}	$-E_{dc}/3$	$1.732E_{dc}/3$
0	1	0	1	0	0	E_{26}	$-4E_{dc}/9$	$3.464E_{dc}/9$
0	1	1	1	0	1	E_{27}	$-5E_{dc}/9$	$1.732E_{dc}/9$
0	1	1	1	0	0	E_{28}	$-2E_{dc}/3$	0
0	1	1	1	1	0	E_{29}	$-5E_{dc}/9$	$-1.732E_{dc}/9$
0	0	1	1	0	0	E_{30}	$-4E_{dc}/9$	$-3.464E_{dc}/9$
0	0	1	1	1	0	E_{31}	$-E_{dc}/3$	$-1.732E_{dc}/3$
0	0	1	0	1	0	E_{32}	$-E_{dc}/9$	$-1.732E_{dc}/3$
1	0	1	1	1	0	E_{33}	$E_{dc}/9$	$-1.732E_{dc}/3$
1	0	1	0	1	0	E_{34}	$E_{dc}/3$	$-1.732E_{dc}/3$
1	0	1	0	1	1	E_{35}	$4E_{dc}/9$	$-3.464E_{dc}/9$
1	0	0	0	1	0	E_{36}	$5E_{dc}/9$	$-1.732E_{dc}/9$

The individual pole voltages of four-level dual VSI are given by (2.14) and (2.15). The phase voltages as a function of resultant pole and common mode voltage are represented by (2.16) and (2.17).

$$\begin{pmatrix} E_{ao} \\ E_{bo} \\ E_{co} \end{pmatrix} = \begin{pmatrix} S_{a1}^{+} \\ S_{b1}^{+} \\ S_{c1}^{+} \end{pmatrix} \frac{2E_{dc}}{3} \tag{2.14}$$

$$\begin{pmatrix} E_{ao}^{,,} \\ E_{bo}^{,,} \\ E_{co}^{,,} \end{pmatrix} = \begin{pmatrix} S_{a2}^{+} \\ S_{b2}^{+} \\ S_{c2}^{+} \end{pmatrix} \frac{E_{dc}}{3} \tag{2.15}$$

$$\begin{pmatrix} E_{aa}^{,} \\ E_{bb}^{,} \\ E_{cc}^{,} \end{pmatrix} = \begin{pmatrix} \Delta E_{aa}^{,} \\ \Delta E_{bb}^{,} \\ \Delta E_{cc}^{,} \end{pmatrix} - \begin{pmatrix} E_z \\ E_z \\ E_z \end{pmatrix} \tag{2.16}$$

$$\begin{pmatrix} E_{aa}^{,} \\ E_{bb}^{,} \\ E_{cc}^{,} \end{pmatrix} = \begin{pmatrix} 2/3 & -1/3 & -1/3 \\ -1/3 & 2/3 & -1/3 \\ -1/3 & -1/3 & 2/3 \end{pmatrix} \begin{pmatrix} \Delta E_{aa}^{,} \\ \Delta E_{bb}^{,} \\ \Delta E_{cc}^{,} \end{pmatrix} \tag{2.17}$$

In above equations, the common mode voltage (2.18) is derived by summing all the resultant pole voltages (2.16) for a balanced 3-phase load.

$$E_z = \frac{\Delta E_{aa}^{,} + \Delta E_{bb}^{,} + \Delta E_{cc}^{,}}{3} \tag{2.18}$$

Therefore, the entire analysis represents mathematical modelling of dual VSI operation in three and four level mode which is suitable for OEWIM drive.

2.4 Co-ordinate frame transformation and space vector representation

Consider a space representation of three phase system (*a*, *b*, *c*) which are displaced by 120^0 apart as presented in Figure 2.6. It is much familiar that all these phases are linearly rely on each other. Therefore, the system modelling becomes complex. To overcome this difficulty and simplify system modelling, the analysis is made in two phase coordinate system. It is stated previously that the system includes three phase IM. Thus, three phase IM electrical quantities such as flux, current and voltage are shifted to two phase stationary (α-β) reference frame.

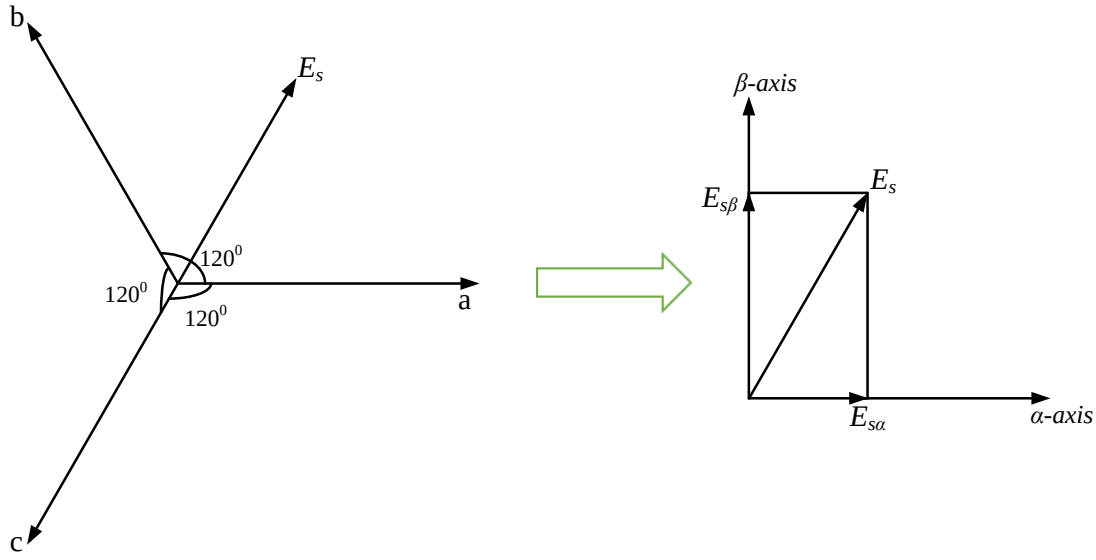

Figure 2.6 Co-ordinate frame transformations

Considering a case with voltage, the three phase voltages (E_a, E_b and E_c) are transferred into two phase ($E_{s\alpha}$ and $E_{s\beta}$) reference frame using Clarke's transformation as (2.19). The same is applicable for the remaining electrical quantities (flux and current). The space vector representation of various electrical quantities is given below:

$$\begin{pmatrix} E_{s\alpha} \\ E_{s\beta} \end{pmatrix} = \frac{2}{3}\begin{pmatrix} 1 & -0.5 & -0.5 \\ 0 & 0.866 & -0.866 \end{pmatrix}\begin{pmatrix} E_a \\ E_b \\ E_c \end{pmatrix} \tag{2.19}$$

Stator voltage: $E_s = E_{s\alpha} + jE_{s\beta}$, Stator current: $i_s = i_{s\alpha} + ji_{s\beta}$, Stator flux: $\lambda_s = \lambda_{s\alpha} + j\lambda_{s\beta}$, Rotor current: $i_r = i_{r\alpha} + ji_{r\beta}$ and Rotor flux: $\lambda_r = \lambda_{r\alpha} + j\lambda_{r\beta}$

2.5 IM's dynamical mathematical modelling

The operation of DTC and PTC schemes require stationary reference frame representation of IM model. The stator side voltage (E_s) and flux (λ_s) equations are represented by (2.20) and (2.21) respectively. In (2.20), stator voltage is written as a function of stator inductance drop and stator resistance drop. Stator inductance is combination of leakage and mutual inductance.

$$E_s = \frac{d\lambda_s}{dt} + R_s i_s \tag{2.20}$$

$$\lambda_s = L_s i_s + L_m i_r \tag{2.21}$$

The rotor side voltage (E_r) and flux (λ_r) equations are given by (2.22) and (2.23) respectively. In (2.22), rotor voltage is made zero, due to the squirrel cage rotor winding of three phase IM. The rotor voltage equation is function of rotor inductance drop, rotor resistance drop and rotational voltage.

$$0 = \frac{d\lambda_r}{dt} + R_r i_r - j\omega_r \lambda_r \tag{2.22}$$

$$\lambda_r = L_r i_r + L_m i_s \tag{2.23}$$

The interaction of stator flux (λ_s) and current (i_s) leads to generation of electromagnetic torque (T_m) given as (2.24). Finally, the motor (T_m) – load (T_l) torque equation is represented by (2.25). The terms ω_m and ω_r are mechanical and electrical speeds which are related as (2.26).

$$T_m = (1.5)\left(\frac{P}{2}\right)\left(\text{imag}\left(\bar{\lambda}_s i_s\right)\right) \tag{2.24}$$

$$T_m = T_l + J\frac{d\omega_m}{dt} \tag{2.25}$$

$$\omega_r = \frac{P}{2}\omega_m \tag{2.26}$$

In (2.20)- (2.26), the indicated motor parameters are inertia constant (J), pole number (P), rotor resistance (R_r), stator resistance (R_s), rotor inductance (L_r), stator inductance (L_s) and mutual inductance (L_m).

By solving equations (2.20)- (2.23), the state variable representation of stator current and flux are given by (2.27) and (2.28) respectively. These are especially used for discretizing IM mathematical model.

$$\frac{di_s}{dt} = B_1\left(B_2\lambda_s - B_3 i_s + B_r\left(E_s + Bi_s - j\omega_r\lambda_s\right) + \frac{j\omega_r i_s}{B_1}\right) \tag{2.27}$$

$$\frac{d\lambda_s}{dt} = \left(E_s + Bi_s\right) \tag{2.28}$$

In (2.27), (2.28), the represented constants are $B = -R_s$, $B_r = L_r/L_m$, $B_1 = L_m/(L_sL_r\text{-}L_m^2)$, $B_2 = R_r/L_m$ and $B_3 = L_sR_r/L_m$

Using Euler's method, the discretization of (2.27), (2.28) can be made. The generalized indication of Euler's formula with any state variable (z) at previous (k-1) and present (k) sample instant is:

$$\frac{dz}{dt} \cong \frac{z(k) - z(k-1)}{T_s} \tag{2.29}$$

where, T_s is sample time.

The equation (2.29) represents backward Euler's approximation. Whereas, the equation (2.30) represents forward Euler's approximation. In (2.30), the terms $z(k)$ and $z(k+1)$ signifies present and future state variables respectively. These approximations are used to represent the discrete model of IM in PTC operation.

$$\frac{dz}{dt} \cong \frac{z(k+1) - z(k)}{T_s} \tag{2.30}$$

2.6 Summary

This chapter describes mathematical modelling of system such as inverter model and IM model. The two configurations of inverter named as two-level VSI and dual VSI which are used in this thesis are mathematically modelled. Their complete voltage switching states and vectors are derived. The co-ordinate transformation from three phase stationary to two phase stationary is briefly discussed and space vector representation is shown. Finally, the IM dynamic modelling equations are presented in stationary reference frame and the method of its discrete modelling is also shown for the sake of DTC and PTC analysis.

Chapter 3

An Improved Direct Torque Control of Three-Level Dual Inverter fed Open-Ended Winding Induction Motor Drive Based on Modified Look-Up Table

Chapter 3

An Improved Direct Torque Control of Three-Level Dual Inverter fed Open-Ended Winding Induction Motor Drive Based on Modified Look-Up Table

3.1 Introduction

At the beginning, DTC scheme is applied for two level VSI supplied IM drives. Later, with the advancement in research, the DTC scheme is extended for multilevel VSI supplied IM drives in medium and high power applications. This chapter introduces DTC scheme for multilevel VSI supplied IM drive. The dual VSI configuration supplied to OEWIM is considered. The motivation behind this selection of particular configuration is briefly discussed in Chapter-1. The dual VSI is operated with equal DC link voltages on its either side as displayed in Figure 3.1. The DC link voltages of dual two-level VSIs (i.e. VSI-1 and VSI-2) are supplied from two individual three phase full bridge diode rectifiers. The common AC input supply is provided to these full bridge diode rectifiers. Therefore, equal DC link voltages (i.e. $E_{dc}/2$ for VSI-1 and $E_{dc}/2$ for VSI-2) are supplied, combined to net DC link voltage of E_{dc} to OEWIM drive. The points O and O' are negative terminals of DC supplies connected to VSI-1 and VSI-2 respectively. The detailed view of this scenario is provided in Appendix-A, Figure A.2.

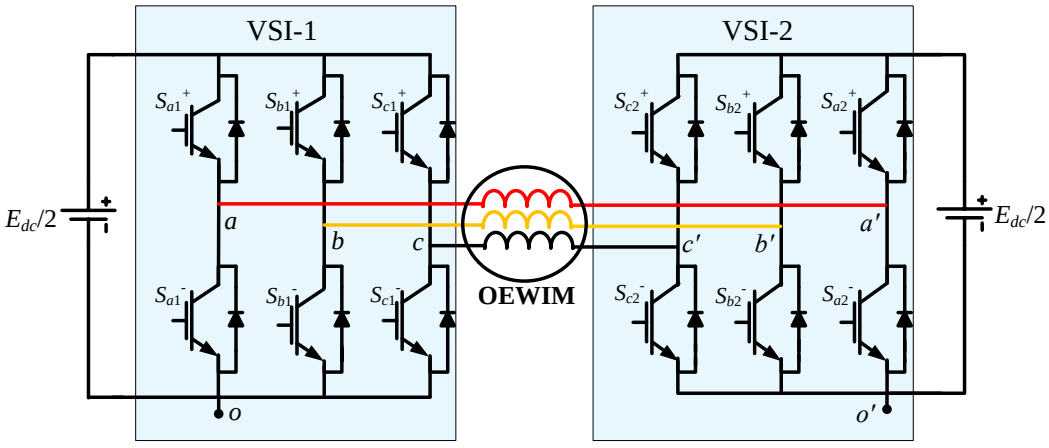

Figure 3.1 Schematic view of three-level dual VSI supplied OEWIM

With the working scheme of three-level dual VSI, the acquired three level voltage space vectors of total 19 are indicated in Figure 3.2. The VVs E_1-E_6 forms a small hexagon group, each having magnitude of $0.33E_{dc}$. Whereas, the VVs E_7-E_{18} forms a large hexagon

group, in which the hexagon corners E_7, E_9, E_{11}, E_{13}, E_{15} and E_{17} are having magnitude of $0.66E_{dc}$, and E_8, E_{10}, E_{12}, E_{14}, E_{16} and E_{18} are having magnitude of $0.57E_{dc}$. The VV N indicates null voltage state with zero magnitude.

Based on the effect of these voltage space vectors, look-up table is formed in DTC operation. Due to its simplicity of operation, DTC scheme became widely popular in electric drives. However, in conventional DTC operation, the identifiable problems are: 1. High torque ripple, 2. High switching frequency and 3. Flux drooping nature at zero speed. The objective of this chapter is to develop an improved DTC scheme for three level dual inverter supplied OEWIM drive and address the mentioned issues. The chapter organization is as follows: section 3.2 provides conventional DTC operation and its application for OEWIM drive supplied from three level dual VSI, limitations with conventional DTC operation. In section 3.3, the proposed DTC scheme is presented which get over the mentioned problems and eventuate an improved performance for OEWIM drive operation. The simulation and real time outcomes of existing and proposed DTC schemes for three level OEWIM drive are discussed in section 3.4. From the overall discussions and observations, the chapter is summarized in section 3.5.

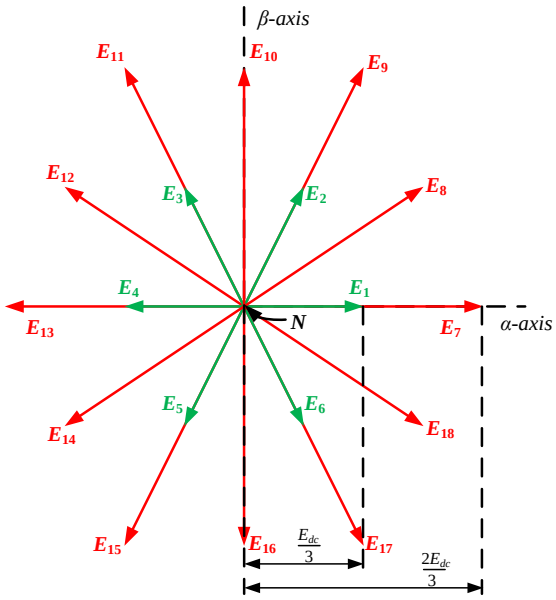

Figure 3.2 Possible VVs generation for three-level dual VSI

3.2 Conventional DTC operation

The conventional DTC functioning block model for three-level dual VSI supplied OEWIM drive is presented in Figure 3.3. The represented blocks in Figure 3.3 are flux, torque and sector estimation. Their realizations are obtained by (3.1)- (3.3). (3.1) indicates present

state (k) stator flux estimation which is function of previous instant stator flux vector at (k-1), stator voltage (E_s) and current (i_s) space vector in a sample period T_s, where R_s is stator resistance. (3.2) denotes stator flux angle calculation. Based on this angle, flux sector estimation is attained. From the stator current and estimated flux space vector, the motor torque is realized by (3.3). The current calculation block involves in the calculation of stator current space vector (i_s) based on the sensed phase currents (i_a, i_b and i_c) through Clarke's transformation. The block voltage calculation provides stator voltage space vector (E_s), through the information of optimal switching states (S_{opt}) and net DC link voltage (E_{dc}) of dual inverter. This can be realized from (2.11)- (2.13) in Chapter-2.

$$\psi_s(k) = \psi_s(k-1) + E_s T_s - R_s T_s i_s \tag{3.1}$$

$$\theta = \tan^{-1}\left(\frac{\psi_{\beta s}}{\psi_{\alpha s}}\right) \tag{3.2}$$

$$T_m = \frac{3}{2}\frac{P}{2}\left(\text{imag}\left(\overline{\psi}_s i_s\right)\right) \tag{3.3}$$

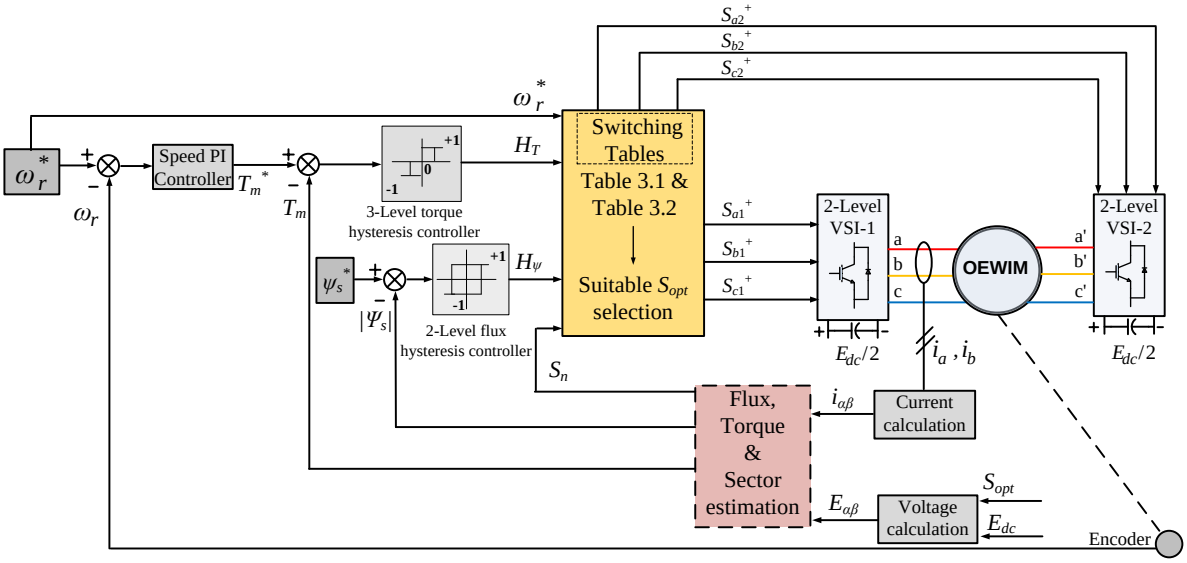

Figure 3.3 Block diagram of OEWIM drive operated with conventional DTC scheme

The difference of given motor reference speed and actual speed provides speed error value. The speed error is fed to PI regulator, which outputs required reference torque value (T_m^*). The actual electromagnetic torque (T_m) is formulated with the information of stator current (i_s) and flux (Ψ_s) vectors as given by (3.3). Thus, with the difference of reference and actual motor torque, the torque error is formed. Similarly, the difference of reference (Ψ_s^*) and actual stator flux ($|\Psi_s|$) forms stator flux error. These flux and torque errors are regulated with in the hysteresis boundaries using three level torque (H_T) and two level flux (H_Ψ)

hysteresis controllers. The outputs of H_T may be +1 or 0 or -1, based on torque error crossing the upper or 0 or lower hysteresis boundaries. Similarly, the outputs of H_Ψ may be +1 or -1, based on flux error crossing the upper or lower hysteresis boundaries. Based on these H_T and H_Ψ outputs and flux sector (S_n) data, the proper VV is chosen from look-up table for DTC operation. In three level dual inverter model, the possible effective voltage space vectors are realized, which are presented in Figure 3.2.

The voltage space vector $\alpha\beta$-plane is divided into 12 sectors, with 30^0 span as presented in Figure 3.4. From these, it is identified that there are 18 active switching states and possible null switching state. The voltage state combinations, E_1-E_6 are assembled as small vector group and E_7-E_{18} are assembled as large vector group. Thus, VV selection for low and high speeds are distinguished based on small and large vector groups respectively. The conventional heuristic look-up table formation for choosing suitable VV based on flux (Ψ_s) sector information (S_n), H_T and H_Ψ conditions during the high and low speeds are displayed in Table 3.1 and Table 3.2 respectively.

These voltage vectors selection from lookup tables are having direct influence on regulation of stator flux and angle between stator and rotor flux as given in Figure 3.5. From Figure 3.5, by applying suitable VV the desired change in flux and torque are brought out for a sample period (T_s), resulting new stator flux position (ψ_s^n) with an angle displacement of (θ^n) between stator and rotor flux. Thus attaining direct torque (3.4) and flux (3.5) controlling for motor drive. In (3.4), the inductance term $L_{ss} = (L_s L_r - L_m^2)/L_r$.

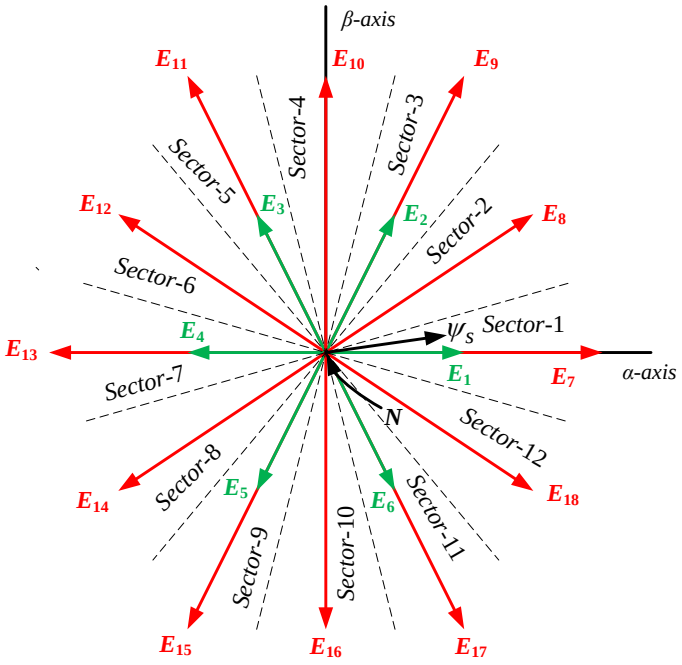

Figure 3.4 Voltage space vector $\alpha\beta$ plane sector divisions

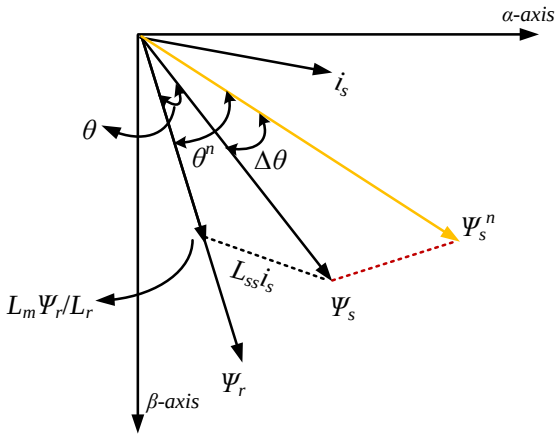

Figure 3.5 Phasor representation of DTC operation

$$\Delta T_m = \frac{3}{2}\frac{P}{2}\frac{L_m}{L_r L_{ss}}\left(|\psi_s + \Delta\psi_s|\right)\left(|\psi_r|\right)\sin(\Delta\theta) \tag{3.4}$$

$$\Delta\psi_s = \left(E_s - R_s i_s\right)\left(\Delta T_s\right) \tag{3.5}$$

Table 3.1 Conventional look-up table for VV selection during high speed condition

H_Ψ	H_T	VV selection based on sector number (S_n)											
		1	**2**	**3**	**4**	**5**	**6**	**7**	**8**	**9**	**10**	**11**	**12**
+1	+1	E_9	E_{10}	E_{11}	E_{12}	E_{13}	E_{14}	E_{15}	E_{16}	E_{17}	E_{18}	E_7	E_8
	0	E_0	E_0	E_0	E_0	E_0	E_0	E_0	E_0	E_0	E_0	E_0	E_0
	-1	E_{17}	E_{18}	E_7	E_8	E_9	E_{10}	E_{11}	E_{12}	E_{13}	E_{14}	E_{15}	E_{16}
-1	+1	E_{11}	E_{12}	E_{13}	E_{14}	E_{15}	E_{16}	E_{17}	E_{18}	E_7	E_8	E_9	E_{10}
	0	E_0	E_0	E_0	E_0	E_0	E_0	E_0	E_0	E_0	E_0	E_0	E_0
	-1	E_{15}	E_{16}	E_{17}	E_{18}	E_7	E_8	E_9	E_{10}	E_{11}	E_{12}	E_{13}	E_{14}

Table 3.2 Conventional look-up table for VV selection during low speed condition

H_Ψ	H_T	VV selection based on sector number (S_n)											
		1	**2**	**3**	**4**	**5**	**6**	**7**	**8**	**9**	**10**	**11**	**12**
+1	+1	E_2	E_2	E_3	E_3	E_4	E_4	E_5	E_5	E_6	E_6	E_1	E_1
	0	E_0	E_0	E_0	E_0	E_0	E_0	E_0	E_0	E_0	E_0	E_0	E_0
	-1	E_6	E_6	E_1	E_1	E_2	E_2	E_3	E_3	E_4	E_4	E_5	E_5
-1	+1	E_3	E_3	E_4	E_4	E_5	E_5	E_6	E_6	E_1	E_1	E_2	E_2
	0	E_0	E_0	E_0	E_0	E_0	E_0	E_0	E_0	E_0	E_0	E_0	E_0
	-1	E_5	E_5	E_6	E_6	E_1	E_1	E_2	E_2	E_3	E_3	E_4	E_4

3.2.1 Limitations of conventional DTC

Generally, H_T band is set to 10% of rated torque while considering the measure of not selecting reverse VV. However, keeping higher H_T band is also not advisable. Besides this, the higher sample time issue in digital implementation of DTC for OEWIM drive is also responsible for reverse VV selection. This results in higher torque ripple in OEWIM drive response with conventional DTC scheme. The three level OEWIM drive is operated with DTC having look-up tables for high and low speed of operation, that are given in Table 3.1 and

Table 3.2 respectively. From this, one can observe that reverse voltage vector selection is during forward motoring mode when H_T and H_Ψ conditions are -1. Similarly, during reverse motoring mode, the reverse voltage vector selection occurs when H_T is +1 and H_Ψ is -1. With this operation, higher torque ripples are noticed in conventional DTC operation and also consequences increase in dual inverter switching frequency.

With the provided look-up Table 3.2 during low speed operation, there exist another problem of flux drooping. One can observe in provided look-up table that the condition H_T is 0 and H_Ψ is 1, results in null voltage vector ($E_s = 0$) selection for long duration. Thus, the change in flux is given by (3.6). But meaning of $H_\Psi = 1$ conveys that the stator flux error crosses upper hysteresis boundaries and need to raise the actual stator flux for maintaining stable flux response. However, the selection of null voltage state in this situation ($H_T = 0$ and $H_\Psi = 1$) consequences further drooping in flux value and not maintaining stable especially in zero speed during start-up process. For high speed operation, the above discussed case ($H_T = 0$ and $H_\Psi = 1$) is acceptable and stable flux is maintained due to shorter duration of null voltage state and more active voltage vectors selection.

$$\Delta\psi_s = \left(-R_s i_s\right)\left(\Delta T_s\right) \tag{3.6}$$

3.3 Proposed DTC operation

The proposed DTC operation is based on modified look-up tables. The block diagram of proposed DTC operation for three-level OEWIM drive is presented in Figure 3.6. The gains of speed PI controller are selected using heuristic approach. The switching tables (Table 3.1 and Table 3.2) in conventional DTC scheme are modified in the proposed DTC scheme for OEWIM drive to answer all the above mentioned limitations of conventional DTC. The modified look-up tables for better VV selection to enhance motor drive response for high and low speeds of operation are presented in Table 3.3 and Table 3.4.

Table 3.3 Proposed look-up table for VV selection during high speed condition

H_Ψ	H_T	Direction of rotation	VV selection based on sector number (S_n)											
			1	**2**	**3**	**4**	**5**	**6**	**7**	**8**	**9**	**10**	**11**	**12**
+1	+1	*Forward/Reverse*	E_9	E_{10}	E_{11}	E_{12}	E_{13}	E_{14}	E_{15}	E_{16}	E_{17}	E_{18}	E_7	E_8
	0		*N*											
	-1		E_{17}	E_{18}	E_7	E_8	E_9	E_{10}	E_{11}	E_{12}	E_{13}	E_{14}	E_{15}	E_{16}
-1	+1	*Forward*	E_{11}	E_{12}	E_{13}	E_{14}	E_{15}	E_{16}	E_{17}	E_{18}	E_7	E_8	E_9	E_{10}
		Reverse	*N*											
	0	*Forward/Reverse*	*N*											
	-1	*Reverse*	E_{15}	E_{16}	E_{17}	E_{18}	E_7	E_8	E_9	E_{10}	E_{11}	E_{12}	E_{13}	E_{14}
		Forward	*N*											

Table 3.4 Proposed look-up table for VV selection during low speed condition

H_Ψ	H_T	Direction of rotation	VV selection based on sector number (S_n)											
			1	**2**	**3**	**4**	**5**	**6**	**7**	**8**	**9**	**10**	**11**	**12**
+1	+1	*Forward/Reverse*	E_2	E_2	E_3	E_3	E_4	E_4	E_5	E_5	E_6	E_6	E_1	E_1
	0	*Forward*	E_8	E_9	E_{10}	E_{11}	E_{12}	E_{13}	E_{14}	E_{15}	E_{16}	E_{17}	E_{18}	E_7
		Reverse	E_{18}	E_7	E_8	E_9	E_{10}	E_{11}	E_{12}	E_{13}	E_{14}	E_{15}	E_{16}	E_{17}
	-1	*Forward/Reverse*	E_6	E_6	E_1	E_1	E_2	E_2	E_3	E_3	E_4	E_4	E_5	E_5
-1	+1	*Forward*	E_3	E_3	E_4	E_4	E_5	E_5	E_6	E_6	E_1	E_1	E_2	E_2
		Reverse	N											
	0	*Forward/Reverse*	N											
	-1	*Reverse*	E_5	E_5	E_6	E_6	E_1	E_1	E_2	E_2	E_3	E_3	E_4	E_4
		Forward	N											

In forward motoring mode, to avoid active reverse VV selection during H_T and H_Ψ are at -1 condition, the active reverse voltage vectors are updated with null voltage states. Similarly, in reverse motoring mode, the active reverse voltage vectors selection is updated with null voltage states during H_T is +1 and H_Ψ is -1 condition. The placement of null voltage states in these conditions ensures torque ripple reduction.

Furthermore, from the possible redundant null VV switching states, the switching combinations providing minimum state transitions to the previously selected VV are chosen. The null VV switching states updation for present sample time (k) depends upon VV applied in previous sample time (k-1). Based on the possible VV group, the null VV switching states selection are listed in Table 3.5, ensuring minimum switching state transitions.

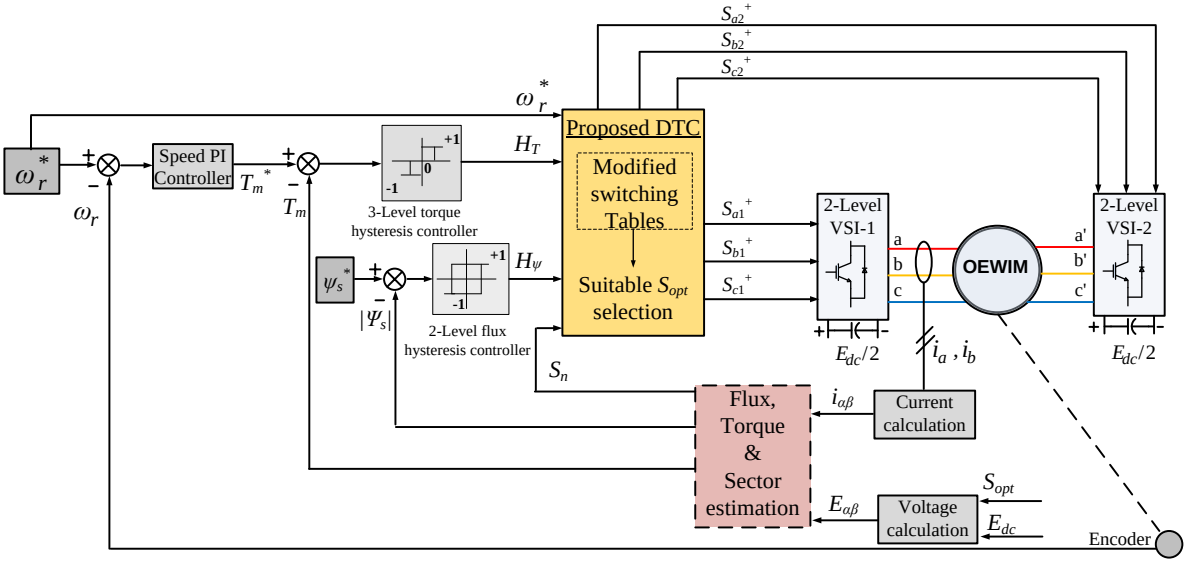

Figure 3.6 Block diagram of OEWIM drive operated with proposed DTC scheme

Thus, the provided modifications in proposed DTC look-up tables ensure overall improved motor torque response and reduction in switching frequency.

Table 3.5 Null VV switching states selection

Voltage vectors $E_s(k\text{-}1)$	**Preferable null voltage switching states** $N(k)= (S_{a1}^+, S_{b1}^+, S_{c1}^+ - S_{a2}^+, S_{b2}^+, S_{c2}^+)$
N	N
E_{10} (0,1,0 - 0,0,1), E_{14} (0,0,1 - 1,0,0), E_{18} (1,0,0 - 0,1,0)	(0,0,0 - 0,0,0)
E_8 (1,1,0 - 0,1,1), E_{12} (0,1,1 - 1,0,1), E_{16} (1,0,1 - 1,1,0)	(1,1,1 - 1,1,1)
E_1 (1,1,0 - 0,1,0), E_3 (0,1,1 - 0,0,1), E_5 (1,0,1 - 1,0,0), E_9 (1,1,0 - 0,0,1), E_{13} (0,1,1 - 1,0,0), E_{17} (1,0,1 - 0,1,0)	(1,1,1 - 0,0,0)
E_2 (0,1,0 - 0,1,1), E_4 (0,0,1 - 1,0,1), E_6 (1,0,0 - 1,1,0), E_7 (1,0,0 - 0,1,1), E_{11} (0,1,0 - 1,0,1), E_{15} (0,0,1 - 1,1,0)	(0,0,0 - 1,1,1)

The null VV selection at $H_T = 0$ and $H_\Psi = 1$ condition is mainly responsible for flux drooping. To obviate this, null VVs at this condition are updated with large active voltage vectors. The large active VVs selection in forward and reverse motoring at low speeds of operation are listed in Table 3.4. These active VVs are mainly responsible to increase flux which is really needed at this condition with negligible effect on torque as the selected active VV is very near to the sector with very small change in θ. Thus, realizing stable flux at zero speed during start-up of OEWIM drive with the modified look-up table.

3.3.1 Proposed DTC operational flowchart

The overall proposed DTC working model for three-level dual VSI supplied OEWIM drive is presented schematically in Figure 3.7 and its operational steps involved are mentioned below.

Step 1: Sense motor phase currents in stationary reference frame ($i_{s\alpha}$ and $i_{s\beta}$), dual inverter combined DC link voltage (E_{dc}), motor speed (ω_r) and optimal switching states (S_{opt}) selected for dual VSIs (S_{a1}^+, S_{b1}^+, S_{c1}^+ for VSI-1 and S_{a2}^+, S_{b2}^+, S_{c2}^+ for VSI-2).

Step 2: Update null VV switching states in modified look-up tables (Table 3.3 and Table 3.4) based on previously selected optimal VV to minimize switching frequency. This updation is done from Table 3.5.

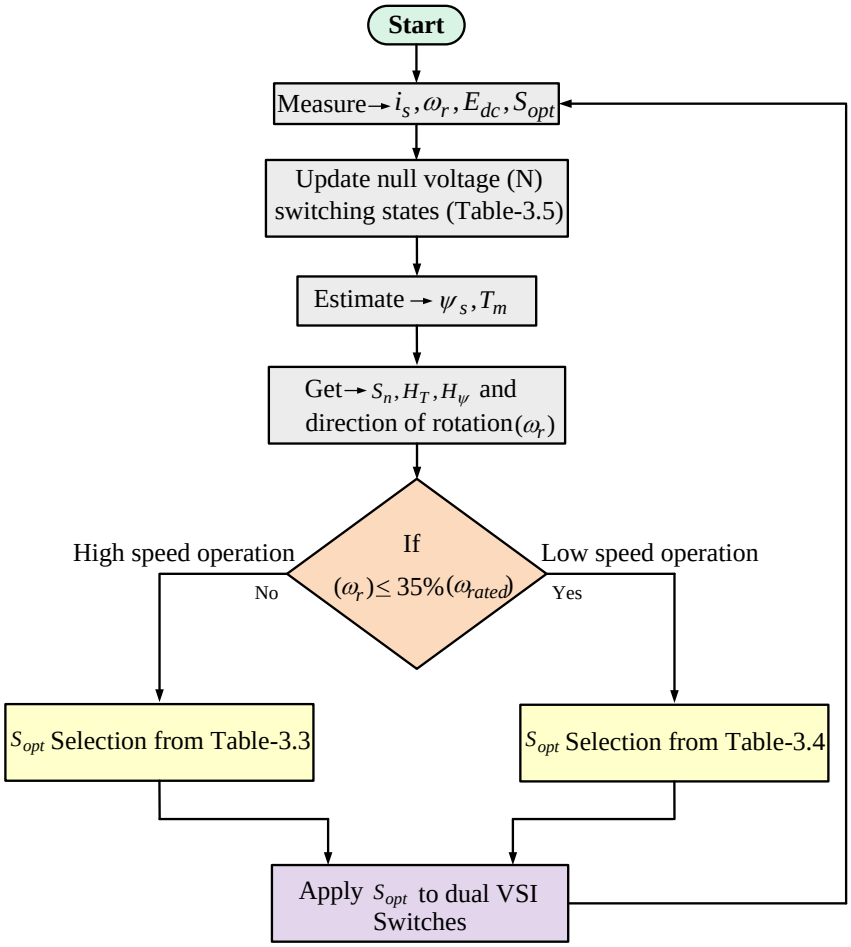

Figure 3.7 Proposed DTC scheme working flowchart

Step 3: Estimate stator flux (ψ_s) and motor torque (T_m) from the machine mathematical modelling. The stator flux magnitude and angle are figured out.

Step 4: If the OEWIM drive is operating at higher speeds, follow look-up Table 3.3 for the optimal switching state selection. Otherwise, follow look-up Table 3.4 for the optimal switching state selection during low speeds.

Step 5: Apply selected optimal switching states (S_{opt}) to the dual VSI switches for DTC operation of OEWIM drive.

Finally, it can be stated that, overall effective modifications performed in proposed DTC look-up table results in better torque response, switching frequency reduction and stable flux maintenance for OEWIM drive operation.

3.4 Results and discussion

The proposed three-level OEWIM drive operated with DTC scheme is verified by conducting tests in MATLAB/Simulink software and practical experimentations using dSPACE platform. The motor drive and load specifications are listed in Table A.1. The obtained results in proposed DTC scheme are compared with existing DTC scheme for highlighting the benefits achieved in proposed DTC scheme. Both DTC schemes are performed with 100 µs sample time. The hysteresis torque and flux bands are maintained at 0.1 Nm and 0.05 Wb for testing both conventional and proposed DTC schemes. The motor operating for the speeds above 500 RPM either in forward or reverse condition are categorized as high speeds. Otherwise, all other motor speeds come under low speed operation category. The simulated and experimental observations are discussed in the following sections below.

3.4.1 Simulation results

The MATLAB/Simulink software is used for executing conventional and proposed DTC schemes for three-level OEWIM drive. The OEWIM drive is mathematically modelled with the motor parameters as given in Table A.1. Dual VSI DC link voltages are kept in 1:1 ratio i.e. both the VSIs are supplied with $E_{dc}/2$ voltage. The net E_{dc} is set to 500 V. Figure 3.8(a) and Figure 3.8(b) indicates steady state performance of OEWIM drive during the control operation of conventional and proposed DTC schemes. The motor reference speeds of 300 RPM and 800 RPM are given to conventional and proposed DTC schemes. The attained steady state condition of motor speed, flux and torque response for conventional and proposed DTC schemes are captured as shown in Figure 3.8. These results represent low and high speed operation of OEWIM drive during no load condition.

From these results, it can be verified that proposed DTC scheme in Figure 3.8(b) exhibits better torque response when related to conventional DTC scheme. This is due to the modified look-up tables (Table 3.3 and Table 3.4) presented in proposed DTC which avoids active reverse VV selection during proposed DTC execution. The average torque ripple is calculated from these simulation results. The average torque ripple is measured by considering sum of the difference between the torque measured and its reference over 20000 samples. At 300 RPM reference speed, the calculated average torque ripple for conventional and proposed DTC are 1.27 Nm and 0.91 Nm. Similarly, at 800 RPM, the calculated average torque ripples are 2.02 Nm and 1.79 Nm for conventional and proposed DTC schemes respectively.

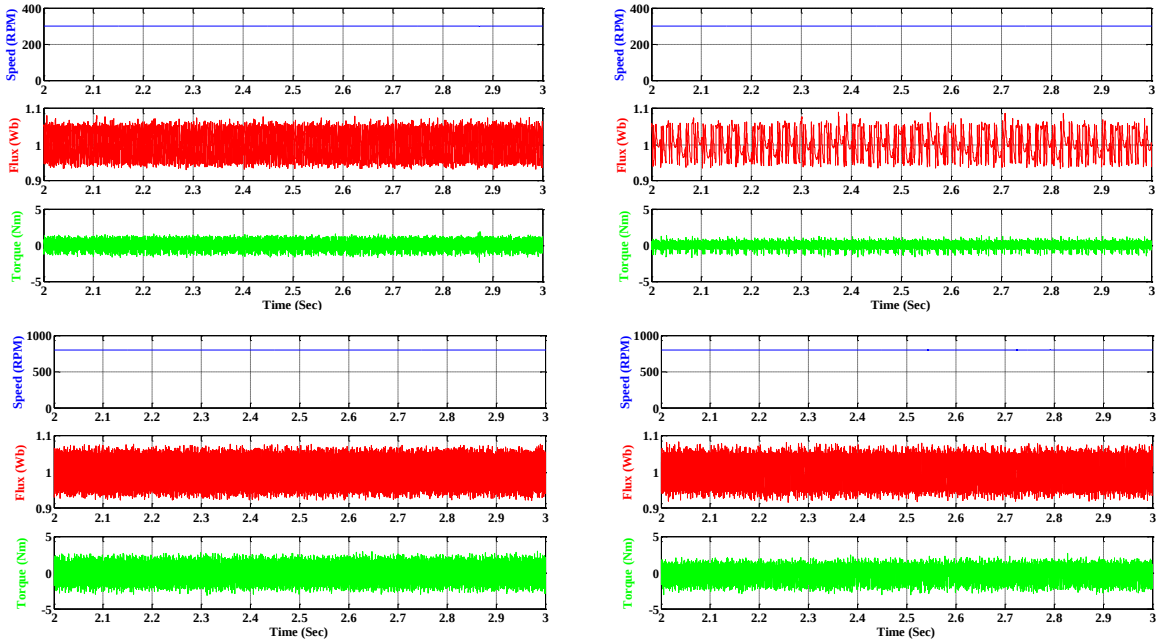

Figure 3.8 OEWIM drive simulated steady-state speed, flux and torque response for low (300 RPM) and high (800 RPM) speeds of operation. (a) Conventional DTC and (b) Proposed DTC

During no load, Figure 3.9(a) and Figure 3.9(b) indicates OEWIM drive speed, flux and torque response under low reference speed step change condition from 300 RPM to 0 RPM. In this operation alone, conventional DTC is operated with H_T band of 2 Nm to observe flux drooping nature at zero speed. In conventional DTC scheme as given in Figure 3.9(a), flux response deteriorated and falls to zero at zero speed condition. This instability in flux response at zero speed is resolved with the modified look-up table and reduced H_T band of 0.1 Nm in proposed DTC scheme, the attained OEWIM drive response is given in Figure 3.9(b). The stable flux response is observed even at zero speed condition as shown in Figure 3.9(b). In Figure 3.9(a), the ripples in torque and flux disappears and falls to zero after the reference speed step change from low to zero. This is due to the prominent occurrence of condition $H_T = 0$ and $H_\Psi = +1$, which selects null VV every time (as from look-up Table 3.2). Therefore, the switching of VVs is absent. In proposed DTC, with the modified look-up table (Table 3.4), the continuous switching of VVs takes place to maintain stable flux as shown in Figure 3.9(b).

The dual inverter switching for conventional and proposed DTC scheme are observed for low (400 RPM) and high (800 RPM) speed operating conditions of OEWIM drive as shown in Figure 3.10(a) and Figure 3.10(b). From Figure 3.10(b), it can be seen that reduction in dual inverter switching transitions for low and high speeds, indicating decrement of average switching frequency for proposed DTC operation. This reduction in switching frequency

response in proposed DTC is due to avoiding reverse active VV selection and utilizing redundant null VV switching states to minimize state transitions from previously applied voltage vector to null voltage vector. The average switching frequency is estimated by counting the total switching state transitions of dual VSI switches of overall 12 over a fixed period of 1 second. The percentage reduction in average switching frequency for proposed DTC with respect to conventional DTC at 400 RPM and 800 RPM is noted as 35.2% and 13.8% respectively.

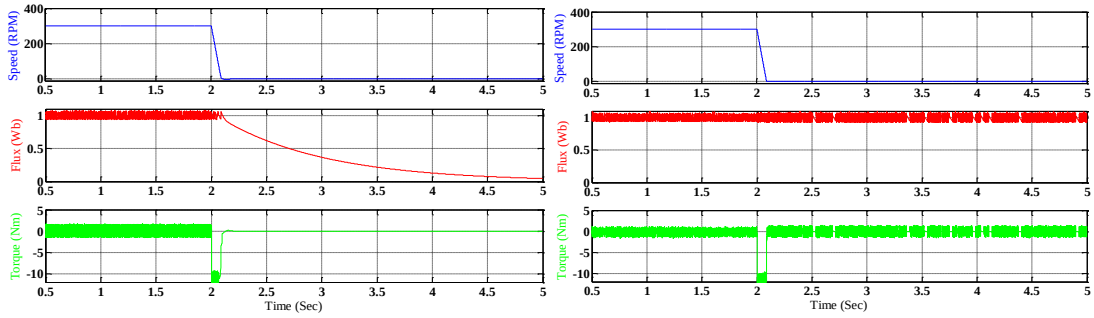

(a) (b)

Figure 3.9 OEWIM drive simulated speed, flux and torque response for reference speed step change from low (300 RPM) to zero. (a) Conventional DTC and (b) Proposed DTC

These simulation results convey primary verification for the proposed DTC scheme and its benefits over conventional DTC scheme such as reduced torque ripples, switching frequency reduction and flux stability at zero speed. Moreover, in depth analysis is performed by conducting various real time experimentations on conventional and proposed DTC scheme for OEWIM drive as followed in section 3.4.2 experimental results.

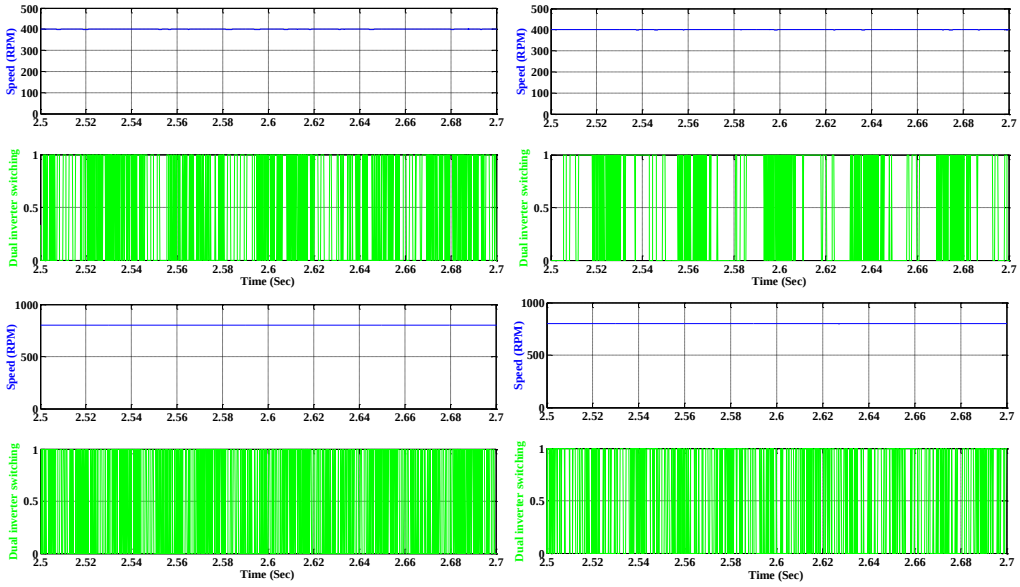

(a) (b)

Figure 3.10 OEWIM drive simulated steady state speed and switching transition response for low (400 RPM) and high (800 RPM) speeds of operation. (a) Conventional DTC and (b) Proposed DTC

3.4.2 Experimental results

The tests for existing and proposed DTC schemes of three level OEWIM drive are conducted on practical setup as shown in Figure A.4. The DC source inputs to the Voltage Source Inverters (VSI-1 and VSI-2) are generated from the two individual three-phase uncontrolled diode bridge rectifier setup. Therefore, both the supplies for VSI-1 and VSI-2 are isolated as shown in Figure 3.1. The MATLAB/Simulink software is interfaced with dSPACE RTI 1104 model in which DTC schemes are implemented. The requirements of DTC operation such as motor speed, phase currents and dual inverter combined DC link voltage are sensed using motor encoder, LA-25 and LV-25 sensors respectively. The motor encoder signal is given to dSPACE incremental encoder channel, LA-25 and LV-25 signals are given to ADC channels which are located on dSPACE control board. The ADC sample frequency is 10 kHz. The speed signal from incremental encoder is filtered with low pass filter having cut-off frequency 10 rad/s. Using dSPACE ControlDesk software, DTC scheme is monitored in real time and several control actions are performed in ControlDesk for changing OEWIM drive speed references. From DTC operation, the obtained optimal switching states are collected at dSPACE control board master bit I/O pins. These optimal switching signals are fed to dual inverter switches.

With this real time OEWIM drive setup, at first steady state analysis is performed for conventional and proposed DTC schemes. The steady state speed, flux and torque response during conventional and proposed DTC operation at no load for the given motor drive reference speeds of 550 RPM and 1000 RPM are presented in Figure 3.11(a) and Figure 3.11(b). The better steady state torque response is observed during the proposed DTC operation of OEWIM drive as shown in Figure 3.11(b). These motor drive operating speeds indicate high speed condition. For testing low speed condition, the motor drive speed reference is set below 500 RPM.

While motor drive in operation at 300 RPM, the observed speed, flux and torque characteristics for conventional and proposed DTC schemes at no load are presented in Figure 3.12(a) and Figure 3.12(b). From these results it can be noted that the decrement in torque ripple for proposed DTC scheme as given in Figure 3.12(b). Therefore, at all the operating speeds the torque response of OEWIM drive is improved for proposed DTC operation when compared to conventional DTC. This is due to the proper VV selection with the modified look-up tables (Table 3.3 and Table 3.4) in proposed DTC operation.

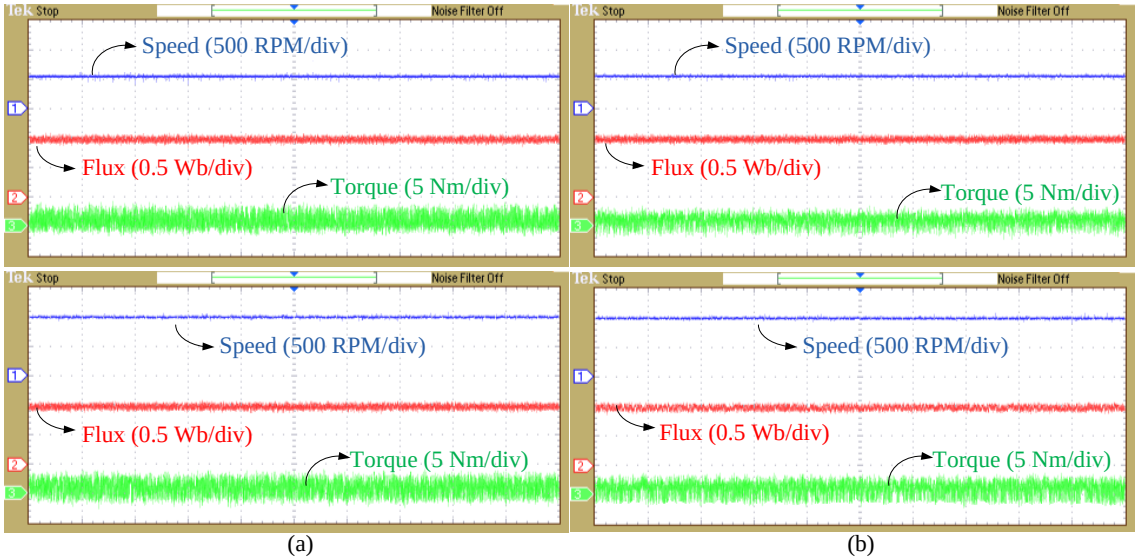

(a) (b)

Figure 3.11 Experimental steady-state speed, flux and torque response for high speed references of 550 RPM and 1000 RPM for OEWIM drive. (a) Conventional DTC and (b) Proposed DTC (Time axis-1 s/div)

Considering the same case of Figure 3.9 i.e. low reference speed step change condition from 300 RPM to 0 RPM, Figure 3.13(a) and Figure 3.13(b) indicates no load OEWIM drive speed, flux and torque response. From Figure 3. 13(a) conventional DTC scheme with the H_T band of 2 Nm, flux response deteriorated and falls to zero at zero speed condition. With the modified look-up table and reduced H_T band of 0.1 Nm in proposed DTC scheme, the instability in flux response is resolved. The attained OEWIM drive response for proposed DTC is given in Figure 3.13(b). From this, stable flux response is observed even at zero speed condition as shown in Figure 3.13(b). In Figure 3.13(a) conventional DTC when speed becomes zero, every time null voltage vector is applied completely with the prominent occurrence of condition $H_T = 0$ and $H_\Psi = +1$ (as from look-up Table 3.2). Therefore, the continuous voltage vector switching is absent. Hence, ripple on flux and torque signal disappears and becomes totally zero. In proposed DTC, with the modified look-up table (Table 3.4), the continuous voltage vector switching is present which avoids flux drooping at zero speed as shown in Figure 3.13(b).

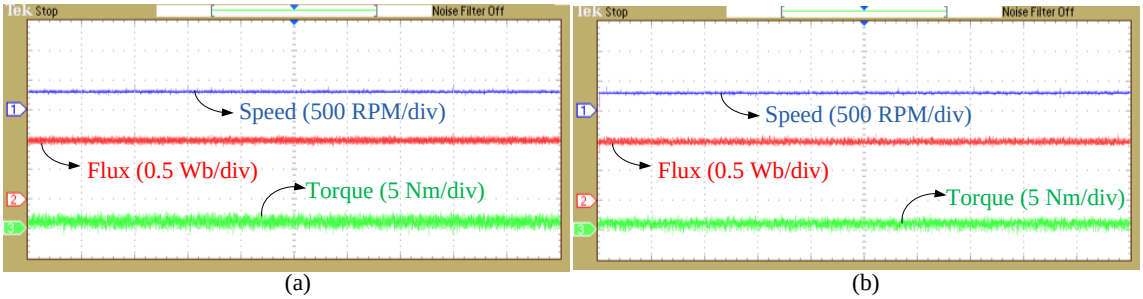

(a) (b)

Figure 3.12 Experimental steady-state speed, flux and torque response for low speed reference of 300 RPM for OEWIM drive. (a) Conventional DTC and (b) Proposed DTC (Time axis-1 s/div)

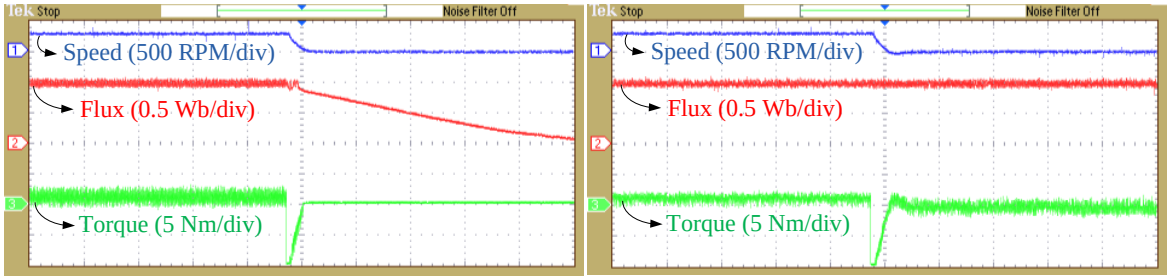

Figure 3.13 OEWIM drive experimental speed, flux and torque response for reference speed step change from low (300 RPM) to zero. (a) Conventional DTC and (b) Proposed DTC (Time axis-1 s/div)

Now the step change in reference speed is considered i.e. 0 to 300 RPM. During this operation, the exhibited motor speed, flux, torque and current response for conventional and proposed DTC scheme are presented in Figure 3.14(a) and Figure 3.14(b). As it is seen from Figure 3.14(a), the conventional DTC lost control over flux at zero speed, it draws huge inrush current the instant when step change in speed is given from zero to 300 RPM. The inrush current is to meet the torque requirement during slow flux build-up process at starting. In proposed DTC scheme, flux is maintained stable even at zero speed and for the step change in reference speed to 300 RPM doesn't effectuate any inrush current as given in Figure 3.14(b). Thus, flux instability issue is addressed in proposed DTC scheme.

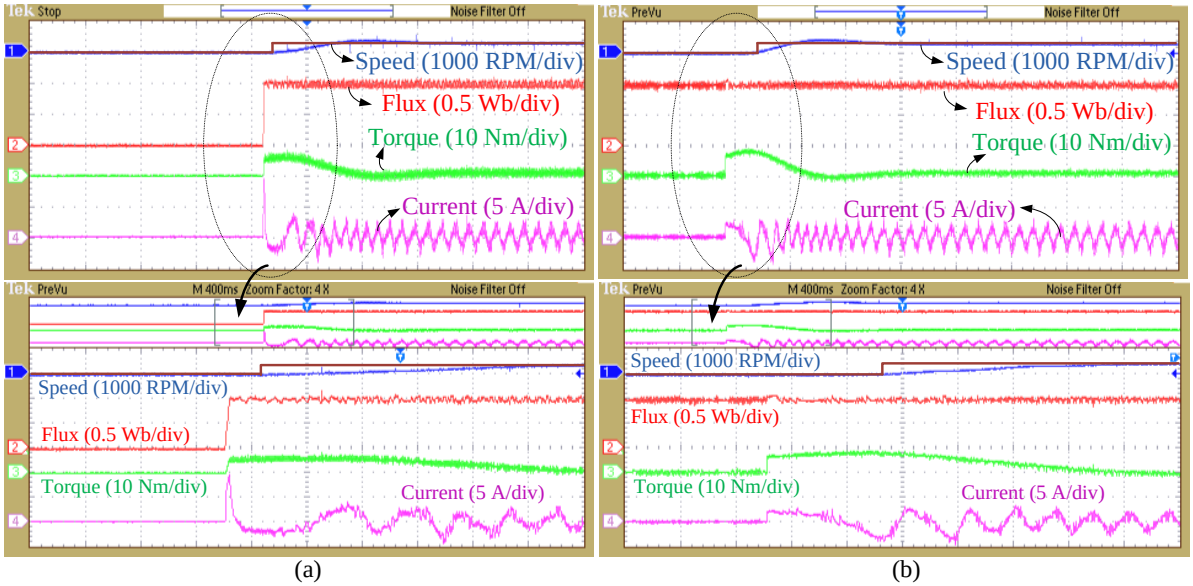

Figure 3.14 Experimental speed, flux, torque and current dynamic response during start-up process. (a) Conventional DTC and (b) Proposed DTC (Time axis-400 ms/div; zoomed time scale-100 ms/div)

In Figure 3.15(a) and Figure 3.15(b), OEWIM drive dynamic response is observed during the operation of conventional and proposed DTC schemes. The reference speed step change in forward direction is performed from low speed to high speed conditions i.e.

300 RPM to 600 RPM and finally 1000 RPM. Both conventional and proposed DTC schemes offer similar dynamic response, but the improved steady state torque characteristics attained for proposed DTC as shown in Figure 3.15(b).

During low and high speed motor drive operation, a forward to reverse reference speed step change is triggered. During low speed forward operation of OEWIM drive at +300 RPM, a reverse reference speed step change is given i.e. -300 RPM. Similarly, for high speed OEWIM drive operations, forward to reverse reference speed step change is given from +600 RPM to -600 RPM. With these OEWIM drive operations, the exhibited motor speed, flux and torque response are captured in Figure 3.16(a) and Figure 3.16(c) for conventional DTC scheme, and Figure 3.16(b) and Figure 3.16(d) for proposed DTC scheme. From these conducted experiments, improved steady state torque response for proposed DTC scheme is observed when related to conventional DTC and the dynamic response for both the conventional and proposed DTC schemes remains the same.

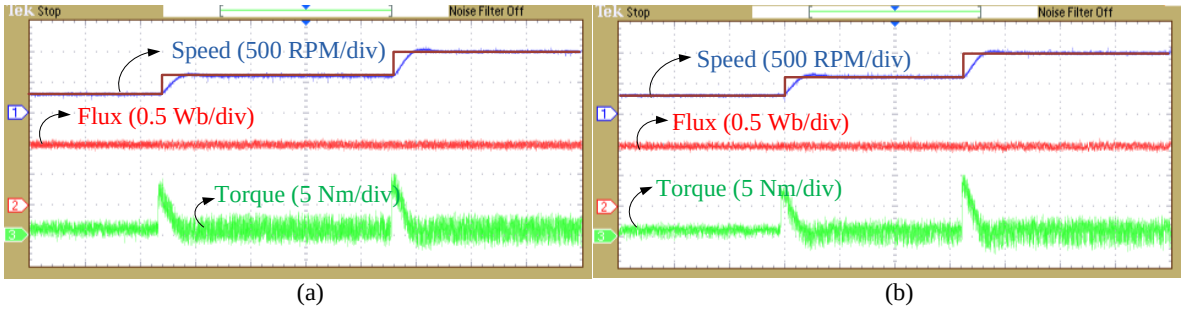

(a) (b)

Figure 3.15 Experimental speed, flux and torque dynamic response for speed reference step change from low to high. (a) Conventional DTC and (b) Proposed DTC (Time axis-1 s/div)

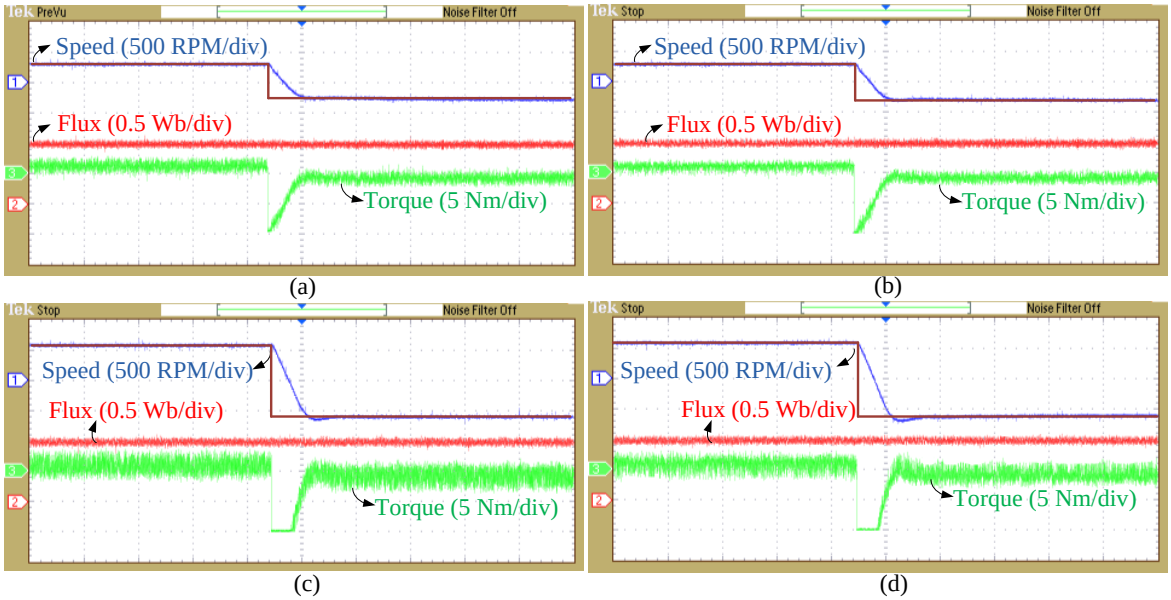

(a) (b)

(c) (d)

Figure 3.16 Experimental speed, flux and torque dynamic response for speed reference step change from forward to reverse. (a, c) Conventional DTC and (b, d) Proposed DTC (Time axis-1 s/div)

In Figure 3.17(a) and Figure 3.17(b), dual inverter switching is observed during high (800 RPM) and low (400 RPM) speed operation of OEWIM drive with conventional and proposed DTC schemes. From Figure 3.17(b), it can be stated that switching transitions are minimized, thereby attaining average switching frequency reduction in proposed DTC operation. The exclusion of reverse active VV selection and utilizing redundant null VV switching states providing minimum state transition from previously applied VV to null VV are the reasons for switching frequency reduction in proposed DTC operation.

Now, the OEWIM drive response under steady state loaded condition and load step change are analysed. For this, OEWIM shaft is coupled with DC generator. By connecting DC generator output to a resistive load bank, electromagnetic load torque is applied on motor shaft. During low (300 RPM) and high (700 RPM) speed motor drive operation, the resistive load bank is switched on, imposing load torque of 50 % of rated motor torque on shaft. After some duration, load torque is made zero by turning off resistive load bank. The OEWIM drive speed, flux, torque and current response during conventional DTC operation is presented in Figure 3.18(a) and Figure 3.19(a). With the same operating circumstances, the OEWIM drive speed, flux, torque and current response with proposed DTC scheme are presented in Figure 3.18(b) and Figure 3.19(b), where the steady state torque response is improved with similar dynamic performance as of conventional DTC scheme.

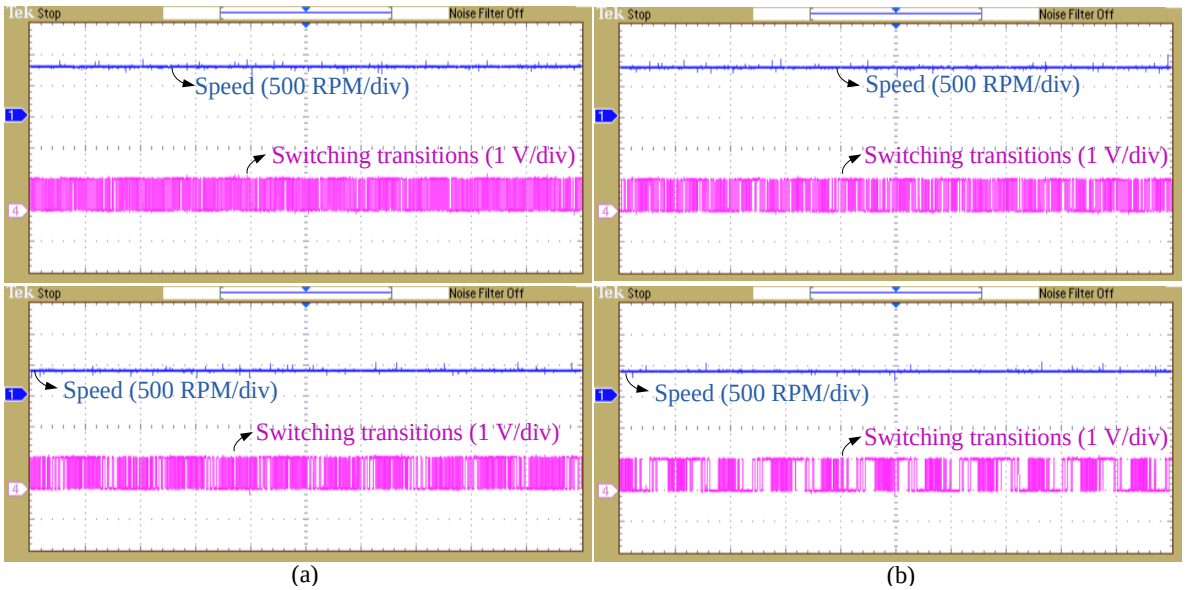

(a) (b)

Figure 3.17 Experimental speed and switching state transitions for high (800 RPM) and low (400 RPM) speed references. (a) Conventional DTC and (b) Proposed DTC (Time axis-40 ms/div)

From these attained results, quantitative analysis is performed at different speed operating conditions as given in Table 3.6 representing average torque ripple and switching frequency for conventional and proposed DTC schemes of OEWIM drive. The average torque ripple is measured by considering sum of the difference between the torque measured and its reference over 20000 samples. Whereas, the average switching frequency is calculated by counting the total switching state transitions of dual VSI switches of overall 12 over a fixed period of 1 second.

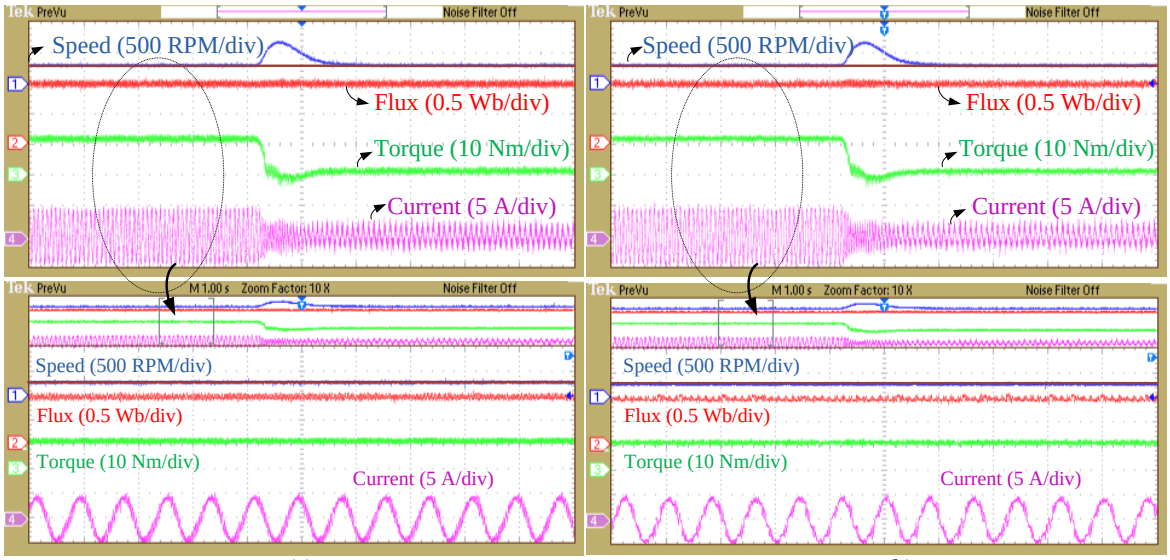

(a) (b)

Figure 3.18 Experimental speed, flux, torque and current response during loaded condition at low (300 RPM) speed reference. (a) Conventional DTC and (b) Proposed DTC (Time axis-1 s/div; zoomed time scale-100 ms/div)

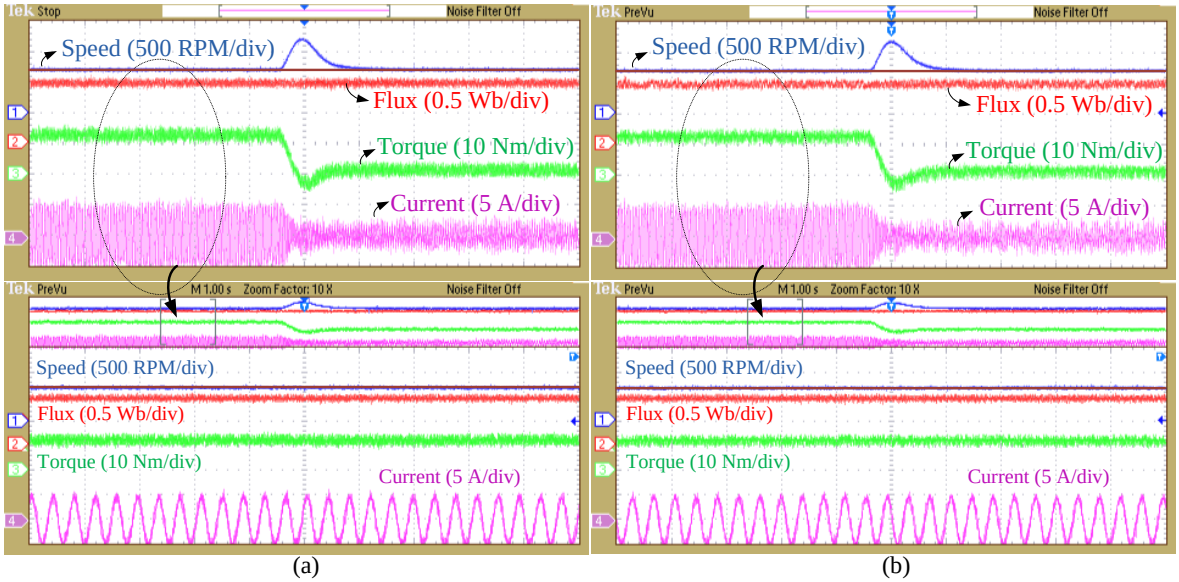

(a) (b)

Figure 3.19 Experimental speed, flux, torque and current response during loaded condition at high (700 RPM) speed reference. (a) Conventional DTC and (b) Proposed DTC (Time axis-1 s/div; zoomed time scale-100 ms/div)

Table 3.6 Real time comparative evaluation of conventional and proposed DTC schemes at various operating conditions

Motor Speed (RPM)	Conventional DTC		Proposed DTC		
	Torque ripple (Nm)	Switching frequency (kHz)	Torque ripple (Nm)	Switching frequency (kHz)	% reduction in switching frequency
300	1.30	1.712	1.01	0.982	42.6
400	1.55	1.457	1.29	0.883	39.3
550	2.01	2.978	1.68	2.250	24.4
800	2.12	2.086	1.81	1.855	11.1
1000	2.25	1.482	1.96	1.275	13.9

From these overall results and discussion, the contributions for proposed DTC are validated in comparison with conventional DTC such as addressing high torque ripples and switching frequency in entire operating speeds (low and high), and flux instability at zero speed in OEWIM drive operation.

3.5 Summary

This chapter presents an enhanced DTC scheme for three-level dual inverter supplied OEWIM drive. The proposed DTC scheme is designed by performing modifications in look-up table for low and high speed conditions, thereby appropriate voltage vector selection is done achieving following benefits: stable flux maintenance at zero speed, torque ripple and switching frequency reduction. Thus, the improved OEWIM drive operation is attained for proposed DTC scheme when related to existing DTC scheme.

To verify the proposed DTC scheme benefits over existing DTC scheme, MATLAB/Simulink and practical tests are performed on OEWIM drive. From these conducted tests and observations, it is proved that proposed DTC exhibits major improvement in OEWIM drive operation and gains the mentioned benefits. Thus, it can be concluded that the proposed DTC scheme is well suited for three-level OEWIM drive operation.

Chapter 4

Enhanced Predictive Torque Control with Auto-Tuning Feature for Induction Motor Drive

Chapter 4

Enhanced Predictive Torque Control with Auto-Tuning Feature for Induction Motor Drive

4.1 Introduction

In earlier chapter, an improved DTC scheme for OEWIM drive is discussed. With the proposed DTC scheme, the problems existing in conventional DTC is solved and torque ripples are minimized to certain extent. However, to establish more accurate control response in DTC, the execution of hysteresis controller requires high sampling frequency. Moreover, the control responses such as flux and torque are dependent on hysteresis boundary conditions and heuristic look-up tables. Now, there is a possibility to improve the motor drive response and further minimising the ripples in torque and flux. This can be achieved with the presence of advanced MPC schemes for the application of motor drives. Among the various divisions in MPC, the thesis concentrates on FCS based MPC. In the field of motor drives, PTC is called as member of FCS MPC scheme. The PTC scheme has notable benefits which are favourable for motor drive application. The features of PTC are direct involvement of multi objectives for intuitive controlling, nonexistence of PWM stage and simple control scheme.

This chapter covers PTC implementation for two-level VSI supplied IM drive. The two-level VSI supplied IM with the possible VV generation is presented in Figure 4.1.

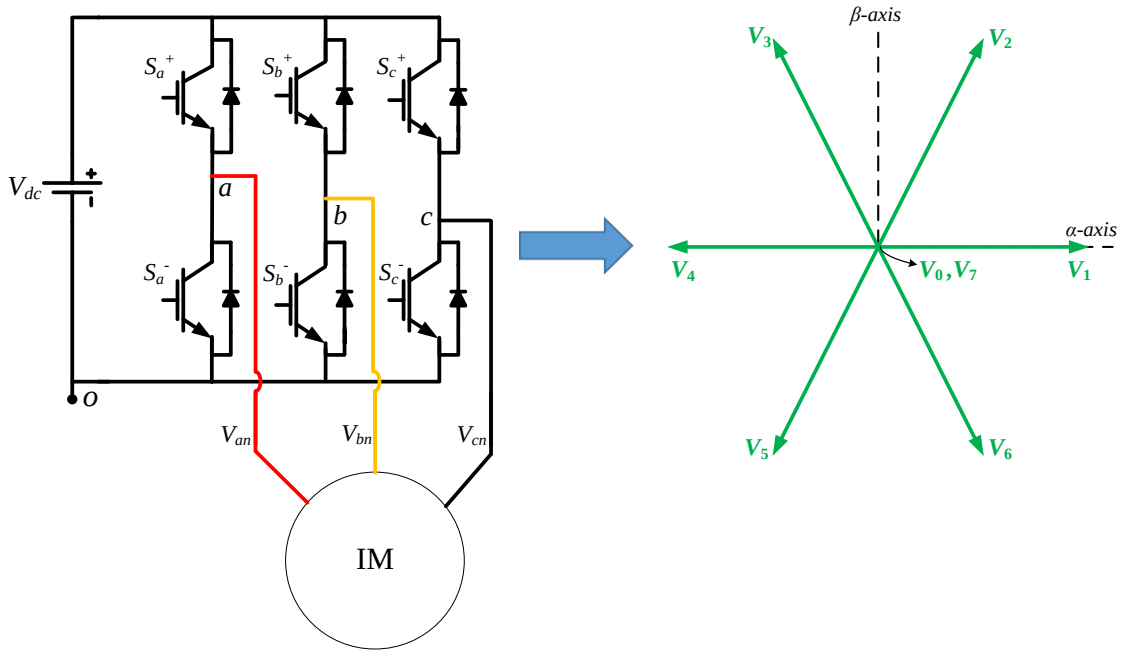

Figure 4.1 Two-level VSI supplied IM with possible VVs generation

The prime steps involved in PTC operation are provided with discrete mathematical analysis. From the literature of PTC in chapter-1, it has been noticed that its operation requires suitable weighting factors choice in cost function for multi objective controlling. The wrong choice of weighting factors has direct influence on control response. Therefore, the choice of weighting factor is considered as one of the main challenges in PTC operation. Several literatures on PTC are presented to solve this issue. This chapter presents an auto tuning based choice of weighting factors. The optimal weight is chosen in online for PTC operation. Thus, desired control response is possible for motor drive operation.

The contents of the chapter are as follows: Explanation of conventional PTC operation for IM drive supplied from two-level VSI in section 4.2, Proposed PTC operation with auto tuning feature in section 4.3, exhibited results in section 4.4 and at the end, summary of the chapter in section 4.5.

4.2 Conventional PTC of IM drive supplied from two-level VSI

Figure 4.2 shows conventional PTC operational block diagram. Torque reference is obtained from speed PI controller. Motor speed (ω_r), measured current (i_s), torque reference (T_{ref}) and flux reference magnitude (λ_s^*) are given to the PTC algorithm for controlling purpose and generation of switching pulses for VSI supplying to IM drive. PTC algorithm contains mathematical model of system in discrete form. The state variable representation of stator current and flux for an IM in stationary reference frame are given as (2.27) -(2.28) in chapter-2. Based on these equations, discretization of IM mathematical model is done using Euler's method. Its basic representations are given as (2.29) and (2.30) in chapter-2. The working of PTC algorithm is established on three key stages. The following of them are discussed below:

4.2.1 Measurements

At first stage, the required measurements for PTC operation are motor speed, DC link voltage supplying to VSI, generated stator flux and current space vector. Among these variables, direct measurable quantities are motor speed, DC link voltage and stator currents. The sensed motor speed and DC link voltage (V_{dc}) are directly fed to PTC algorithm. The stator current space vector measurement is as follows:

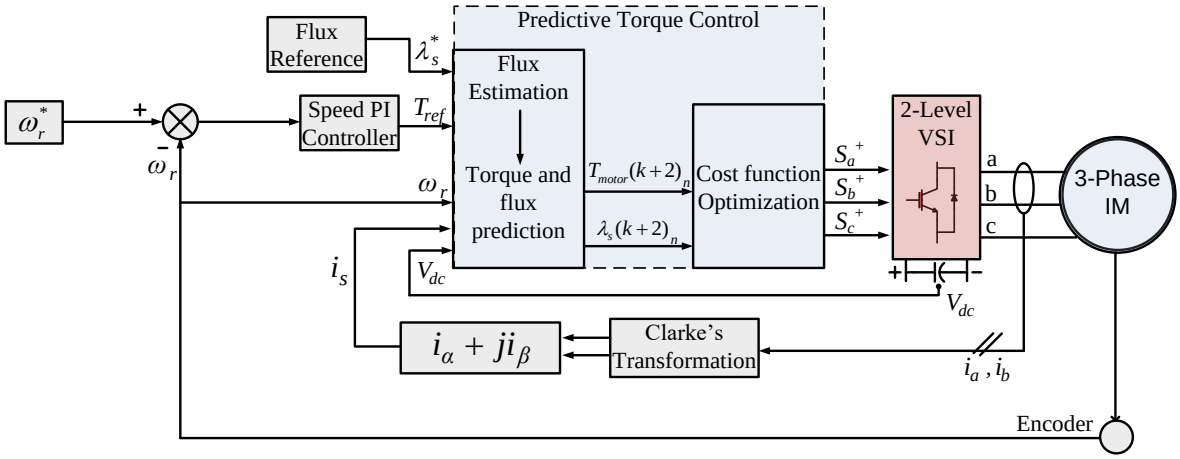

Figure 4.2 Conventional PTC for IM drive fed by two-level VSI

(a) Stator current (i_s) measurement

Stator currents can be directly measured from motor phases. The measured currents i_a, i_b and i_c (= -(i_a + i_b); balanced three phase load) through motor *a*, *b*, *c* phases are converted to i_α and i_β using Clarke's transformation (as discussed in Chapter-2). From this, generated current space vector ($i_s = i_\alpha + \mathrm{j}\, i_\beta$) is obtained.

(b) Stator flux (λ_s) estimation

Machine stator flux cannot be measured directly. Therefore, by using Euler mathematical analysis, stator flux (λ_s) has to be estimated. Considering stator voltage space vector equation (2.28) from Chapter-2, the stator flux at present state (*k*) can be estimated using previous (*k*-1) sample instant data as,

$$\lambda_s(k) = \lambda_s(k-1) + V_s T_s - A T_s i_s \tag{4.1}$$

where, V_s belongs to voltage space vector applied in previous sample state and T_s is sample time.

4.2.2 Predictions

After gaining the knowledge of required variables at first stage, the second stage follows, that is prediction of stator flux, current and torque. Prediction is done for all the available switching vectors relating to a given inverter. For a 2-level VSI, there are '8' possible switching vectors as given in Table 2.1 in stationary reference frame in Chapter-2. Their locations in α-β plane are also presented in Figure 4.1. Using the information of present state variables (flux and current), the possible future predictions at one step ahead for stator

flux, current and torque with all 8 prediction VVs are calculated. The computation of stator flux, current and torque predictions are as follows:

Stator flux prediction: $(\lambda_s(k+1))_n = \lambda_s(k) + T_s((V_s)_n - Ai_s(k))$ (4.2)

Stator current prediction:

$$i_s(k+1)_n = i_s(k) + T_s\left(A_1\left(\begin{matrix} A_2\lambda_s(k) - A_3 i_s(k) + K_r\left((V_s)_n - Ai_s(k) - j\omega_r\lambda_s(k)\right) \\ + \dfrac{j\omega_r i_s(k)}{A_1} \end{matrix} \right) \right)$$

(4.3)

Finally, the motor torque prediction using (4.2) and (4.3) as,

$$(T_{motor}(k+1))_n = \frac{3}{2}\frac{P}{2}\left(\text{imag}\left(\bar{\lambda}_s(k+1)_n i_s(k+1)_n\right)\right) \quad (4.4)$$

In the above discretized prediction equations, the subscript *n* indicates VV number i.e. zero to 7. Moreover, the represented constants in (4.1) – (4.3) are noted as below.

$A = R_s$, $A_1 = \dfrac{L_m}{L_s L_r - {L_m}^2}$, $A_2 = \dfrac{R_r}{L_m}$, $A_3 = \dfrac{L_s R_r}{L_m}$, $K_r = \dfrac{L_r}{L_m}$

4.2.3 Cost function assessment

Cost function is composed of multi-objective terms which have to be controlled. For all the switching states, predicted values of control parameters are compared with their reference values. The switching state which realizes predicted value closeness to reference value is selected as optimum. The basic representation of cost function with two control objectives (torque and flux) can be given as follows,

$$G_n = \left|T_{ref} - T_{motor}(k+1)_n\right| + W\left|\lambda_s^* - \left|\lambda_s(k+1)_n\right|\right| \quad (4.5)$$

Where, *W* is the flux weighting factor which signifies importance between torque and stator flux control objectives comparatively. The terms T_{ref} represents reference torque generated by speed PI controller and λ_s^* is the reference stator flux magnitude.

The above equations of torque, current and flux predictions (4.2)- (4.4) represents one step ahead. Owing to the practical sample delay problems in the PTC algorithm, two step ahead prediction (*k*+2) is preferred. The modified prediction equations can be expressed as,

$$(\lambda_s(k+2))_n = \lambda_s(k+1) + T_s((Vs)_n - Ai_s(k+1)) \quad (4.6)$$

$$i_s(k+2)_n = i_s(k+1) + T_s\left(A_1\left(\begin{array}{l} A_2\lambda_s(k+1) - A_3 i_s(k+1) + K_r\left((V_s)_n - A i_s(k+1) - j\omega_r\lambda_s(k+1)\right) \\ + \dfrac{j\omega_r i_s(k+1)}{A_1} \end{array} \right) \right) \tag{4.7}$$

$$(T_{motor}(k+2))_n = \frac{3}{2}\frac{P}{2}\left(\text{imag}\left(\bar{\lambda}_s(k+2)_n i_s(k+2)_n\right)\right) \tag{4.8}$$

With the obtained two step predicted torque and flux (4.6) - (4.8), cost function can be reformulated and is given by (4.9),

$$G_n = \left|T_{ref} - T_{motor}(k+2)_n\right| + W\left|\lambda_s^{\,*} - \left|\lambda_s(k+2)_n\right|\right| \tag{4.9}$$

In (4.9), weighting factor is pointed as the ratio of nominal values of motor torque and flux. It is represented as,

$$W = \frac{T_{nom}}{\lambda_{nom}} \tag{4.10}$$

However, this value of weighting factor (*W*) is considered only at initial point of time and it may vary in real time implementation for proper tuning.

4.3 Proposed PTC of IM drive

The paramount steps in PTC are: 1. Measurement and estimation of unknown variables, 2. Prediction of system behaviour and 3. Output optimization based on cost function minimization. Owing to the multiple control objectives in single cost function (toque and flux), weighting factor has direct impact on selection of optimal voltage vector and thereby control performance of motor drive. Figure 4.3 represents block diagram of proposed PTC for IM drive fed by 2-level VSI. In this, weighting factor is tuned to an optimum value for every sampling time. This tuned value of weighting factor is applied in cost function to obtain optimal control response. The view of the control process is shown in Figure 4.4.

Consider an objective function (flux) for which the weighting factor is assigned. From cost function (4.9) it is given as,

$$K = \left|\lambda_s^{\,*} - \left|\lambda_s(k+2)_n\right|\right| \tag{4.11}$$

For all '8' switching states, '*K*' is computed and minimum of '*K*' value is selected. Variables 'p_1' and 'p_2' are selected as considerably small numbers to minimize torque and flux ripples. Here, 'p_1' value is set to 0.05 m which is maximum permissible flux ripple and

'p_2' value is set to 5 which is multiplication factor for flux weighting factor (W_{opt}). If the minimum value of 'K' is less than or equal to 'p_1', optimal weighting factor is selected as (4.13). It indicates that the flux response is in permissible level while increasing the contribution of torque control objective in cost function, thereby reduction in torque ripple.

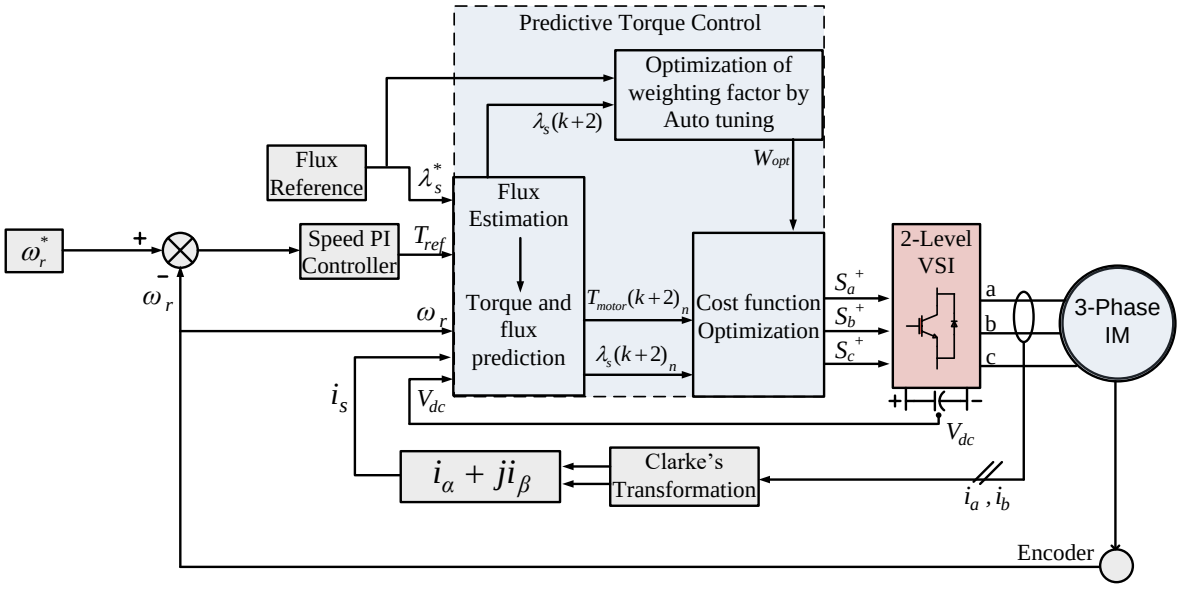

Figure 4.3 Block diagram of proposed PTC

$$\text{Minimum } (K) <= p_1 \tag{4.12}$$

$$W_{opt} = p_2 \tag{4.13}$$

If the above condition (4.12) is not satisfied, it implies that flux ripple is more. Then it checks for the condition (4.14).

$$\text{Minimum } (K) <= mp_1 \tag{4.14}$$

If this condition (4.14) is satisfied, then optimal weighting factor is set to,

$$W_{opt} = mp_2 \tag{4.15}$$

In the above terms, 'm' belongs to natural numbers set (N). In this auto-tuning process, natural number set is considered till the value of 15. As the value of 'p_2' is set to 5, the maximum tuned weighting factor value is 75.

It means that, if the flux control objective function minimum value does not satisfy the stipulation (4.12), it checks the condition (4.14) for every value of N. With the satisfaction of condition (4.14), weighting factor increases its magnitude by multiplying 'm' times with 'p_2' as given in (4.15). Therefore, increase in the value of W_{opt} results in increasing the contribution

of flux control objective in cost function and thereby reduction in flux ripple. The optimum value of weighting factor (W_{opt}) is substituted in cost function as shown in (4.16).

$$G_n = \left|T_{ref} - T_{motor}(k+2)_n\right| + W_{opt}\left|\lambda_s^{*} - \left|\lambda_s(k+2)_n\right|\right| \tag{4.16}$$

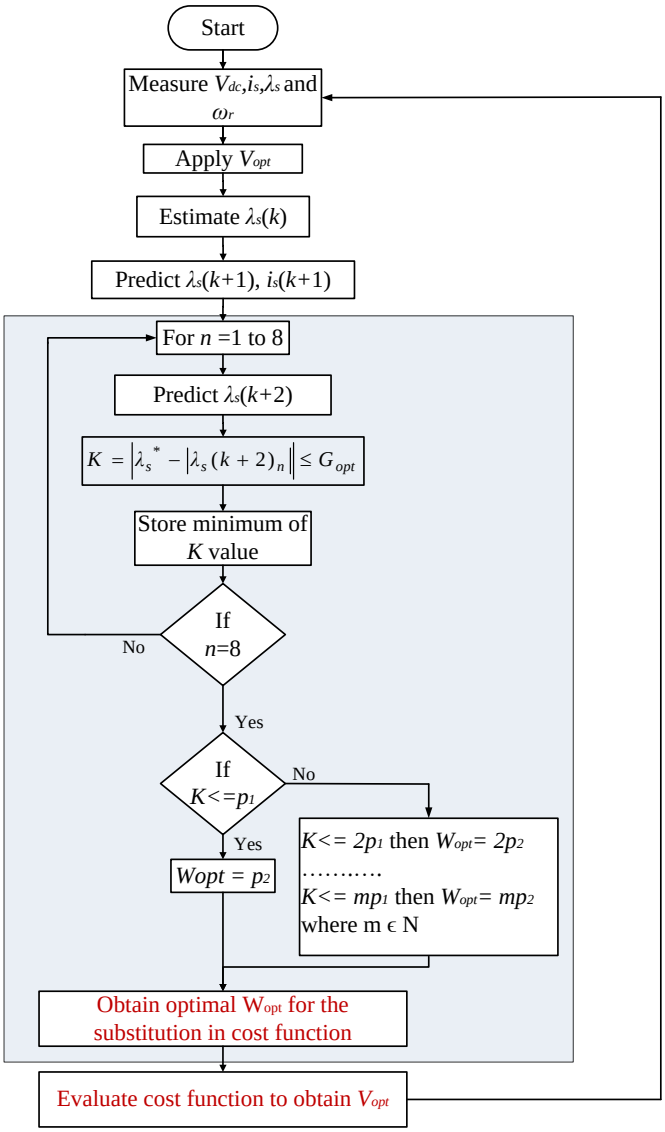

Figure 4.4 Proposed PTC flowchart

This process repeats for every sample interval. With this system, optimization is done online and optimal value of W_{opt} is selected in every sample period based on flux control objective. The modified cost function with the optimized tuned weight is given by (4.16) and it is assessed for all 8 switching states of inverter. The switching state providing minimum cost function value is selected for switching in next sample interval. This auto-tuning feature helps in the selection of optimal voltage vector (V_{opt}) to enhance the motor torque and flux response achieving minimum torque and flux ripples.

4.4 Results and discussion

To verify the proposed control strategy as shown in Figure 4.3, IM is modelled using mathematical equations (as presented in Chapter-2) in MATLAB/Simulink environment. The real time machine parameters are tabulated as shown in Table A.1. To compare the effectiveness of proposed model, both conventional and proposed PTC are performed on IM drive. Simulations are configured with the sampling time of 50 μs. Inverter DC link voltage is considered as 540 V. The machine flux reference magnitude is set to 1 Wb. For comparing proposed PTC simulation results with the conventional, a conventional weighting factor is selected empirically in conventional PTC. While in the proposed PTC of IM drive, optimum weighting factor is selected in every sampling interval automatically with the incorporation of auto tuning feature.

4.4.1 Simulation results

At first steady state behaviour of machine is analysed for proposed PTC in comparison with the conventional model. Figure 4.5 illustrates the steady state behaviour of machine at reference electrical speed of 200 rad/s till the simulation time of 3 s exhibiting forward motoring operation. A step change in reference speed of -200 rad/s is triggered at the time instant of 3 s. Thus, motor exhibited dynamic characteristics from the instant of 3 s to 3.25 s is analysed. After the time instant of 3.25 s, motor starts rotating in reverse direction, thus exhibiting steady state reverse motoring characteristics.

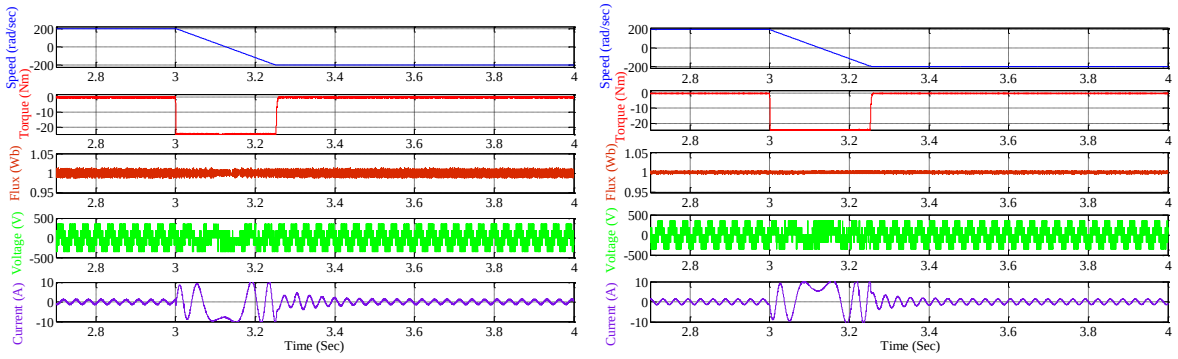

Figure 4.5 Motor Speed, torque, flux, phase voltage and current characteristics. (a) Conventional PTC of IM drive and (b) Proposed PTC of IM drive

Figure 4.5 represents the characteristics of motor speed, torque, flux, phase voltage and current under various operating conditions of reference speeds at no-load. From these results, it is conveyed that the proposed PTC of IM drive exhibits optimal steady state torque

and flux response when compared with the conventional PTC scheme. Both these schemes exhibit similar dynamic response during the step change in motor reference speed. Now the IM drive is operated at the rated reference electrical speed (301 rad/s) and full load torque (24.5 Nm) conditions. The exhibited motor speed, torque and flux steady state characteristics are shown in Figure 4.6.

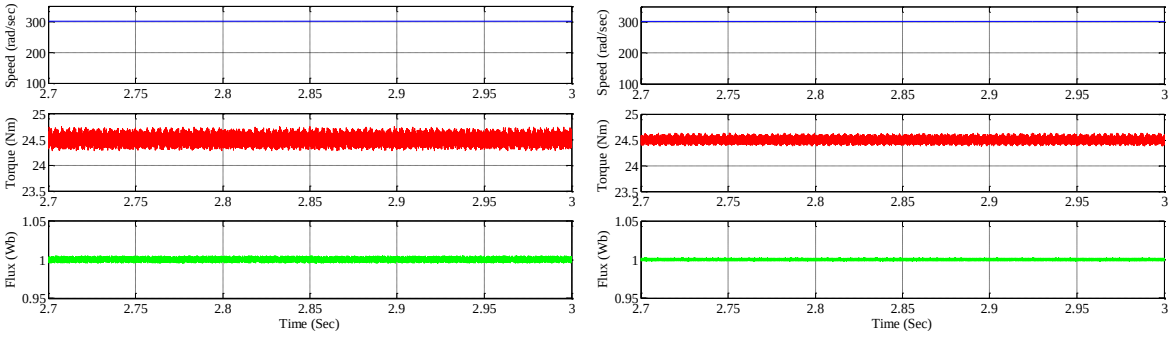

Figure 4.6 Motor Speed, torque and flux steady state characteristics. (a) Conventional PTC of IM drive and (b) Proposed PTC of IM drive

From all the above results, it is evident that the online based optimization of weighting factor in proposed PTC results in overall better performance of motor torque and flux in comparison with the conventional PTC of IM drive.

4.4.2 Experimental results

To validate the proposed PTC of IM drive practically, experimentation is performed on 5 HP, 1440 RPM IM drive fed by two-level VSI. The machine parameters are displayed in Table A.1. The experimental test rig of IM drive is presented in Figure A.3. The proposed PTC algorithm is programmed in dSPACE (RTI 1104) platform with the sampling time of 50 µs. The motor speed is measured using Encoder and interfaced to dSPACE incremental encoder. The IM drive phase currents and DC link voltage are measured using current sensors (LA-25) and voltage sensor (LV-25) respectively. Thus, the required measurements are sensed and fed to predictive control algorithm with the help of dSPACE ADC BNC connectors. Based on the cost function minimization, switching pulses are generated for the two-level VSI. These pulses are collected from the digital I/O connectors of dSPACE controller board and interfaced to inverter switches.

Experimental results of proposed PTC are exhibited in Figures (4.7)- (4.13) in comparison with the conventional PTC of IM drive, to validate its effectiveness. The steady state motor speed, torque, phase voltage and current characteristics under the reference speed

of 250 rad/s and load torque of 14 Nm are exhibited in Figure 4.7. It is observed that the motor torque response is improved for the proposed PTC in comparison with the conventional scheme. In conventional PTC, with the adjustment of weighting factor by trial and error method, better results can be obtained, where as in proposed PTC, weighting factor is auto tuned and optimal value is selected for the better control response of IM drive.

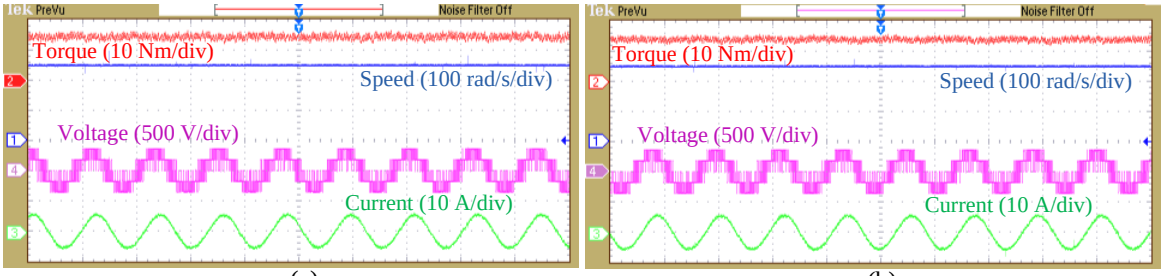

(a) (b)

Figure 4.7 Steady state motor speed, torque, current and voltage for reference speed 250 rad/s and load torque 14 Nm. (a) Conventional PTC (b) Proposed PTC (X-axis time scale – 20 ms/div)

To analyse the motor response for step changes in reference speed, dSPACE ControlDesk software is used for the provision of instant step changes in motor reference speed. To verify the dynamic response of IM drive, step change in reference speed of IM is set from 150-200 rad/s and then 200-250 rad/s at no load. Its related motor speed, torque and flux characteristics are shown in Figure 4.8(a) and 4.8(b) for the conventional and proposed PTC of IM drive respectively. These results represent forward motoring. The same can be verified in reverse motoring i.e. from -150 to -200 rad/s and then -200 to -250 rad/s. Its respective motor speed, torque and flux characteristics are shown in Figure 4.8(c) and 4.8(d) for the conventional and proposed PTC of IM drive respectively. From these results it can be verified that the proposed PTC of IM drive exhibits better steady state torque and flux response having low ripples when compared to conventional scheme.

A step change in reference speed is given from forward motoring at 200 rad/s to reverse motoring at -200 rad/s. The response of torque, flux, and motor phase current along with its speed are shown in Figure 4.9(a) and 4.9(b) for the conventional and proposed PTC of IM drive respectively.

From these results, it can be observed that both of the schemes of IM drive exhibits similar dynamic characteristics with improved steady state performance in proposed scheme. To examine the performance of conventional and proposed PTC of IM drive under load variation conditions, IM is coupled to DC generator. By loading DC generator with a resistive load bank, step changes in motor load torque is performed while motor is operating at speed

of 200 rad/s. Its motor speed, torque, current and flux characteristics are shown in Figure 4.10 (a) and 4.10 (b) for the conventional and proposed PTC of IM drive for step change in load torque from no load to 12.25 Nm (50% load).

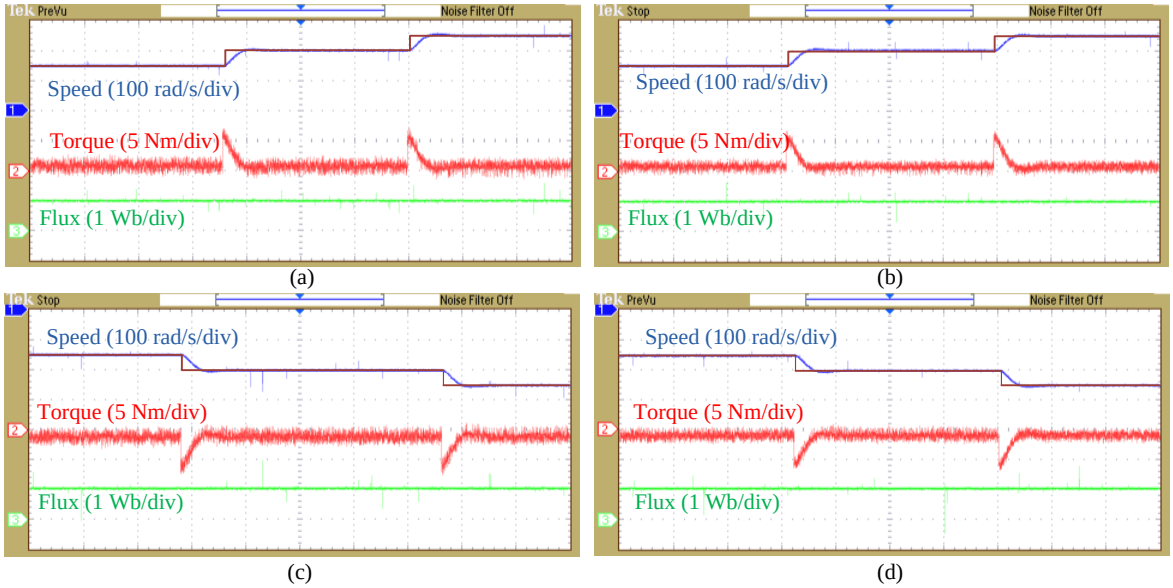

Figure 4.8 Motor speed, torque and flux characteristics with change in reference speed. For forward motoring (a) in Conventional PTC and (b) in Proposed PTC. For reverse motoring (c) in Conventional PTC and (d) in Proposed PTC (X-axis time scale – 1 s/div)

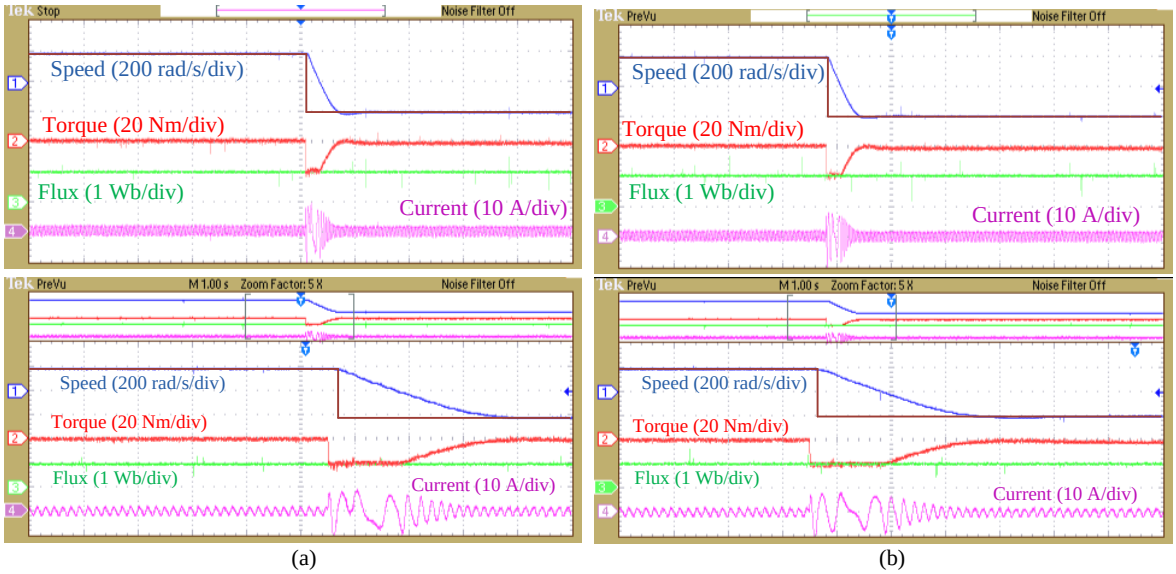

Figure 4.9 Motor speed, torque, flux and current characteristics with change in reference speed from forward to reverse. (a) in Conventional PTC and (b) in Proposed PTC (X-axis time scale – 1 s/div; zoomed time scale– 200 ms/div)

Figure 4.10(c) and 4.10(d) represents motor steady state speed, torque, current and flux characteristics at 50% of motor load torque for the conventional and proposed PTC of IM drive. These results convey improved steady state performance of motor torque and flux for the proposed PTC. Both of these results convey similar dynamic response. Finally, testing

is done for conventional and proposed PTC of IM drive at rated electrical speed (301 rad/s) and full load torque (24.5 Nm) condition. Its results are shown in Figure 4.11.

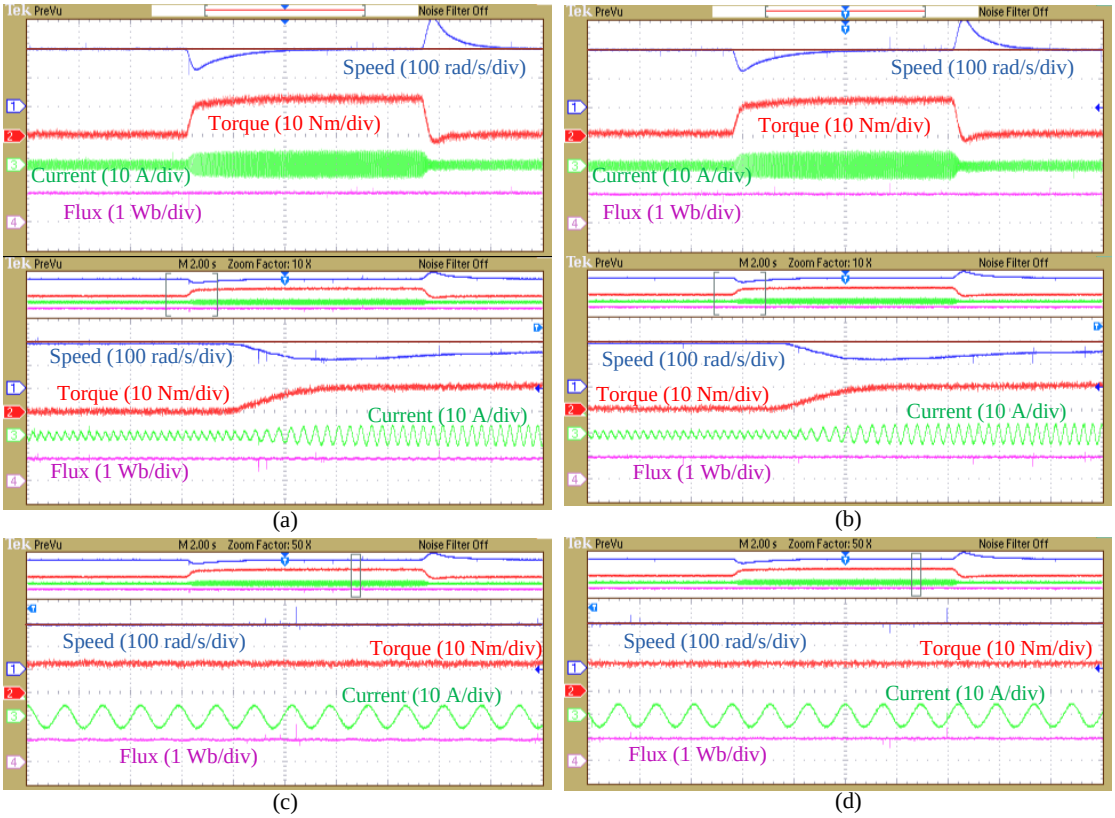

Figure 4.10 Motor speed, torque, flux and current characteristics with step changes in load torque. (a) and (c) Conventional PTC, (b) and (d) Proposed PTC (X-axis time scale – 2 s/div; zoomed time scale (a, b)– 200 ms/div; zoomed time scale (c, d)– 40 ms/div)

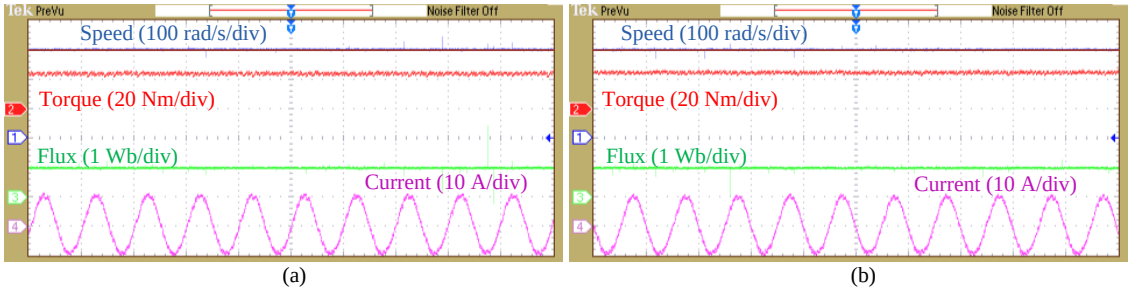

Figure 4.11 Motor speed, torque, flux and current characteristics. (a) Conventional PTC and (b) Proposed PTC (X-axis time scale – 20 ms/div)

The response of IM drive supplied from two-level VSI is checked against DTC and PTC schemes also. From Figure 4.12, it has been observed that PTC schemes are exhibiting good steady state performance of torque and flux for various operating speeds.

The motor torque and flux are measured for 125000 samples. From the above conducted results of conventional and proposed PTC of IM drive, the average torque and flux ripples are evaluated considering the sum of the difference between the measured and

reference values over 125000 samples. The comparison table is prepared to show the effectiveness of proposed PTC over conventional PTC and DTC scheme of IM drive and are listed in Table 4.1. The characteristics of weighting factor tuning in proposed PTC for the electrical speeds 140 rad/s (mechanical – 668.4 RPM) and 210 rad/s (mechanical – 1002.6 RPM) are shown in Figure 4.13. The weighting factor tuning in each sample interval is observed till the value of 75.

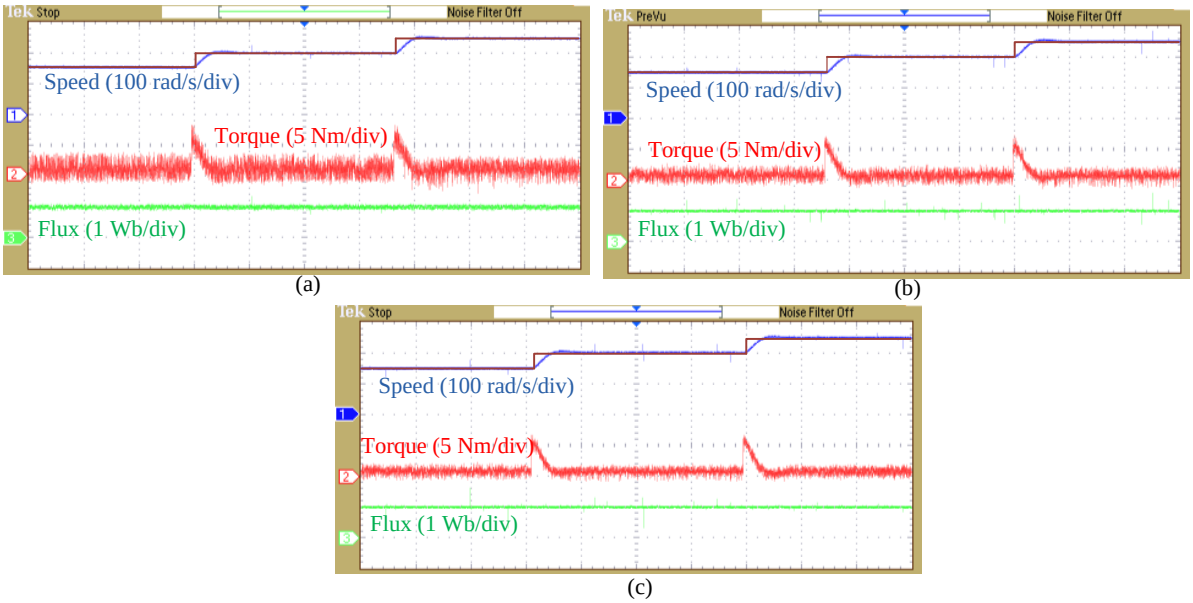

Figure 4.12 IM drive response for step changes of speed (150 rad/s – 200 rad/s – 250 rad/s). (a) DTC technique, (b) Conventional PTC technique and (c) Proposed PTC technique (X-axis time scale – 1 s/div)

Table 4.1 Comparison table under various operating conditions of speed

Control scheme	Speed (electrical)	Torque ripple (Nm)	Flux ripple (Wb)
DTC	150 rad/s	2.58	0.064
Conventional PTC		1.52	0.032
Proposed PTC		1.44	0.029
DTC	200 rad/s	2.45	0.058
Conventional PTC		1.501	0.028
Proposed PTC		1.42	0.026
DTC	250 rad/s	2.32	0.044
Conventional PTC		1.48	0.024
Proposed PTC		1.40	0.022

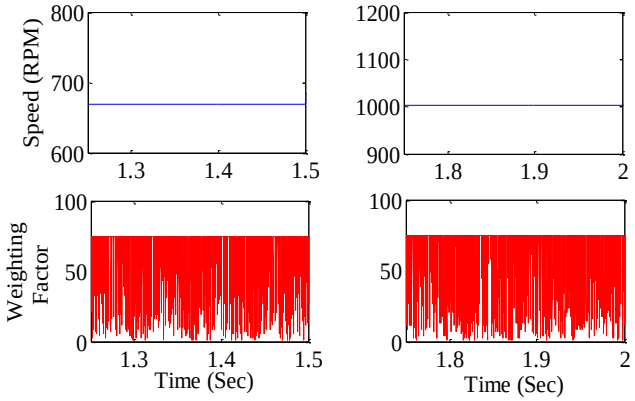

Figure 4.13 Weighting factor tuning

The average computation time for the conventional PTC is 20.25 µs and for the proposed PTC with the involvement of auto-tuning feature, the computation time increased to 28.5 µs. However, it is a good solution for better response of motor drive because the weighting factor is auto-tuned and leads to optimal control response. Finally, it is validated that the auto tuning of flux weighting factor (W_{opt}) facilitates an improved steady state performance of torque and flux of IM drive while implementing the proposed PTC.

4.5 Summary

The selection of weighting factor and its adjustment is the main challenge in PTC execution. This chapter presents an auto tuning based weighting factor selection for IM drive fed by two-level VSI. The proposed feature enables optimization of weighting factor in every sampling time. This optimization is based on minimization of control objective function. The cost function is formulated with the optimized weighting factor and optimal switching states are selected while minimizing the cost function.

The proposed PTC strategy is verified with the both simulation and experimentation on IM drive. The obtained steady state motor torque and flux characteristics under various operating conditions demonstrates the improved performance of IM drive without any manual tuning as in the case of conventional PTC. In addition, the proposed PTC exhibits similar dynamic characteristics to that of conventional scheme. Finally, an effective and simple application of torque and flux control of IM drive with the proposed PTC scheme is possible.

Chapter 5

Enhanced Predictive Torque Control for Open End Winding Induction Motor Drive without Weighting Factor Assignment

Chapter 5

Enhanced Predictive Torque Control for Open End Winding Induction Motor Drive without Weighting Factor Assignment

5.1 Introduction

In earlier chapter, PTC implementation and its superior control response over DTC are discussed. Besides this, modifications are incorporated in basic PTC by applying auto tuning of flux weighting factor to improve further its control response to drive IM. However, the extra auto tuning algorithm is getting added for PTC operation. Moreover, the tuned set of weighting values are limited. In this chapter, flux weighting factor independent operation is attained using modified cost function, where the single control objective is framed to replace two individual flux and torque control objectives. Thus, omitting flux weighting factor and performing PTC operation with modified cost function. The basic PTC operation exhibit variable switching frequency without any limitation on it. Thereby, switching frequency could be higher during PTC operation. The limitation on switching frequency can be imposed by adding additional control objective to the existing ones in cost function. However, the addition cannot be direct, since the control objectives are different. Therefore, it has to be weighted sum. The placement of switching frequency weighting factor again in cost function and its fine adjustment has direct influence on overall control response of motor drive. To obviate tedious tuning of this weighting factor, ranking analysis is used. Therefore, complete weighting factor independent PTC operation is gained in this chapter.

In earlier chapter, PTC is applied for IM drive fed by two-level VSI. However, for medium and high power application, the use of multilevel VSI is appropriate for several reasons. With the developments in digital field, PTC started its application for motor drives supplying from multilevel VSI. This thesis concentrates on dual VSI model, owing to its favourable benefits. The dual VSI model supplying to OEWIM is presented in Figure 5.1(a). In this chapter, dual VSI is functioned in four-level mode, where the DC link voltages V_{dc1} of VSI-1 and V_{dc2} of VSI-2 are $2V_{dc}/3$ and $V_{dc}/3$ correspondingly. The detailed view of this scenario for obtaining DC supply for OEWIM drive is provided in Appendix-A, Figure A.2. During this mode of operation, the generated effective VVs are also presented in Figure 5.1. From Figure 5.1(b), by four-level dual VSI functioning, it has been taken notice of overall 37

effective VVs (36 active VVs + 1 null VV). These are named as prediction VVs in PTC operation.

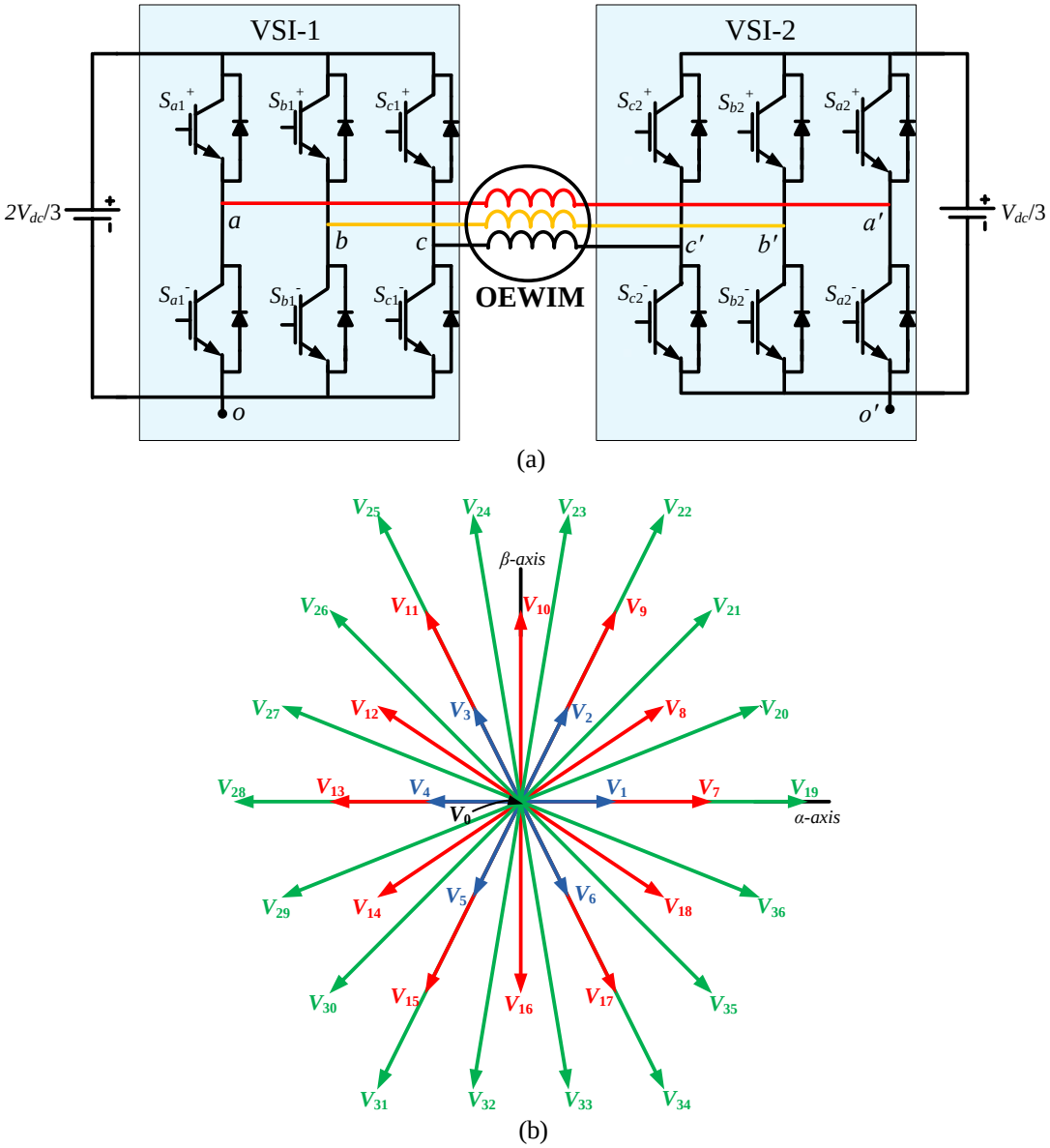

Figure 5.1 (a) Four-level dual VSI supplied OEWIM and (b) possible VVs generation

The participation of all these prediction VVs in PTC operation impose computational burden. Therefore, PTC operation for four-level dual VSI supplied OEWIM drive becomes complex. In this chapter, the prediction VVs of dual VSI are reduced, so that minimizing the computational burden for PTC operation. The objectives of the work for PTC of OEWIM drive supplied from four-level dual VSI are as follows: 1. Permitting PTC operation independent from weighting factors, 2. Reduce the complexity of control algorithm by limiting the prediction VVs, 3. Exhibiting better torque and flux response and 4. Switching frequency limitation. The chapter coordination is as follows: Section 5.2 discusses the

operation of conventional PTC for OEWIM drive supplied from four-level dual VSI. In section 5.3, four-level dual VSI supplied OEWIM drive operation using proposed PTC is explained. The conducted simulation and experimentations, their exhibited results are discussed in section 5.4. Finally, the chapter summary is provided in section 5.5.

5.2 Conventional PTC of four-level dual VSI supplied OEWIM drive

The required inputs for conventional PTC implementation of OEWIM drive are: motor speed (ω_r), stator current (i_s), combined DC link voltage (V_{dc}), reference torque (T_m^*- generated from speed PI controller) and reference flux magnitude (λ_s^*). Its operational block diagram is shown in Figure 5.2. The main steps engaged in PTC of OEWIM drive are explained as follows:

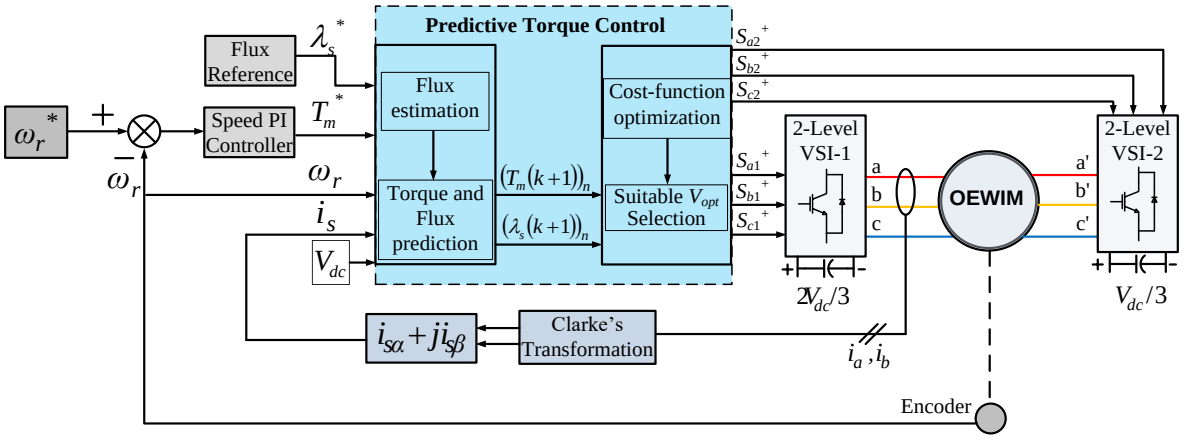

Figure 5.2 Conventional PTC for four-level OEWIM drive

5.2.1 Measurement and estimation

The motor speed (ω_r), current (i_s) and combined DC link voltage can be sensed directly. Here, combined DC link voltage V_{dc} represents V_{dc1}+V_{dc2}, owing to the dual VSI arrangement. As stated earlier in Chapter-2, stator flux which is not directly measurable can be estimated using Euler's formula (5.1). The present state (k) stator flux is mentioned using variables at previous (k-1) sample state as,

$$\lambda_s(k) = \lambda_s(k-1) + V_s T_s - A T_s i_s \tag{5.1}$$

5.2.2 Predictions

With the available switching states of inverter configuration, predictions are done for stator current, flux and torque of a machine. For a dual inverter fed OEWIM, there are '37'

effective possible inverter voltage states out of '64' switching combinations. The dual inverter voltage space vectors are stated in Chapter-2 of (2.11) and (2.12). From these, net voltage space vector (V_s) is realized for a given OEWIM drive as in Chapter-2 of (2.13). With these 37 VVs (as indicated in Figure 5.1 (b)) and present state variables of OEWIM drive, the stator current, flux and torque predictions for one step ahead (k+1) are stated by (5.2)- (5.4).

Stator flux prediction: $$(\lambda_s(k+1))_n = \lambda_s(k) + T_s((V_s)_n - Ai_s(k)) \tag{5.2}$$

Stator current prediction:

$$i_s(k+1)_n = i_s(k) + T_s\left(A_1\left(\begin{matrix} A_2\lambda_s(k) - A_3 i_s(k) + K_r\left((V_s)_n - Ai_s(k) - j\omega_r\lambda_s(k)\right) \\ + \dfrac{j\omega_r i_s(k)}{A_1} \end{matrix} \right) \right) \tag{5.3}$$

Finally, the motor torque prediction using (5.2) and (5.3) as,

$$(T_m(k+1))_n = \frac{3}{2}\frac{P}{2}\left(\text{imag}\left(\bar{\lambda}_s(k+1)_n i_s(k+1)_n\right)\right) \tag{5.4}$$

In the above discretized prediction equations, the subscript n indicates VV number i.e. zero to 36. Moreover, the represented constants in (5.1) – (5.3) are noted as below.

$$A = R_s,\ A_1 = \frac{L_m}{L_s L_r - {L_m}^2},\ A_2 = \frac{R_r}{L_m},\ A_3 = \frac{L_s R_r}{L_m},\ K_r = \frac{L_r}{L_m}$$

5.2.3 Formulation of cost function

Cost function deals with number of control objectives. As it involves different objectives, relative balance among them is mandatory. The control action and switching state realization is to minimize the cost function. For IM drive applications, basic cost function is stated by (5.5). Here, 'W' is the weighting factor providing relative importance between torque and flux. At starting, the value of W is assigned as the ratio of nominal torque and flux, which is later adjusted by manual tuning. When number of objectives are more, weighting factors adjustment for every objective is difficult and has direct impact on optimal voltage vector selection. Therefore, the only adjustable term 'W' is influencing the control performance of PTC.

$$G_n = \left|T_m^{\ *} - T_m(k+1)_n\right| + W\left|\lambda_s^{\ *} - \left|\lambda_s(k+1)_n\right|\right| \tag{5.5}$$

Here, reference stator flux magnitude and motor torque are denoted by λ_s^* and T_m^* respectively.

In PTC operation of four-level dual inverter supplied OEWIM drive, total 37 evaluations are required at each stage of prediction and cost-function assessment. Thus, overall complexity grows in operation.

5.3 Proposed PTC for OEWIM drive

In conventional PTC, the cost function is formulated with the control objectives of torque and magnitude of stator flux as stated by (5.5). This demands flux weighting factor ('*W*') assignment in it. To alleviate the problem of '*W*' selection for torque and flux control, this chapter introduces stator flux space vector control. The proposed PTC block diagram for four level OEWIM drive operation is shown in Figure 5.3. The new control objective is formulated with the reference and predicted stator flux space vector as stated by (5.6). The main idea here is that the predicted stator flux space vector is made close to the generated reference stator flux space vector. This stator flux space vector (SFSV) control objective performs combined control of flux and torque.

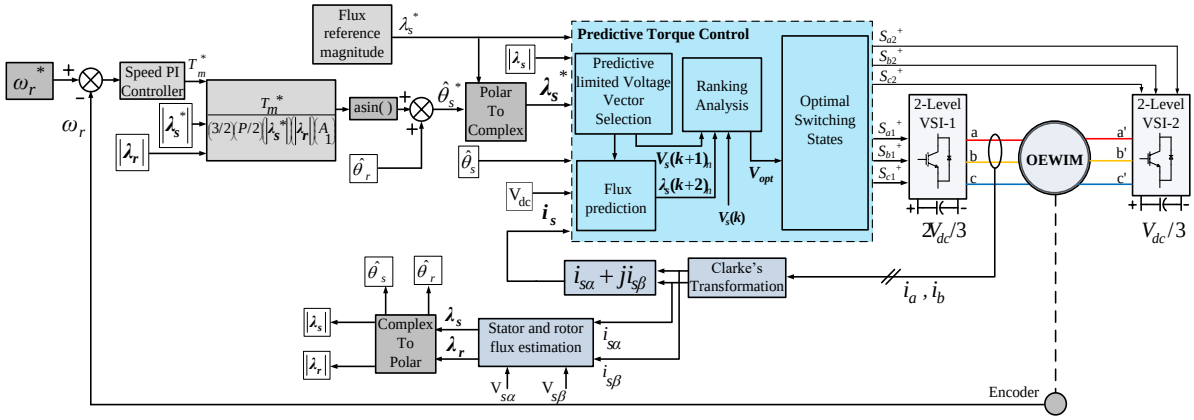

Figure 5.3 Proposed PTC block diagram for four-level OEWIM drive

The procedure for reference stator flux space vector (λ_s^*) generation is as indicated in Figure 5.3. Speed PI controller generates reference motor torque needed to maintain the actual speed of motor at a given reference speed value. The machine actual stator and rotor flux estimation is done using the mathematical equations as presented in chapter 2. The reference stator flux magnitude is set to machine nominal value. Thus, with the information of reference motor torque, reference stator flux magnitude, rotor flux magnitude and angle, the reference stator flux angle (θ_s^*) is figured out. Therefore, the reference stator flux magnitude and angle (which is in polar form) undergoes polar to complex form conversion, resulting the generated

reference stator flux space vector (λ_s^*). By evaluating modified cost-function (5.6) with all the possible VVs, the VV is identified which provides minimum cost-function value serving the accurate tracking of predicted real and imaginary flux components with the reference real and imaginary flux components, and it is considered as optimal. The optimal selected VV guarantees combined control of flux and torque. This results in simplified PTC operation overcoming the obstacle of weighting factor selection and providing optimal flux and torque response for OEW-IM drive.

$$G_n = \left| \boldsymbol{\lambda}_s^* - \boldsymbol{\lambda}_s(\boldsymbol{k}+\boldsymbol{1})_n \right| \tag{5.6}$$

However, weighting factors cannot be eliminated when additional control objectives are included in cost function as stated by (5.7). Here, *'N'* represents weighting factor for switching frequency control objective. The other concern is regarding high switching frequency in motor drive operation. The reduction in switching frequency of dual inverter is possible when number of voltage vector state transitions are less. Thus, control objective for switching frequency reduction is formulated with the previously applied and present applicable voltage vectors. This can be stated by (5.8).

$$G_n = \left| \boldsymbol{\lambda}_s^{\ *} - \boldsymbol{\lambda}_s(\boldsymbol{k}+\boldsymbol{1})_n \right| + N \left| f_{sw} \right| \tag{5.7}$$

$$\text{where: } f_{sw} = \boldsymbol{V}_s(\boldsymbol{k}-\boldsymbol{1}) - \boldsymbol{V}_s(\boldsymbol{k})_n \tag{5.8}$$

Thus, the proposed scheme is extended to alleviate weighting factors burden completely using ranking analysis. The step by step procedure for it is explained as follows:

Step 1: *Multiobjective separation*

Stator flux space vector and switching frequency control objectives are considered separately. Owing to the sample delay problem, two step ahead prediction is desired. Therefore, control objectives are represented as (5.9) and (5.10).

$$(G_1)_n = \left| \boldsymbol{\lambda}_s^{\ *} - \boldsymbol{\lambda}_s(\boldsymbol{k}+\boldsymbol{2})_n \right| \tag{5.9}$$

$$(G_2)_n = \left| \boldsymbol{V}_s(\boldsymbol{k}) - \boldsymbol{V}_s(\boldsymbol{k}+\boldsymbol{1})_n \right| \tag{5.10}$$

$$\text{where: } \boldsymbol{\lambda}_s(\boldsymbol{k}+\boldsymbol{2})_n = \boldsymbol{\lambda}_s(\boldsymbol{k}+\boldsymbol{1}) + T_s\left((\boldsymbol{V}_s(\boldsymbol{k}+\boldsymbol{1}))_n - A\boldsymbol{i}_s(\boldsymbol{k}+\boldsymbol{1}) \right) \tag{5.11}$$

Step 2: *Assessment and ranking*

The control objectives (G_1 and G_2) are assessed for every available voltage vector. Lower rank of '1' is assigned to the voltage vector for which control

objective value is minimum compared to remaining values. From this value, ranking increases with increase in control objective value. As two control objectives are considered, every voltage vector is associated with two ranks (R_1 and R_2).

Step 3: *Selection of optimal switching state*

After assessment and ranking, the averaged rank value is determined for every voltage vector as stated by (5.12). The voltage vector having minimum averaged rank value is considered as optimal switching state for the next sample interval.

$$\boldsymbol{V_{opt}} = VV\left[\min\left(\frac{R_1 + R_2}{2}\right)\right] \tag{5.12}$$

5.3.1 Voltage vector selection

It is known that dual inverter fed OEWIM offers '37' effective voltage states. Thus, all these states can be considered for control process. But it demands more computational burden. To reduce this computational burden, voltage vectors should be limited. This can be possible by knowing the stator flux position and flux error. Considering the instant where stator flux vector location is in sector-1 and flux error ($\Delta\lambda_s = |\lambda_s^*| - |\lambda_s|$) is ≥ 0, the voltage vectors made available to increase flux magnitude are as shown in Figure 5.4(a) (Dark side of plane). Likewise, for the similar location of stator flux vector, when flux error is < 0, the voltage vectors made available to decrease flux magnitude are located at light side of plane as shown in Figure 5.4(a). Thus, with this technique number of prediction voltage vectors are limited to '20'. It is also possible to find the limited prediction vectors, considering torque error ($T_m^* - T_m$). Figure 5.4(b) shows limited prediction vectors made available to increase torque when flux vector is situated in sector-1 and error in torque (ΔT) is ≥ 0. But here, prediction voltage vector number increased to '22' compared to flux error based technique, where it is '20'. Therefore, former technique is used for finding the limited voltage vector predictions.

Table 5.1 represents limited voltage vector predictions in six sectors based on stator flux error condition. Null state (V_0) is always involved with the active vectors (V_1 to V_{36}) for minimizing torque and flux ripples. With this, there are only '20' prediction voltage vectors selected out of '37' in each sample period and made available for multi-objective ranking analysis. This simplifies control process and computational burden is reduced.

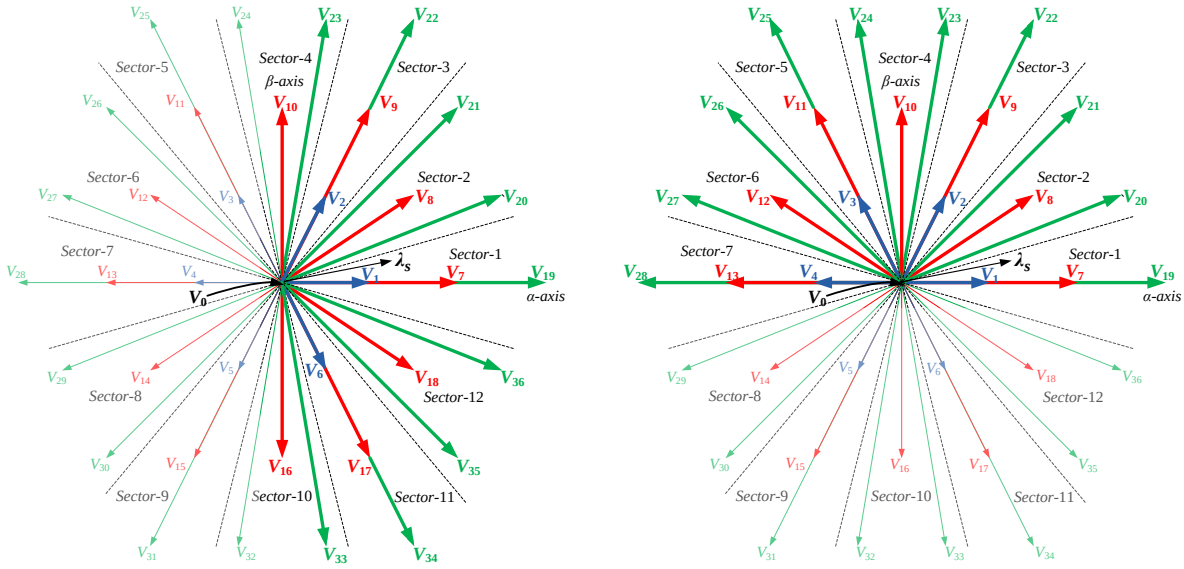

Figure 5.4 With the location of stator flux space vector in sector 1, possible prediction voltage vectors in dark colour (a) for $\Delta\lambda_s \geq 0$ and (b) for $\Delta T \geq 0$

Table 5.1 Possible set of voltage vector predictions

Sector number	Set of Voltage vectors for $\Delta\lambda_s \geq 0$	Set of Voltage vectors for $\Delta\lambda_s < 0$
1	V_0, V_6, V_1, V_2, V_{16}, V_{17}, V_{18}, V_7, V_8, V_9, V_{10}, V_{33}, V_{34}, V_{35}, V_{36}, V_{19}, V_{20}, V_{21}, V_{22}, V_{23}	V_0, V_{24}, V_{25}, V_{26}, V_{27}, V_{28}, V_{29}, V_{30}, V_{31}, V_{32}, V_{10}, V_{11}, V_{12}, V_{13}, V_{14}, V_{15}, V_{16}, V_3, V_4, V_5
2	V_0, V_{18}, V_7, V_8, V_9, V_{10}, V_{11}, V_{12}, V_1, V_2, V_3, V_{36}, V_{19}, V_{20}, V_{21}, V_{22}, V_{23}, V_{24}, V_{25}, V_{26}	V_0, V_{27}, V_{28}, V_{29}, V_{30}, V_{31}, V_{32}, V_{33}, V_{34}, V_{35}, V_{12}, V_{13}, V_{14}, V_{15}, V_{16}, V_{17}, V_{18}, V_4, V_5, V_6
3	V_0, V_8, V_9, V_{10}, V_{11}, V_{12}, V_{13}, V_{14}, V_2, V_3, V_4, V_{21}, V_{22}, V_{23}, V_{24}, V_{25}, V_{26}, V_{27}, V_{28}, V_{29}	V_0, V_{30}, V_{31}, V_{32}, V_{33}, V_{34}, V_{35}, V_{36}, V_{19}, V_{20}, V_{14}, V_{15}, V_{16}, V_{17}, V_{18}, V_7, V_8, V_5, V_6, V_1
4	V_0, V_{10}, V_{11}, V_{12}, V_{13}, V_{14}, V_{15}, V_{16}, V_3, V_4, V_5, V_{24}, V_{25}, V_{26}, V_{27}, V_{28}, V_{29}, V_{30}, V_{31}, V_{32}	V_0, V_{33}, V_{34}, V_{35}, V_{36}, V_{19}, V_{20}, V_{21}, V_{22}, V_{23}, V_{16}, V_{17}, V_{18}, V_7, V_8, V_9, V_{10}, V_6, V_1, V_2
5	V_0, V_{12}, V_{13}, V_{14}, V_{15}, V_{16}, V_{17}, V_{18}, V_4, V_5, V_6, V_{27}, V_{28}, V_{29}, V_{30}, V_{31}, V_{32}, V_{33}, V_{34}, V_{35}	V_0, V_{36}, V_{19}, V_{20}, V_{21}, V_{22}, V_{23}, V_{24}, V_{25}, V_{26}, V_{18}, V_7, V_8, V_9, V_{10}, V_{11}, V_{12}, V_1, V_2, V_3
6	V_0, V_{14}, V_{15}, V_{16}, V_{17}, V_{18}, V_7, V_8, V_5, V_6, V_1, V_{30}, V_{31}, V_{32}, V_{33}, V_{34}, V_{35}, V_{36}, V_{19}, V_{20}	V_0, V_{21}, V_{22}, V_{23}, V_{24}, V_{25}, V_{26}, V_{27}, V_{28}, V_{29}, V_8, V_9, V_{10}, V_{11}, V_{12}, V_{13}, V_{14}, V_2, V_3, V_4

Figure 5.5 displays the proposed PTC flow graph. The proposed control technique is examined for one sample period. Table 5.2 represents control objective values for the available limited voltage vectors in particular sample period and its corresponding rankings. It is observed that the voltage vector V_7 exhibits minimum averaged rank value which is selected as optimal state for dual inverter switching in the next sample interval.

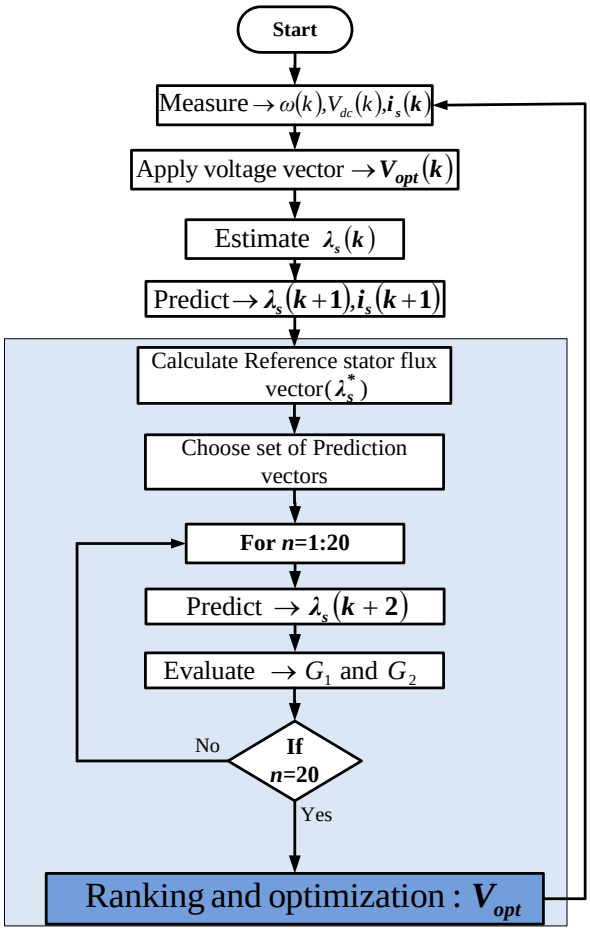

Figure 5.5 Proposed PTC flow graph

Table 5.2 Control operation during one sample interval

Voltage vectors (V_s)	G_1	G_2	R_1	R_2	$0.5*(R_1+R_2)$
V_0	0.0144	222.222	13	4	8.5000
V_1	0.0088	111.111	6	2	4.0000
V_2	0.0101	192.45	7	3	5.0000
V_6	0.0164	192.45	14	3	8.5000
V_7	**0.0033**	**0**	**1**	**1**	**1.0000**
V_8	0.0045	111.111	3	2	2.5000
V_9	0.0121	222.222	10	4	7.0000
V_{10}	0.0176	293.972	15	5	10.0000
V_{16}	0.024	293.972	19	5	12.0000
V_{17}	0.0184	222.222	16	4	10.0000
V_{18}	0.0108	111.111	9	2	5.5000
V_{19}	0.0086	111.111	5	2	3.5000
V_{20}	0.0043	111.111	2	2	2.0000
V_{21}	0.0065	192.45	4	3	3.5000
V_{22}	0.0141	293.972	12	5	8.5000
V_{23}	0.0197	333.333	17	6	11.5000
V_{33}	0.026	333.333	20	6	13.0000
V_{34}	0.0205	293.972	18	5	11.5000
V_{35}	0.0129	192.45	11	3	7.0000
V_{36}	0.0107	111.111	8	2	5.0000

Finally, a weighting factor independent PTC operation for four level dual VSI supplied OEWIM drive is achieved along with reduced prediction VVs.

5.4 Results and discussion

To check the performance of proposed PTC of OEWIM drive, simulation and experimental tests are conducted on existing 3.7 kW, 1440 RPM OEWIM. The machine parameters are listed in Table A.1. Results are presented in comparison with conventional PTC to accentuate the merits of proposed PTC. For this, conventional PTC weighting factor in cost function is opted empirically.

5.4.1 Simulation results

The proposed PTC scheme for OEWIM drive is simulated in MATLAB/Simulink software. The dual inverter fed OEWIM is mathematically modelled using the framed equations in Chapter-2. The DC link voltages of dual inverter are maintained at 333.33 V and 166.67 V i.e. in the ratio of ($2V_{dc}/3$) and ($V_{dc}/3$). Here V_{dc} corresponds to combined DC link voltage which is set to 500 V. The reference stator flux magnitude ($|\lambda_s^*|$) is set to a nominal value of 1 Wb. The performed simulation results are shown in Figures (5.6)- (5.8).

Figure 5.6 shows the motor speed and phase voltage simulated waveforms at the reference speed of 250 rad/s (electrical). Steady state characteristics of machine (Speed, motor torque and stator flux) at the reference speed of 200 rad/s are shown in Figure 5.7. The steady state current trace is also indicated at reference speed of 250 rad/s.

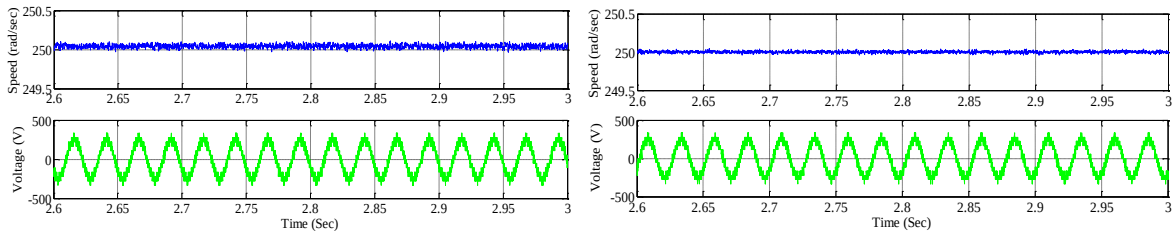

Figure 5.6 Simulated steady state waveforms of speed and voltage at reference speed of 250 rad/s. (a) Conventional PTC and (b) Proposed PTC

The dynamic performance of a machine is analysed with a step changes in reference speed (100 rad/s to 200 rad/s and then 250 rad/s) at no load. Its motor speed, torque and flux characteristics are shown in Figure 5.7. A step change in load torque is performed from no load to 6 Nm. It is observed that motor torque is tracking load torque with low ripple content for the proposed PTC of OEWIM drive. Its dynamic characteristics such as speed, torque,

flux and current at the reference speed of 200 rad/s are shown in Figure 5.8. These results reveal that the proposed PTC of OEWIM drive exhibits optimal control response having low steady state torque and flux ripples.

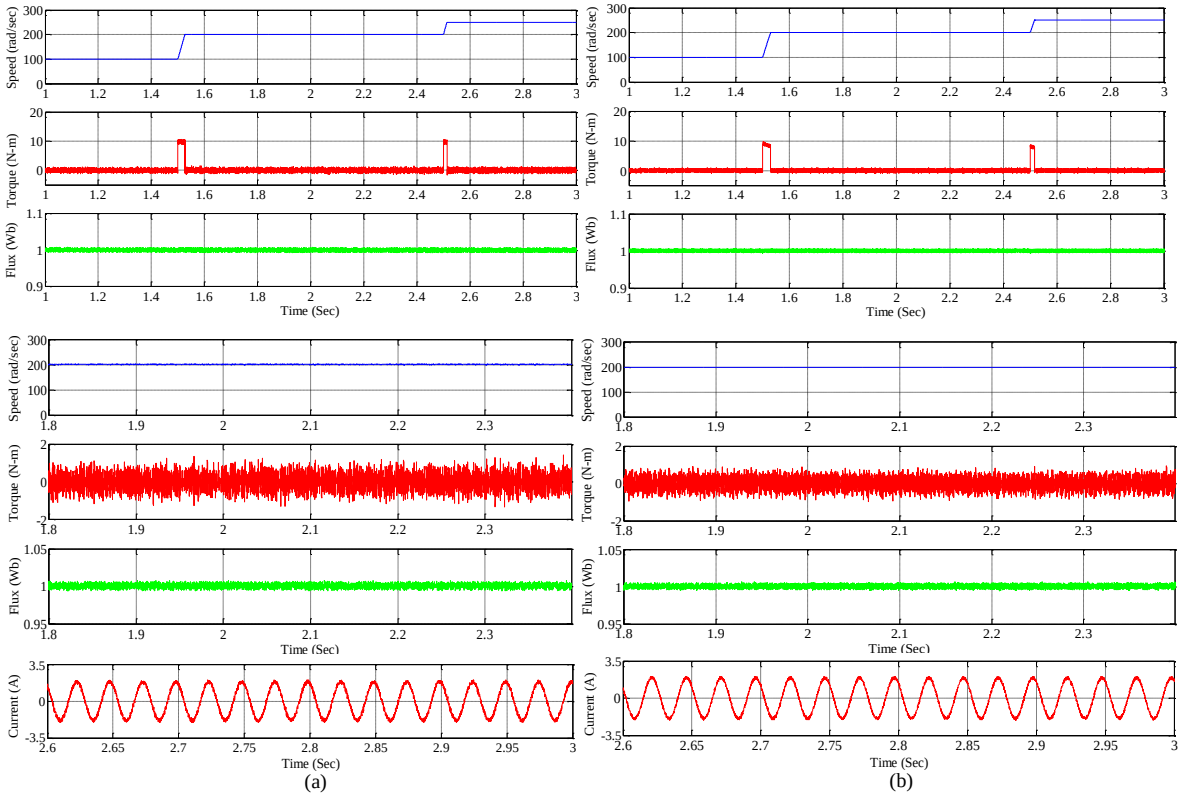

Figure 5.7 Speed, torque, flux and current characteristics. (a) Conventional PTC and (b) Proposed PTC

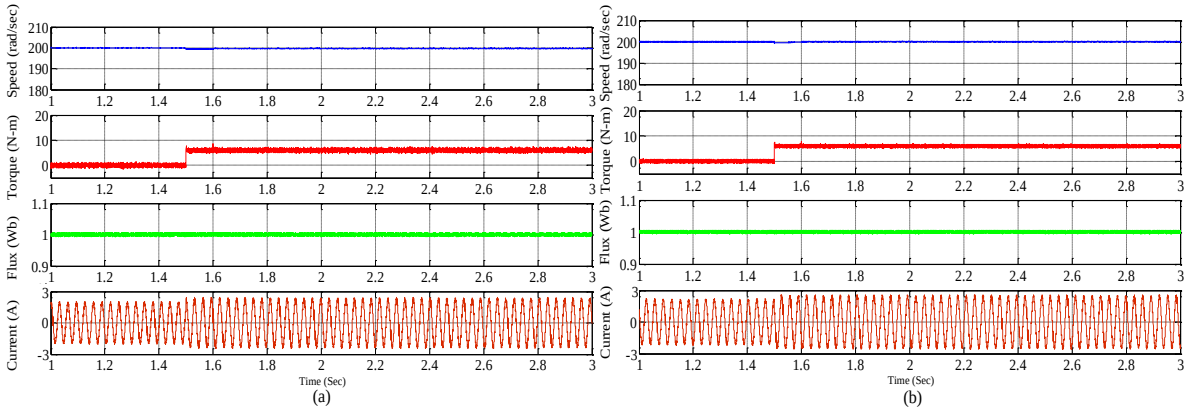

Figure 5.8 Simulated dynamic response of motor speed, torque, flux and current at reference speed of 200 rad/s with the step change in load torque. (a) Conventional PTC and (b) Proposed PTC

5.4.2 Experimental results

The hardware setup of existing machine as shown in Figure A.4 is used for real time execution of PTC schemes for OEWIM drive. The control algorithms are implemented in discrete platform using dSPACE Real Time Interfacing (RTI-1104). The sensed DC link

voltages from voltage sensor (LV-25) and stator currents from current sensor (LA-25) are given to ADC BNC connectors of dSPACE controller board interfacing. From motor encoder, speed is measured and interfaced to dSPACE incremental encoder. The controlled switching pulses are acquired at digital I/O pins and processed to interface with inverter switches. The conducted experimental results are shown in Figures (5.9)- (5.14).

During no load operation, motor speed, phase voltage and current at the reference motor speed of 250 rad/s are shown in Figure 5.9. For online step changes in reference speed, ControlDesk software is used. Thus, the dynamic performance of machine is examined by step changes in reference speeds (100 rad/s to 200 rad/s and then 250 rad/s) at no load as shown in Figure 5.10. Figure 5.11 shows forward to reverse motoring operation at no load, when step change in reference speed is given from 200 rad/s to -200 rad/s.

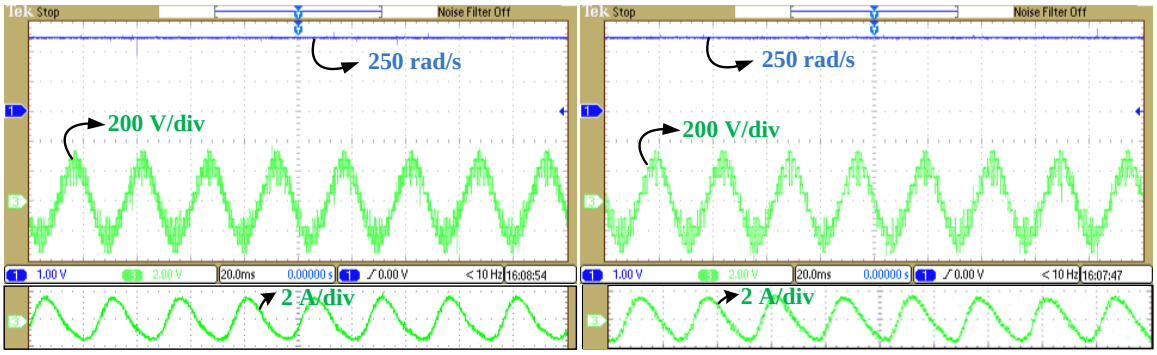

Figure 5.9 Steady state speed, voltage and current at reference speed of 250 rad/s. (a) Conventional PTC and (b) Proposed PTC

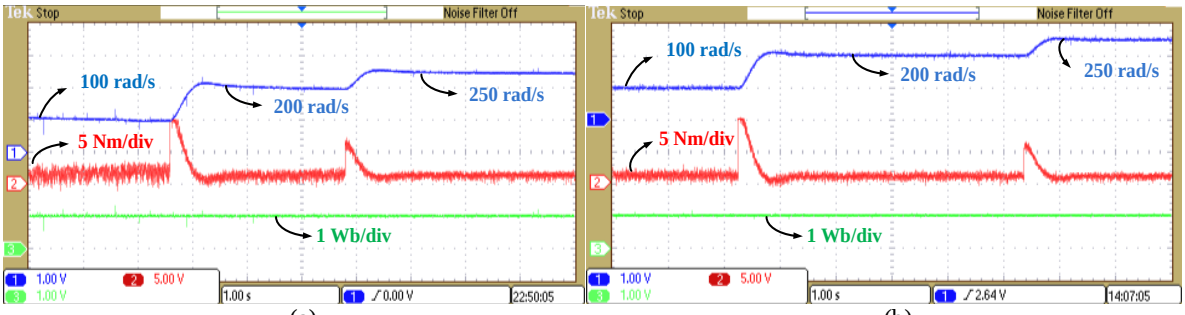

Figure 5.10 Dynamic characteristics of motor speed, torque and flux at no load. (a) Conventional PTC and (b) Proposed PTC

For applying load torque, an equivalent resistive load is connected to a DC generator which is coupled to OEWIM. Thus, by loading DC generator with a resistive load, step changes in load torque is performed when motor is operating at speed of 150 rad/s and 200 rad/s. These dynamic load step change experimental results are shown in Figures 5.12 and 5.13. Steady state performance under loaded condition is also shown in Figure 5.13. From

these experimental results, it is evident that the proposed PTC exhibits improved steady state torque and flux response when compared to conventional PTC, whereas the dynamic response of both the PTC schemes remains same.

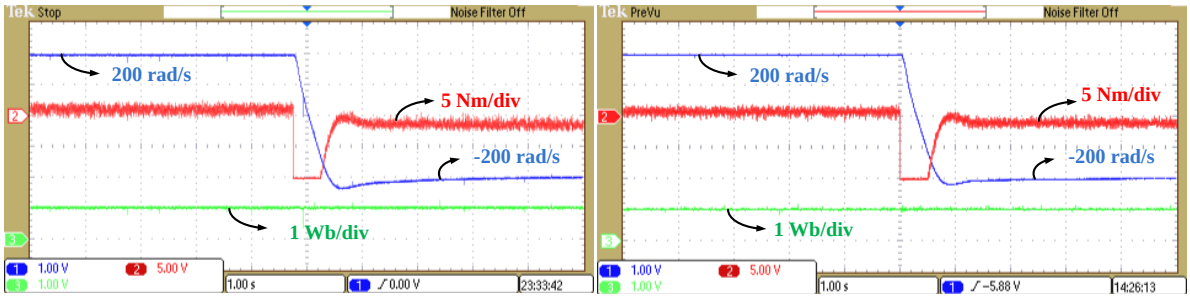

(a) (b)

Figure 5.11 Speed, torque and flux dynamic characteristics during forward to reverse motoring operation. (a) Conventional PTC and (b) Proposed PTC

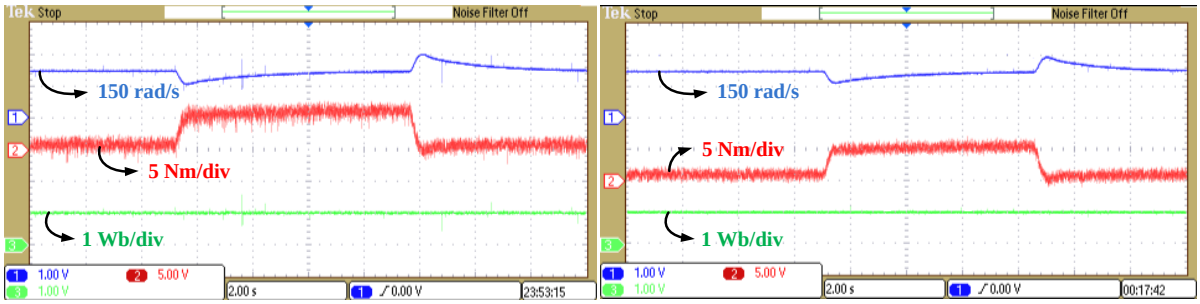

(a) (b)

Figure 5.12 Speed, torque and flux dynamic characteristics during load step change. (a) Conventional PTC and (b) Proposed PTC

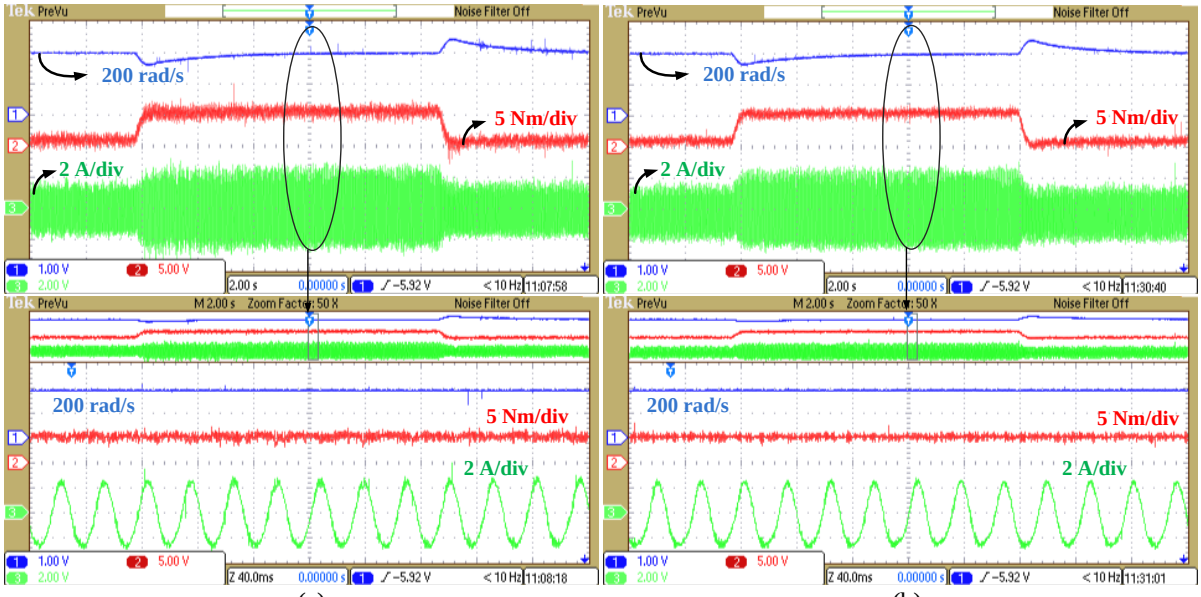

(a) (b)

Figure 5.13 Motor Speed, torque and current dynamic characteristics with step changes in load torque. (a) Conventional PTC and (b) Proposed PTC

While in operation, dual inverter switching states attained for conventional and proposed PTC are shown in Figure 5.14. From this, minimum switching state transitions are observed for the proposed PTC scheme indicating lower switching frequency. Finally, a comparative table is prepared for flux and torque ripple, and switching frequency achieved in conventional and proposed PTC of OEWIM drive as listed in Table 5.3. These results indicate effectiveness of proposed PTC over conventional PTC scheme.

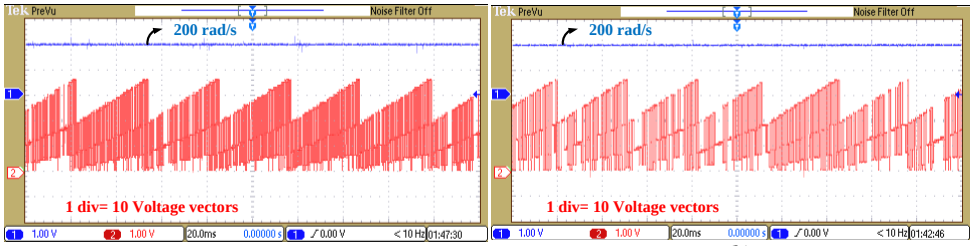

(a) (b)

Figure 5.14 Switching state transitions at speed of 200 rad/s. (a) Conventional PTC and (b) Proposed PTC

Table 5.3 Comparative analysis

Control scheme	Speed	Torque ripple (Nm)	Flux ripple (Wb)	Switching Frequency (Hz)
Conventional PTC	100 rad/s	1.47	0.033	2009
Proposed PTC		1.22	0.028	1310
Conventional PTC	200 rad/s	1.24	0.022	2362
Proposed PTC		1.08	0.018	1610
Conventional PTC	250 rad/s	1.09	0.017	2229
Proposed PTC		0.97	0.011	1492

5.5 Summary

In this chapter, modified PTC for OEWIM drive application has been introduced and implemented. This approach eliminates flux weighting factor assignment and provides combined torque and flux control by introducing stator flux space vector based control in cost function. However, when additional control objective i.e. switching frequency is involved in single cost function, the proposed scheme is extended to eliminate weighting factors completely using multi objective ranking analysis. To reduce control algorithm complexity, prediction voltage vectors of OEWIM drive are limited by stator flux error strategy.

The proposed PTC for OEWIM drive is verified by conducting simulation and experimental tests. These results are examined in comparison with the conventional PTC scheme. It is observed that OEWIM drive exhibits better torque and flux response for the proposed PTC. Switching frequency of dual inverter also reduced compared to the conventional PTC scheme. Finally, an improvised predictive torque control is accomplished for OEWIM drive.

Chapter 6

A Simplified Predictive Torque Control Scheme for Open End Winding Induction Motor Drive

Chapter 6
A Simplified Predictive Torque Control Scheme for Open End Winding Induction Motor Drive

6.1 Introduction

In earlier chapter, weightless PTC operation for four-level dual VSI supplied OEWIM drive is investigated. To achieve this, stator flux space vector objective and further ranking analysis are applied. However, the process creates extra computational burden. This is due to the involvement of following: determination of reference stator flux space vector, application of ranking methodology and calculation of actual flux space vector for knowing its sector information. In the present work, a simplified PTC is proposed for four-level dual VSI supplied OEWIM drive. Usually, the weighting factor choice in basic cost function plays a key role in selecting optimal voltage vector for better torque and flux response. Several analytical and empirical methods are introduced for optimal selection of weighting factor, which demands additional computational burden. This work aims to develop modified PTC, eliminating flux weighting factor. The flux control objective in cost function is replaced by an equivalent reactive torque control. Thus, forming two control objectives of same units and eliminating the requirement of flux weighting factor in cost function. Furthermore, nearest voltage vector selection strategy is introduced to limit the number of prediction voltage vectors in each sampling period. This selection of limited voltage vectors also helps in switching frequency reduction. The objectives of this work are presented below: 1. Formation of simplified PTC operation and further improvement in limiting prediction voltage vectors, thereby reduction in computational burden of operation. 2. Elimination of weighting factor through the modifications in PTC operation to obviate its tedious tuning process. 3. Development of OEWIM drive performance such as better torque and flux response along with switching frequency limitation. Therefore, simplified PTC operation for four-level Open End Winding Induction Motor Drive is formed in this chapter.

The conventional PTC operation of four-level dual VSI supplied OEWIM drive which involves three main steps (measure and estimation, predictions, and cost function assessment) is already explained in chapter-5 (section-5.2). Now, this chapter includes the following contents: section 6.2 deals with operation of proposed PTC for four-level OEWIM drive,

section 6.3 presents the monitored results of proposed PTC and conventional PTC. Thus, proposed PTC operation is verified. Finally, in section 6.4, the chapter summary is mentioned.

6.2 Proposed PTC for OEWIM drive

From the discussion of conventional PTC, it is observed that the only term needs to tune in cost function is weighting factor (W) and its improper selection leads to distortions in motor torque and flux response. Therefore, its proper tuning in order to achieve optimal control response of motor drive becomes one of the major problem. To solve this problem, various control methods are introduced in literature. In conventional PTC of OEWIM, heuristic procedure is followed for weight determination achieving better torque and flux control response. However, it is a time taking process. In previous work (Chapter-5), flux weighting factor is completely eliminated by modifying the cost function. New control objective is formulated having the reference and predicted values of stator flux vector. Thus, the combined torque and flux control is possible with a single control objective, thereby eliminating weighting factor for PTC operated OEWIM drive. However, the calculation of reference stator flux space vector involves trigonometric functions and parameter dependent.

In this study, an improved and simple PTC for OEWIM drive is introduced. Figure 6.1 shows functioning block diagram of the proposed PTC. For four-level dual VSI operation, two VSIs are supplied with unequal DC link voltages, where terms C_1 and C_2 are 2/3 and 1/3.

6.2.1 Modified cost function formulation

In conventional PTC cost function, the difference in control objectives of motor torque and flux, demands weighting factor to provide the relative importance between them. In this chapter, a reactive torque control objective is introduced, which is equivalent to the flux control. The modified cost function is stated as,

$$G_n = \left|T_m^{\,*} - T_m(k+1)_n\right| + \left|T_r^{\,*} - T_r(k+1)_n\right| \tag{6.1}$$

In (6.1), T_r^* is the reference reactive torque generated from the flux PI controller. The flux in a machine is related to the reactive torque. The basic representation of reactive torque is stated in [15], which is given as (6.2),

$$T_r = \frac{3}{2}\frac{P}{2}\left(\text{real}\left(\bar{\lambda}_s i_s\right)\right) \tag{6.2}$$

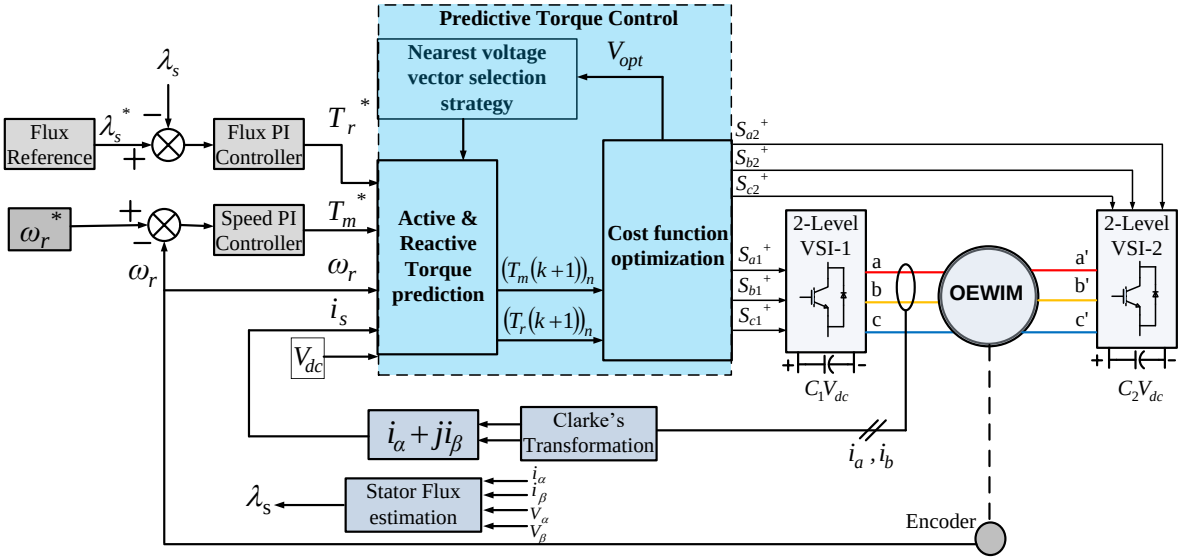

Figure 6.1 Proposed PTC operational block diagram

The one step ahead prediction for the reactive torque is given as (6.3),

$$(T_r(k+1))_n = \frac{3}{2}\frac{P}{2}\left(\text{real}\left(\bar{\lambda}_s(k+1)_n i_s(k+1)_n\right)\right) \tag{6.3}$$

Thus, the closeness of predicted value of reactive torque ($T_r(k+1)$) with the generated reference reactive torque value (T_r^*) ensures flux control. From (6.1), it is observed that the first control objective represents electromagnetic torque control and the second control objective represents reactive torque control which is an equivalent flux control, thus ensuring both the control objectives are of same units. The similarity in control objectives alleviate flux weighting factor assignment in cost function. Thereby, an improved predictive torque and flux control of OEWIM drive is achieved with the modified cost function, eliminating weighting factor.

6.2.2 Nearest voltage vector selection

In PTC of OEWIM drive, the optimal voltage vector is the one which gives minimum cost function value. Thus, for optimal selection of voltage vector, the modified cost function (6.1) value needs to be determined for all 37 dual inverter voltage states in every sample period. In order to reduce the computational burden of control process, number of prediction voltage vectors available in each sample interval has to be limited. Based on the data of stator flux error and sector identification of stator flux vector, set of limited voltage vectors can be made available for the predictions and evaluation of cost function. This requires stator flux vector sector information using inverse trigonometric function. However, it demands

additional computational burden and also number of voltage vectors required for prediction depends on sector information. Hence it needs more number of voltage vectors.

In this chapter, prediction voltage vectors are limited by nearest voltage vector selection strategy. It does not require any information about the stator flux vector position and sector. In this, number of prediction voltage vectors are limited by considering only nearest voltage vectors to the optimal one, which is selected in previous step. With the information of previous optimal voltage vector state, form the nearest voltage vectors set. The set of nearest voltage vectors to the optimal one are determined in such a way that it includes at least one from small vector group, at least four from medium vector group and at least four from large vector group. With this all the group of voltage vector candidates (small, medium and large) are get involved and thus forming overall 12 limited prediction voltage vectors including null vector. This set of 12 limited prediction voltage vectors are made available for cost function evaluation and from this set, optimal switching state is figured out which gives minimum cost function value (6.1). Its corresponding switching states are fed to dual inverter switches. This process keeps on continuing.

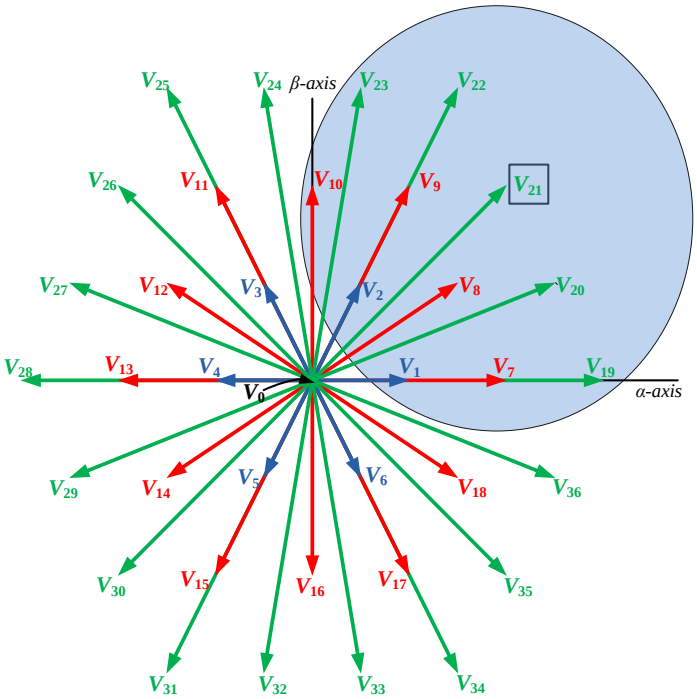

Figure 6.2 Possible limited prediction vectors selection for next sample interval when the present optimal vector is V_{21}

Considering the case where the voltage vector V_{21} is selected as optimal, now the set of voltage vectors nearer to the optimal vector V_{21} are: V_0, V_1, V_2, V_7, V_8, V_9, V_{10}, V_{19}, V_{20}, V_{22}, V_{23}. Figure 6.2 illustrates the instant of selecting the set of nearest voltage vectors to the optimal voltage vector V_{21}. Here, the voltage vectors (V_1, V_2) represents small vectors, (V_7,

V_8, V_9, V_{10}) represents medium vectors and (V_{19}, V_{20}, V_{22}, V_{23}) represents large vectors. Null vector (V_0) is always engaged with the active vectors (V_1 to V_{36}) for reduction of torque and flux ripples. These voltage vectors (as in Figure 6.2) along with V_{21} are made available for the next sample interval as a set of prediction voltage vectors for the cost function evaluation. Consider one more case, where the null voltage vector V_0 is selected as optimal, in this situation the previous set of prediction voltage vectors are considered for the present cost function evaluation.

Thus in each sample interval, cost function is evaluated for only 12 prediction voltage vectors, instead of evaluating for all 37 voltage vectors. This proposed feature permits reduction in computational burden of control process and also it adds switching frequency limitation as the next selecting optimal voltage vector is nearer to the previously selected optimal voltage vector. The overall control steps involved in proposed PTC are exhibited in Figure 6.3 and are discussed as follows:

Step 1: Measure combined DC link voltage (V_{dc}), stator current space vector (i_s) and motor speed (ω_r).

Step 2: Estimate present stator flux ($\lambda_s(k)$) with the information of previously applied optimal voltage vector ($V_s(k\text{-}1)$), stator flux and current.

Step 3: Follow the nearest voltage vector strategy (Set of voltage vectors nearer to the $V_s(k\text{-}1)$) and limit the number of prediction voltage vectors for the prediction in next sample interval.

Step 4: With the help of limited prediction voltage vectors, predict stator flux ($\lambda_s(k+1)$) and current ($i_s(k+1)$), which further provides active torque ($T_m(k+1)$) and reactive torque ($T_r(k+1)$) predictions.

Step 5: Evaluate the modified cost function G_n (6.1), with the limited predicted values of active torque and reactive torque (Obtained from the limited prediction voltage vectors).

Step 6: Select the optimal voltage vector for the next sample interval providing minimum cost function value and apply its corresponding switching states to the dual inverter.

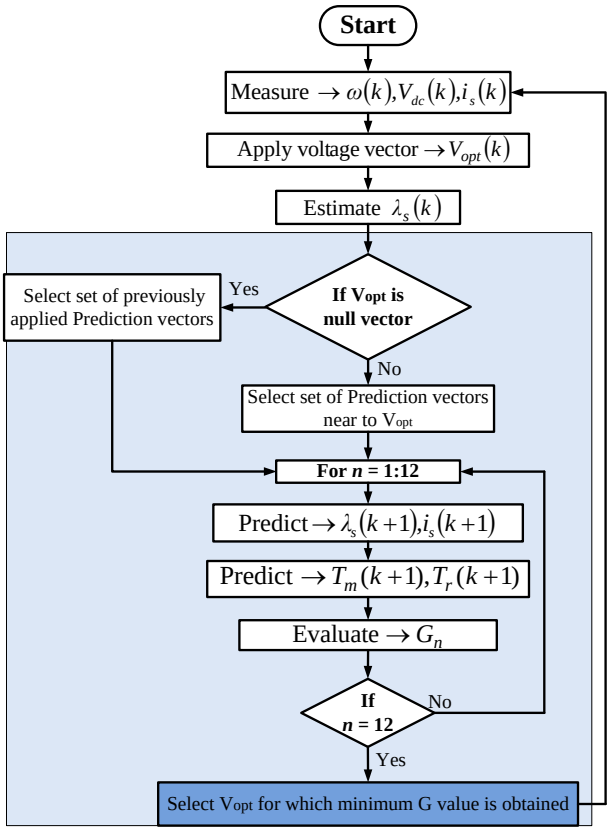

Figure 6.3 Proposed PTC flow graph

Thus, a simplified PTC of OEWIM drive, eliminating weighting factor requirement in cost function and limiting prediction voltage vectors without any additional computational burden is achieved.

6.3 Results and discussion

The proposed PTC for OEWIM drive is verified by performing real time experimentation. The machine parameters of real time test setup are given in Table A.1. The obtained results of proposed PTC are compared with the conventional PTC scheme. For this, conventional PTC is executed with the basic cost function having weighting factor and evaluated for all 37 prediction voltage vectors of dual inverter in each sample period. In conventional PTC, for weighting factor determination, heuristic procedure is followed.

6.3.1 Experimental results

The real time validation of proposed PTC is exhibited by performing experimentation on 3.7 kW OEWIM drive. The OEWIM is coupled with DC generator, in order to apply load torque on motor by loading DC generator with a resistive load. Figure A.4 indicates experimental test setup of OEWIM drive. For real time execution, MATLAB/Simulink

software is interfaced with dSPACE RTI 1104 controller. The inputs to the PTC algorithm are combined DC link voltage (V_{dc}), motor speed (ω_r) and current (i_s). Motor speed is measured with encoder and connected to dSPACE incremental encoder. DC link voltage and motor phase currents are sensed from the sensors LV-25 and LA-25 respectively. These sensed signals are given to ADC-BNC connectors of dSPACE control board. The optimal switching states of dual inverter achieved from the PTC algorithm are given to the dSPACE Master bit I/O pins and thereby interfacing with the dual inverter switches. The conducted experimentation results of both conventional and proposed PTC for various operating conditions of motor are shown in Figures (6.4) - (6.9). The speed and flux PI regulator gains are tuned empirically. In fact, the tuning of PI regulator is easier when compared to the weighting factor tuning [90].

During no load condition, motor is operated at the reference speeds 200 rad/s and 250 rad/s (electrical). Its steady state speed, phase voltage and current are shown in Figure 6.4. Figure 6.4(a) and Figure 6.4(c) exhibits the OEWIM drive response at reference speeds 200 rad/s and 250 rad/s when conventional PTC technique is operated. At the same speeds, Figure 6.4(b) and Figure 6.4(d) displays the OEWIM drive response obtained for the proposed PTC scheme.

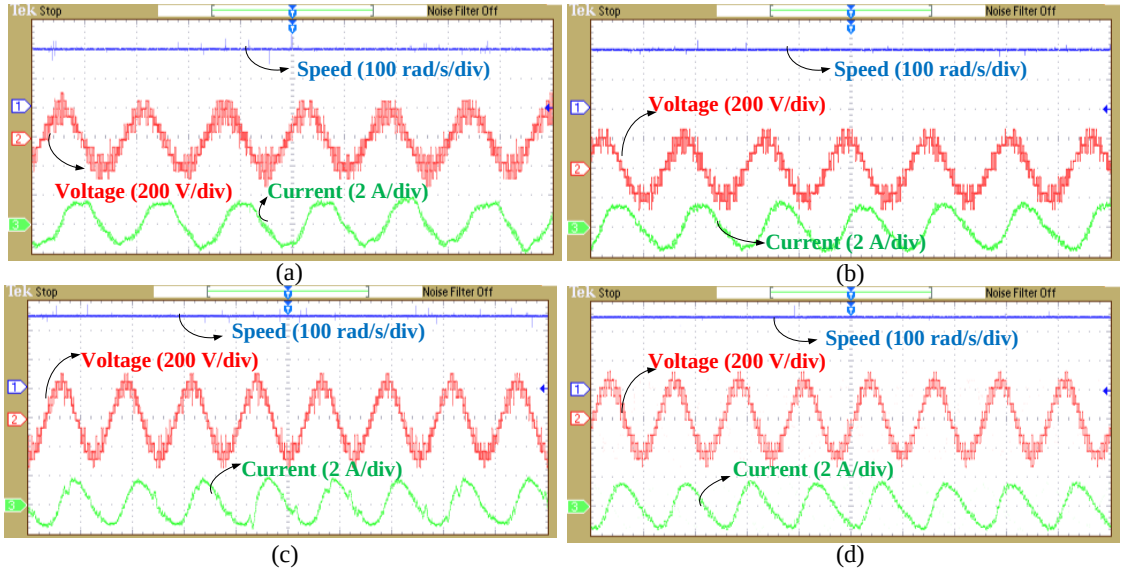

Figure 6.4 Experimental steady state motor speed, voltage and current response. (a) With Conventional PTC and (b) with Proposed PTC of OEWIM running at 200 rad/s. (c) With Conventional PTC and (d) with Proposed PTC of OEWIM running at 250 rad/s (X-axis time scale- 20 ms/div)

When the motor reference speed is set to 200 rad/s, the response of motor speed and dual inverter switching transitions are shown in Figure 6.5. Figure 6.5(a) and Figure 6.5(b) shows the experimental response for conventional and proposed PTC scheme respectively.

With the help of nearest voltage vector selection strategy in proposed PTC, the nearest limited voltage vectors set to the optimal one (which is selected in previous state) is made available for the present cost function evaluation. Thus, the optimal voltage vector selection for the next sample interval is mostly nearer to the previous one. Thereby, reducing switching state transitions. In Figure 6.5(b), less dual inverter switching state transitions are observed in proposed PTC compared to conventional PTC scheme. Number of switching state transitions in a fixed time period decides the dual inverter average switching frequency. Thus, the average switching frequency reduction is achieved in proposed PTC scheme.

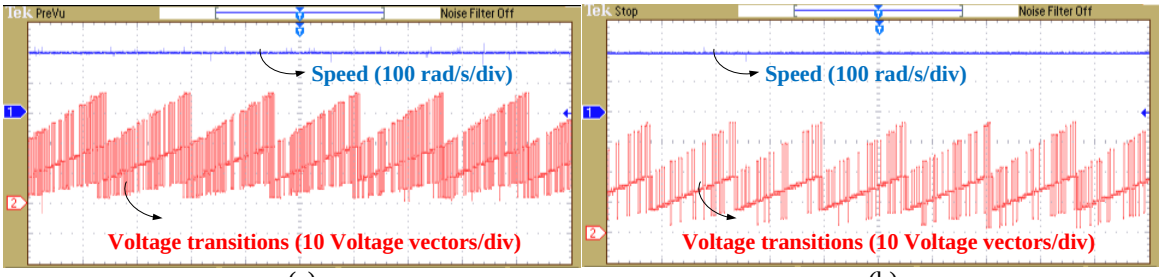

(a) (b)

Figure 6.5 Dual inverter voltage state transitions at motor speed of 200 rad/s. (a) Conventional PTC and (b) Proposed PTC (X-axis time scale- 20 ms/div)

In Figure 6.6, the effect of Common Mode Voltage (CMV) is observed. The reduction in CMV is observed for the proposed PTC as the proposed PTC of OEWIM drive operates at lower switching frequency. The observed CMV rms values at motor speed of 200 rad/s for the conventional and proposed PTC are 67.7 V and 50.1 V respectively. At the reference speed of 100 rad/s, 150 rad/s and 200 rad/s, the steady state motor speed, torque and flux response are shown in Figure 6.7. Figure 6.7(a) represents the experimental response obtained for conventional PTC of OEWIM running at 100 rad/s, 150 rad/s and 200 rad/s. At the same speeds, Figure 6.7(b) represents the motor response obtained for the proposed PTC scheme, where the optimal torque and flux response are observed. Thus, reduction in motor steady state torque and flux ripple are achieved in proposed PTC scheme for OEWIM.

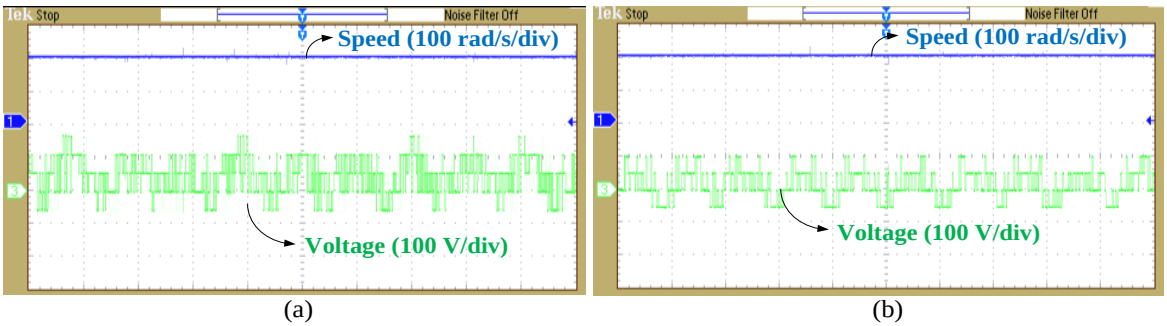

(a) (b)

Figure 6.6 OEWIM drive CMV response at reference speed of 200 rad/s. (a) Conventional PTC and (b) Proposed PTC (X-axis time scale- 10 ms/div)

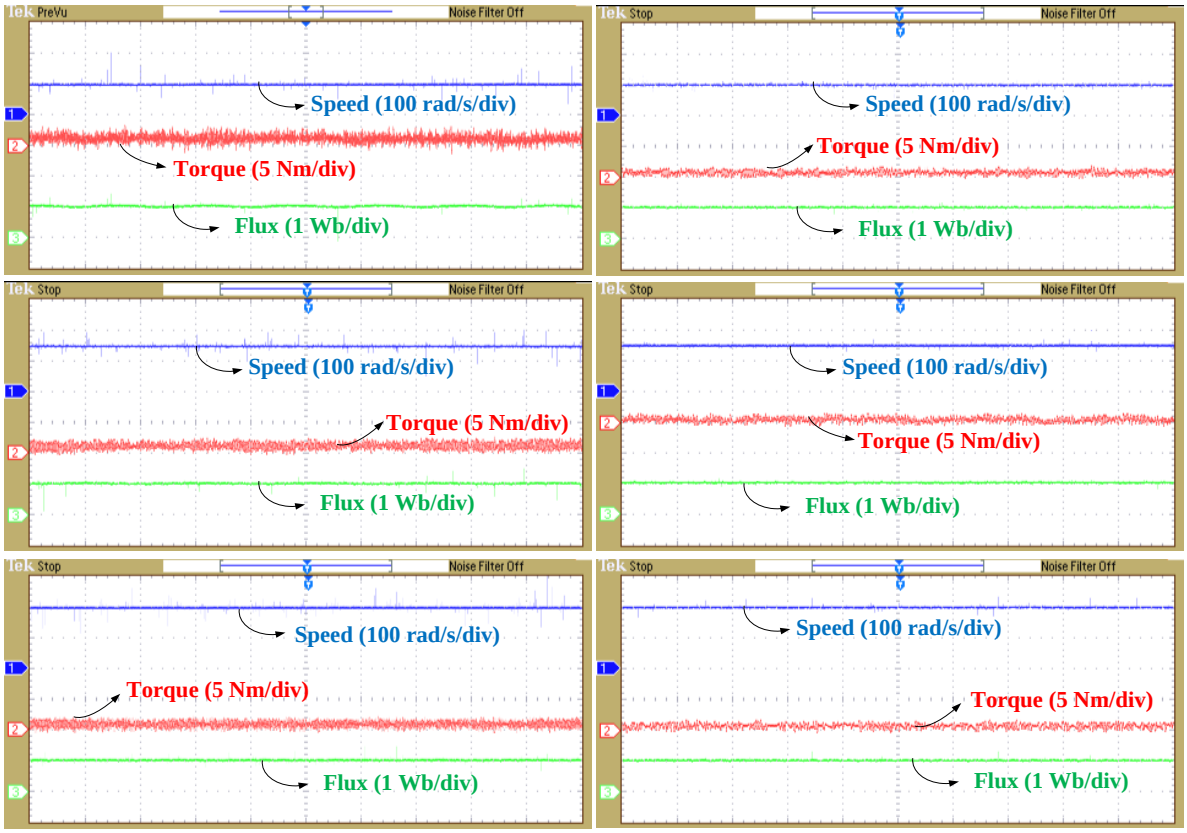

(a) (b)

Figure 6.7 Experimental steady state motor speed, torque and flux response. (a) With Conventional PTC and (b) with Proposed PTC of OEWIM running at 100 rad/s, 150 rad/s and 200 rad/s (X-axis time scale- 20 ms/div)

In Figure 6.8, dynamic response of OEWIM drive is observed during forward to reverse motoring operation. For dynamic analysis of motor, dSPACE Control Desk software is used to trigger the reference speeds online. While motor is operating in forward direction at a speed of +220 rad/s, step change of -220 rad/s is triggered. During this operation, motor speed, torque and flux response for both conventional and proposed PTC are shown in Figure 6.8(a) and Figure 6.8(b) respectively.

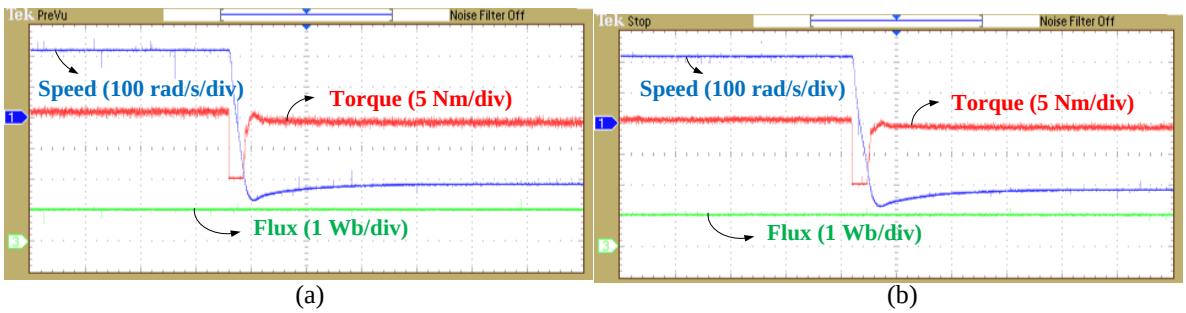

(a) (b)

Figure 6.8 Experimental dynamic response of OEWIM drive from forward (+220 rad/s) to reverse motoring (-220 rad/s). (a) With Conventional PTC and (b) with Proposed PTC (X-axis time scale- 2 s/div)

In Figure 6.9, dynamic response of OEWIM drive with load disturbance is observed. During no load, while motor is operating at the speed of 200 rad/s, load torque of 5 Nm is applied and removed after certain time. The exhibited motor dynamic speed, torque and current response for both conventional and proposed PTC scheme are shown in Figure 6.9(a) and Figure 6.9(b) respectively.

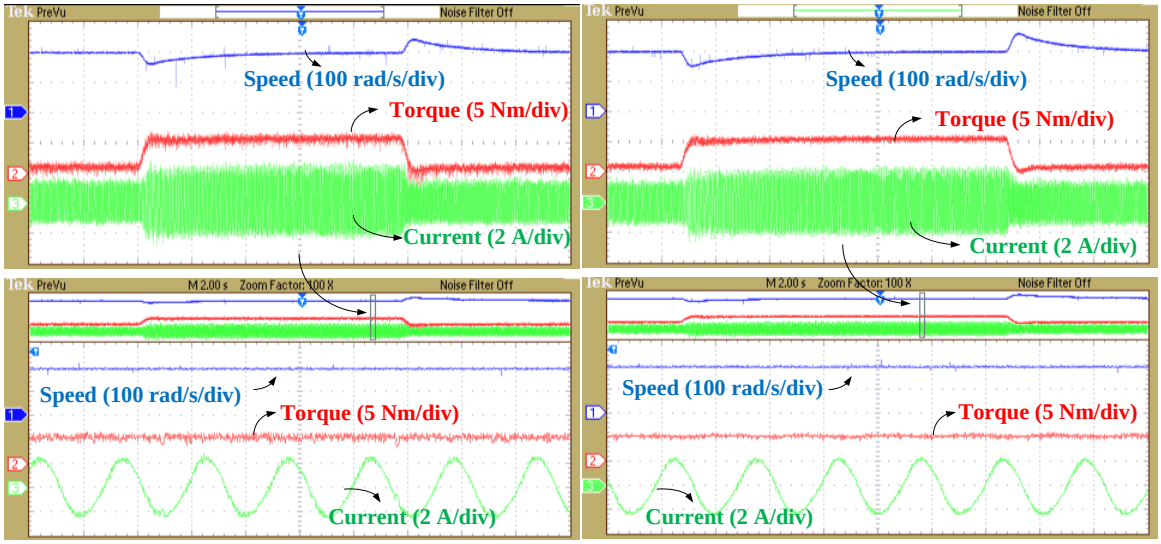

(a) (b)

Figure 6.9 Experimental dynamic response of OEWIM drive with the load disturbance operating at speed of 200 rad/s. (a) With Conventional PTC and (b) with Proposed PTC (X-axis time scale- 2 s/div, zoomed view X-axis time scale- 20 ms/div)

From these experimental results, it is observed that both conventional and proposed PTC schemes exhibited almost similar dynamic characteristics during step change in reference speed and load torque disturbance. The prominence of proposed PTC is observed during the steady state operation of motor exhibiting low torque and flux ripple at different operating speeds compared to conventional PTC scheme. Thus, the weighting factor elimination in modified cost function of proposed PTC results in better control response of motor drive i.e. improved torque and flux regulation. Furthermore, the nearest voltage vector selection scheme facilitates the benefits of reduced computational time and switching frequency reduction.

Comparison of torque, flux ripple and average switching frequency at various operating speeds between the conventional PTC and Proposed PTC of OEWIM drive are listed in Table 6.1. The torque and flux ripples are calculated by considering the sum of the difference between the measured and reference over 125000 samples. From these results, it is validated that proposed PTC exhibits better steady state torque and flux response along with switching frequency reduction.

Table 6.1 Comparison of torque ripple, flux ripple and average switching frequency

Motor speed (rad/s)	Torque ripple (Nm)		Flux ripple (Wb)		Switching frequency (Hz)	
	Conventional PTC	Proposed PTC	Conventional PTC	Proposed PTC	Conventional PTC	Proposed PTC
100	1.47	1.11	0.033	0.023	2009	1264
200	1.24	1.02	0.022	0.015	2362	1552
250	1.09	0.88	0.018	0.010	2229	1481

Furthermore, the proposed PTC requires only 12 prediction voltage vectors without any additional computational burden in control process. The total computational time for the proposed PTC of OEWIM drive in comparison with conventional PTC are listed in Table 6.2.

Table 6.2 Comparison of computational times

Implementation method	Overall Computational time
Conventional PTC	60.93 µs
Proposed PTC	34.20 µs

Thus, from the entire results, it is evident that the proposed PTC of OEWIM drive facilitate simple control structure, optimal torque and flux response, and switching frequency reduction with low computational burden when compared to the conventional PTC implemented with OEWIM drive.

6.4 Summary

In this chapter, an improved predictive torque and flux control scheme for OEWIM drive with four level inversion has been proposed which is independent from flux weighting factor. To achieve this, flux control objective is replaced by an equivalent reactive torque control. Furthermore, number of prediction voltage vectors selection in each sample interval is reduced to 12 from 37 which are used in the case of conventional PTC. The reduction in number of prediction voltage vectors in each sample interval is achieved by nearest voltage vector selection strategy, which allows switching frequency reduction and thereby decrease in CMV. Thus, providing overall simple control without any additional complex calculations and alleviating the problems faced by conventional PTC of OEWIM drive.

The reliability of proposed PTC is verified by conducting experimental assessment on dual inverter fed OEWIM drive. From the conducted tests, it is evident that the proposed PTC offers improved steady state torque and flux response. Lower torque, flux ripple and average switching frequency reduction are observed for different operating conditions of OEWIM

drive when compared to the conventional PTC. Furthermore, the proposed PTC offers lower computational time when compared to the existing PTC scheme of OEWIM drive. In future, the proposed PTC scheme can be extended to improve its robustness towards the model parameter variations. Therefore, it is clear that the proposed PTC gains all these benefits and this simple improved control technique is applicable for OEWIM drive.

Chapter 7

An Effective Predictive Torque Control Technique for Open-Ended Winding Induction Motor Drive

Chapter 7
An Effective Predictive Torque Control Technique for Open-Ended Winding Induction Motor Drive

7.1 Introduction

In the previous chapter, the four-level dual VSI prediction VVs are limited to 12 out of 37 in PTC operation. In this chapter, an attempt is made to limit the prediction VVs further. The reference stator flux vector generation which is used for flux weighting factor elimination (in chapter-5) is also applied in this work. Furthermore, the same reference stator flux vector is used for effective limitation of the prediction VVs for PTC operation of four-level dual VSI fed OEWIM drive. Therefore, the reference flux space vector generation only helps in both weighting factor elimination and prediction VVs limitation. The chapter formation is as follows: The proposed PTC for four-level dual VSI supplied OEWIM drive operation and the process of prediction VV limitation is elucidated in section 7.2. Besides this, switching frequency limitation in proposed PTC operation is also explained in the same section. Results of existing and proposed PTC operation are presented in section 7.3. In section 7.4, summary is provided for the chapter.

7.2 Proposed PTC for four-level OEWIM drive

In conventional PTC, tracking of flux and torque magnitudes with their references is attained using two separate control objectives in a single cost-function. The relative balancing between these two different control objectives is provided by *W*. To obviate *W* and to realize weighting factor independent PTC operation in the proposed technique as presented in Figure 7.1, Stator flux space vector (SFSV) control objective is used. The modified cost-function is represented by (7.1). The SFSV control objective performs combined control of flux and torque. Using the data of reference stator flux magnitude and torque, rotor flux angle and its magnitude, the reference SFSV is determined. The in detail view of generating reference SFSV is presented in Figure 7.1. By evaluating the modified cost-function (7.1) with all the possible VVs, the VV is identified which provides minimum cost-function value serving the accurate tracking of predicted real and imaginary flux components with the reference real and imaginary flux components, and it is considered as optimal. The optimal

selected VV guarantees combined control of flux and torque. This results in simplified PTC operation overcoming the obstacle of weighting factor selection and providing optimal flux and torque response for OEW-IM drive.

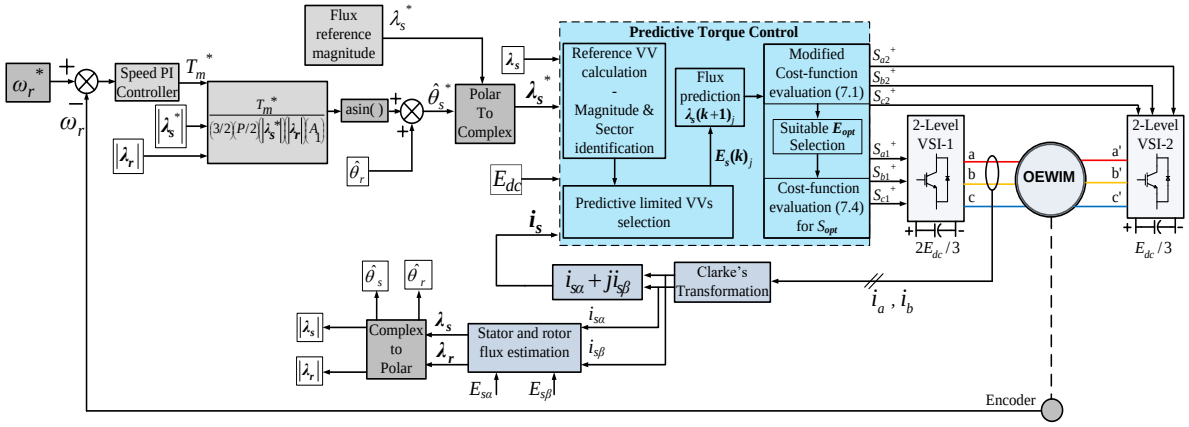

Figure 7.1 OEW-IM drive working block diagram using proposed PTC

$$G_j = \left|\lambda^*_{s\alpha} - \lambda_{s\alpha}(k+1)_j\right| + \left|\lambda^*_{s\beta} - \lambda_{s\beta}(k+1)_j\right| \tag{7.1}$$

The key contributions of this work for proposed PTC of four-level OEW-IM drive involves in: (1) Reducing prediction VVs selection and (2) Switching frequency reduction. The following are discussed below:

7.2.1 Reduced prediction VV selection

The condition of optimal VV selection is checked usually by evaluating modified cost-function (7.1) for all the possible 37 VVs. However, it is computationally not efficient. In proposed PTC, the number of VVs for prediction and cost-function evaluation are limited and so it avoids performing computations for all 37 VVs. This reduction in prediction VVs can be attained by calculating reference voltage space vector from the determined reference SFSV. The reference voltage space vector is calculated to maintain the closeness of predicted ($\boldsymbol{\lambda_s}(k+1)$) and reference ($\boldsymbol{\lambda_s}^*$) SFSV. Using this relation, the reference voltage space vector ($\boldsymbol{E_s}^*$) is determined as (7.2)- (7.3), where the term $B = -R_s$.

$$\boldsymbol{\lambda_s}^* = \boldsymbol{\lambda_s(k+1)} = \boldsymbol{\lambda_s(k)} + T_s\left(\boldsymbol{E_s}^* + B\boldsymbol{i_s(k)}\right) \tag{7.2}$$

$$\boldsymbol{E_s}^* = \frac{\boldsymbol{\lambda_s}^* - \boldsymbol{\lambda_s(k)}}{T_s} - B\boldsymbol{i_s(k)} \tag{7.3}$$

Now the limited possible discrete VVs are to be identified based on reference voltage space vector to reduce the number of computations required for prediction and cost-function

evaluation in each sample time. This study aims at maximum reduction of prediction VVs selection, which is based on voltage space vector α-β plane partitions into number of sectors. The voltage space vector plane is partitioned into 12 sectors i.e. sector-1 to 12 having the span of 30^0 each. These sectors are further subdivided into two equal parts named as (a) and (b) as presented in Figure 7.2, to identify the specific location of $\boldsymbol{E_s}^*$ within the sector. The determined reference voltage space vector ($\boldsymbol{E_s}^*$) ensures combined control of flux and torque, since it is calculated from (7.2) to maintain the closeness of predicted ($\boldsymbol{\lambda_s}(k+1)$) and reference ($\boldsymbol{\lambda_s}^*$) SFSV. Hence, instead of selecting all the possible discrete prediction VVs for modified cost-function evaluation (7.1), the only limited prediction VVs which falls in the vicinity of $\boldsymbol{E_s}^*$ are considered in every sample period.

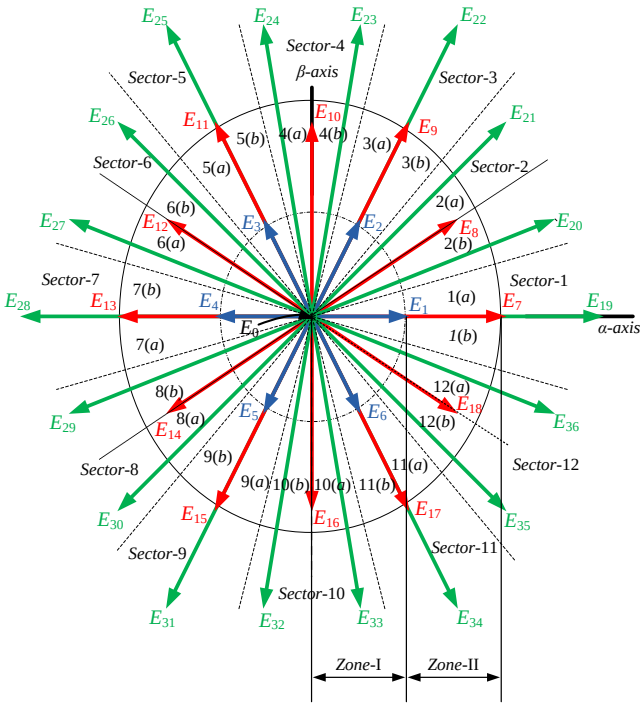

Figure 7.2 Voltage space vector α-β plane divisions

The determined reference voltage space vector magnitude and angle information gives the position in a sector (S_n) under which it falls. Now, to identify the level of VVs (null, blue-small VVs, red-medium VVs and green-large VVs) in the vicinity of $\boldsymbol{E_s}^*$, the voltage space vector plane is divided into two zones in magnitude wise, such as zone-I with 0 to (2/9)E_{dc} and zone-II with (2/9)E_{dc} to (4/9)E_{dc} as shown in Figure 7.2. In a subsector, if the amplitude of $\boldsymbol{E_s}^*$ falls in zone-I, only null and small VVs are considered and as per the situation existing either two or three of them are chosen, that are nearer to $\boldsymbol{E_s}^*$. If $\boldsymbol{E_s}^*$ falls in zone-II, the small and medium VVs are considered, as per the prevailing situation either three or four VVs are picked up which are nearer to $\boldsymbol{E_s}^*$. Similarly, if $\boldsymbol{E_s}^*$ falls above zone-II, the medium and large

VVs are considered, in any situation four VVs are chosen that are nearer to $\boldsymbol{E_s}^*$. These set of limited chosen VVs in the vicinity of $\boldsymbol{E_s}^*$ participate in cost-function evaluation process and the finalized optimal VV from cost-function evaluation ensures combined control of flux and torque, which also represents most nearer to $\boldsymbol{E_s}^*$ when compared to the other limited VVs.

Consider an instant as shown in Figure 7.3, where the reference voltage space vector is in sector-1(b) and its magnitude is 0 to (2/9)E_{dc} (i.e. magnitude of $\boldsymbol{E_s}^*$ falls in zone-I).

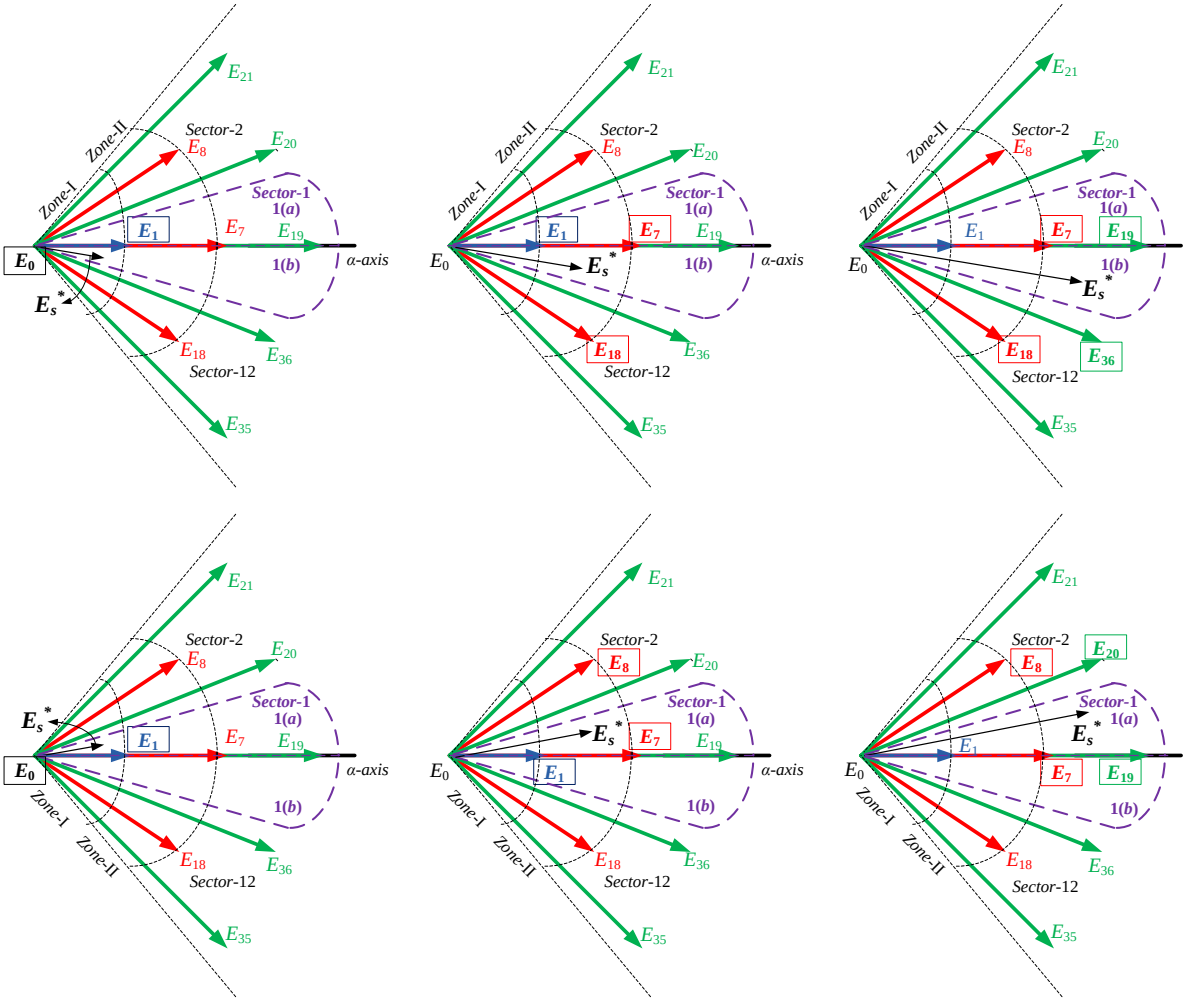

Figure 7.3 Limited VVs set selection for various situations when $\boldsymbol{E_s}^*$ is in sector-1(b) and sector-1(a)

In this scenario, the possible VVs set in the vicinity of $\boldsymbol{E_s}^*$ are selected as E_0 and E_1, forming set of two limited VVs. In the same sector-1(b) location, if the $\boldsymbol{E_s}^*$ magnitude is in the range of (2/9)E_{dc} to (4/9)E_{dc} (i.e. magnitude of $\boldsymbol{E_s}^*$ falls in zone-II), the possible VVs set in the vicinity of $\boldsymbol{E_s}^*$ are selected as E_1, E_7 and E_{18}. Therefore, set of three limited VVs are formed. Similarly, if the $\boldsymbol{E_s}^*$ magnitude falls above (4/9)E_{dc} (i.e. magnitude of $\boldsymbol{E_s}^*$ falls above zone-II), the possible VVs set is considered as E_7, E_{18}, E_{19}, and E_{36} forming set of four limited

VVs. The similar cases are also represented in Figure 7.3 considering $\boldsymbol{E_s}^*$ in sector-1(a). Therefore, when $\boldsymbol{E_s}^*$ is located in sector-1, the possible number of limited VVs are 2, 3 and 4 depending on $\boldsymbol{E_s}^*$ amplitude. In every instant, the selected possible limited VVs set is provided for cost function evaluation. From the cost-function evaluation, the optimal VV is finalized which indicates most nearer to $\boldsymbol{E_s}^*$ and applied for next sample interval for combined flux and torque control.

Figure 7.4 represents the case for limited VVs selection when $\boldsymbol{E_s}^*$ is located in sector-2. In all these instants, the selected set of VVs in the vicinity of $\boldsymbol{E_s}^*$ are represented by distinctly indicating VV in a box as shown in Figure 7.4. In this sector-2, the possible range of limited VVs number is noticed as three to four. The similar method of limited VVs selection is followed for other sectors also. From the overall observations, it is identified that when $\boldsymbol{E_s}^*$ falls in odd number of sectors, the possible range of limited VVs selection lies among two to four, which is based on $\boldsymbol{E_s}^*$ magnitude. Similarly, when $\boldsymbol{E_s}^*$ falls in even number of sectors, the possible range of limited VVs selection lies among three to four. Therefore, the overall maximum limited VVs selection is four in entire PTC operation. This limited VVs (m) set in every instant is provided for cost-function evaluation to determine optimal VV among them for applying in next sample interval.

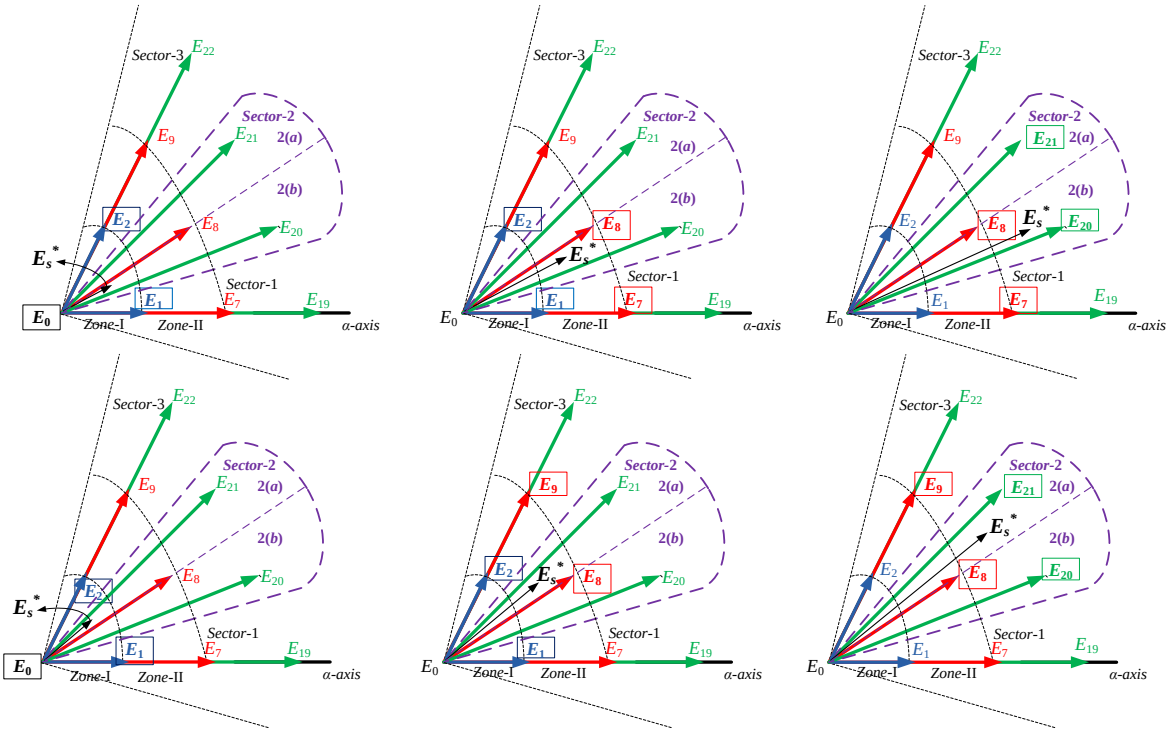

Figure 7.4 Limited VVs set selection for various cases when $\boldsymbol{E_s}^*$ is in sector-2(b) and sector-2(a)

Lastly, it can be stated that the pre selection of limited VVs set in the vicinity of $\boldsymbol{E_s}^*$ for cost-function evaluation process and the finalized optimal VV from cost-function evaluation contributes optimization which is applied for next sample interval. With this, the proposed technique allows an effective reduction of prediction VVs number in PTC operation of four-level OEW-IM drive.

7.2.2 Switching frequency reduction

In conventional PTC technique, only one switching state of VV is utilized for OEW-IM drive operation. However, in dual inverter switching, the null and active VVs can be generated using redundant switching states as mentioned in Table 2.5 of Chapter-2. This redundancy in VVs is utilized in proposed PTC technique to minimize the switching frequency of dual inverter. Based on optimal VV switching states applied in previous sample time, the next applicable optimal VV switching states are to be decided, that are to be applied confirming minimum state transitions between them. To attain this, a separate cost-function (7.4) is considered, which compares previous VV switching combination ($S_{opt}(k\text{-}1)$) with the redundant switching combinations (r) of final optimal VV ($S_{opt}(k)$). The redundant switching combination of optimal VV is selected for which minimum value of cost-function (7.4) is achieved, thus providing minimum switching frequency in proposed PTC operation.

$$S_r = \sum_{i=1}^{6} \left| \left(S_{opt}(k-1) \right)_i - \left(S_{opt}(k)_i \right)_r \right| \tag{7.4}$$

where, subscript i denotes dual-VSI leg number i=1 to 6.

Therefore, switching frequency reduction is achieved for the proposed PTC scheme without including the switching frequency control objective and its weighting factor in main cost-function (7.1).

The overall working process of proposed PTC technique for four-level OEW-IM drive is given below and also presented in Figure 7.5.

Step 1: Measure OEW-IM actual speed (ω_r), stator current ($\boldsymbol{i_s}$), dual VSI DC link voltage (E_{dc}) and optimal VV applied ($\boldsymbol{E_{opt}}$) in previous sample time having switching states of S_{opt}.

Step 2: Estimate present state stator flux space vector using the previous sample instant data such as optimal VV, stator flux and current.

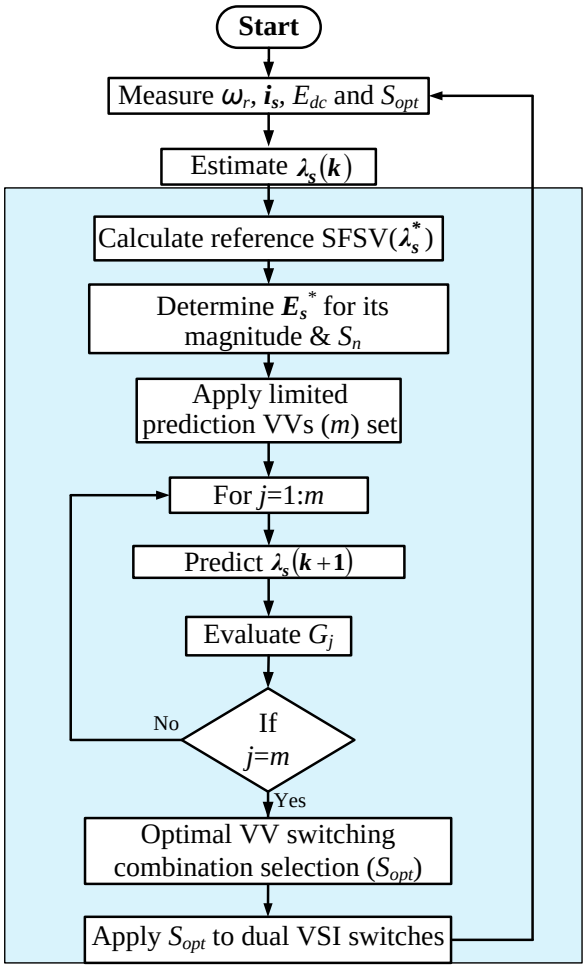

Figure 7.5 Proposed PTC operational process

Step 3: Calculate the reference SFSV ($\boldsymbol{\lambda_s}^*$) and from this the reference voltage space vector ($\boldsymbol{E_s}^*$) is determined.

Step 4: The sector location (S_n) and magnitude of reference voltage space vector are figured out to limit the prediction VVs (m) for reduced computations.

Step 5: Predict stator flux for one step ($\boldsymbol{\lambda_s(k+1)}$) ahead using the identified limited prediction VVs (m) set.

Step 6: Evaluate modified cost-function (7.1) to choose the optimal VV of next sample time for flux and torque ripple reduction.

Step 7: Assess the cost-function (7.4), for selecting optimal VV switching combination to provide minimum switching state transitions.

Step 8: Apply the selected optimal VV having switching states of S_{opt} to dual VSI switches for proposed PTC operation.

Finally, it can be stated that the effective and simplified proposed PTC technique is having less computations, exhibits optimal flux and torque response for OEW-IM drive with reduced switching frequency.

7.3 Results and discussion

The four-level OEW-IM drive performance is tested using existing and proposed PTC techniques in terms of average torque and flux ripples, and switching frequency. Table A.1 represents the parameters of existing OEW-IM on which tests are conducted. In all the practical tests 100 µs sample time is set for existing and proposed PTC executions in digital platform. The conventional PTC is operated with heuristic process of weighting factor value selection. In conventional PTC operation all 37 VVs are provided, whereas for the proposed PTC operation reduced number of VVs are selected based on subsector and magnitude of $\boldsymbol{E_s}^*$.

7.3.1 Experimental results

To validate the effectiveness of proposed PTC over existing PTC technique, various practical tests are performed for both the techniques on four-level OEW-IM drive, and they are presented in this section. The practical test setup is presented in Figure A.4 having Dual VSI and OEW-IM. A DC generator is coupled with OEW-IM shaft and loading the DC generator with resistive load bank, load torque is enforced on shaft. For measuring motor speed, phase currents, dual VSI DC link voltage the measurement devices such as Encoder, LA-25 and LV-25 are used. The existing and proposed PTC techniques are executed in dSPACE-1104 environment. The sensed signals from encoder, LA-25 and LV-25 are linked to dSPACE control board having incremental encoder and ADC channels to realize them in digital platform for PTC operation. The attained control switching states from PTC operation are collected through dSPACE master bit I/O pins which are to connect to dual VSI switches. The complete PTC operations are supervised in dSPACE ControlDesk software.

The investigations are made on steady state flux and torque response at various functioning motor speed conditions. The low motoring reference speed of 200 RPM is given to conventional, proposed PTC and SFSV objective with all 37 possible VVs operated PTC. The exhibited performance of OEW-IM drive such as speed, flux and torque are presented in Figure 7.6(a), Figure 7.6(b) and Figure 7.6(c) when performed with mentioned PTC techniques. Similarly, at high motoring reference speeds of 800 RPM and 1000 RPM, the OEW-IM drive speed, flux and torque response are presented in Figure 7.7(a), Figure 7.7(b)

and Figure 7.7(c) when performed with mentioned PTC techniques. From these comparisons, the optimal flux and torque response is observed in proposed PTC and SFSV objective with all 37 possible VVs operated PTC, which performs weighting factor independent operation. From these results, it can be stated that both the effective limited VVs of proposed PTC and 37 VVs operated PTC with SFSV control objective attain almost similar level of ripples when calculated. This validates effectiveness of reduction in prediction VVs number in proposed PTC operation. Therefore, the proposed PTC is more advantageous than SFSV control objective operated PTC with all 37 possible VVs and conventional PTC technique for OEW-IM drive.

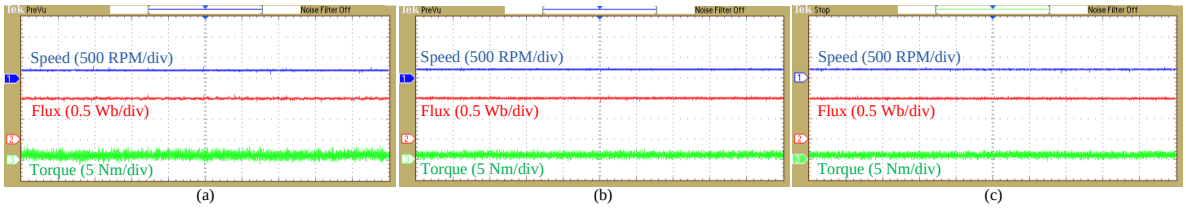

Figure 7.6 Practical response of steady state speed, flux and torque at low speed reference of 200 RPM. (a) Conventional PTC, (b) Proposed PTC and (c) SFSV objective operated PTC with all 37 VVs (X-axis scale- 200 ms/div)

Next, the OEW-IM drive dynamic behaviour is investigated. Using ControlDesk software the reference speed variations are performed during OEW-IM drive operation. The reference speed variations are initiated from 600 RPM to 800 RPM, and at last 800 RPM to 1100 RPM. During this dynamic speed reference variations, the OEW-IM drive performance such as speed, flux and torque are observed when conducted with conventional, proposed PTC and SFSV objective operated PTC with all 37 VVs as presented in Figure 7.8(a), Figure 7.8(b) and Figure 7.8(c).

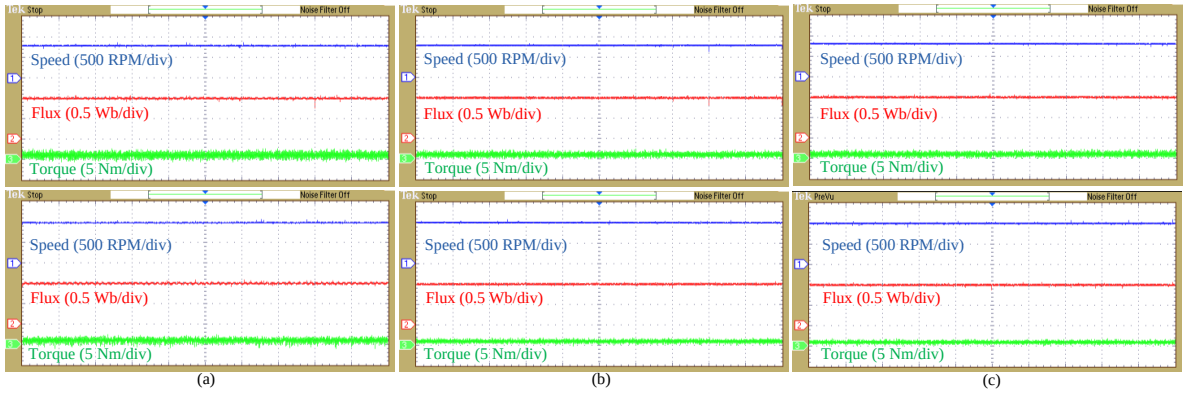

Figure 7.7 Practical response of steady state speed, flux and torque at high speed references of 800 RPM and 1000 RPM. (a) Conventional PTC, (b) Proposed PTC and (c) SFSV objective operated PTC with all 37 VVs (X-axis scale- 200 ms/div)

The OEW-IM drive operation from onward to backward rotation is analysed. For this to perform, sudden variations are made in reference speed from +900 RPM to -900 RPM. The exhibited OEW-IM drive characteristics such as speed, flux and torque when performed with conventional, proposed PTC and SFSV objective operated PTC with all 37 VVs are presented in Figure 7.9(a), Figure 7.9(b) and Figure 7.9(c). From these dynamic speed reference variations, it can be seen that the exhibited dynamic characteristics for proposed PTC technique are almost same as the existing PTC techniques, but with better steady state characteristics when related to conventional PTC.

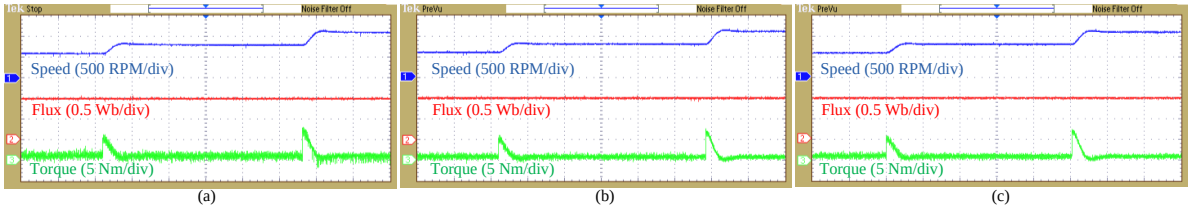

Figure 7.8 Dynamic response of speed, flux and torque with sudden variations in onward reference speeds during practical operation. (a) Conventional PTC, (b) Proposed PTC and (c) SFSV objective operated PTC with all 37 VVs (X-axis scale- 1 s/div)

Now the OEW-IM drive test in the presence of dynamic load torque is performed. By turning on and off the resistive load bank connected to DC generator, the load torque variations on shaft are attained. Here, load torque is suddenly varied from half of the rated motor torque (12.5 Nm) to zero condition during operating speed of 1000 RPM. In this situation, the OEW-IM drive steady state and dynamic characteristics such as speed, flux, torque and current are observed when performed with conventional, proposed PTC and SFSV objective operated PTC with all 37 VVs as presented in Figure 7.10(a), Figure 7.10(b) and Figure 7.10(c). From these results, it can be seen that all the control techniques attain similar dynamic response, but the steady state performance is improved in proposed PTC when related to conventional PTC.

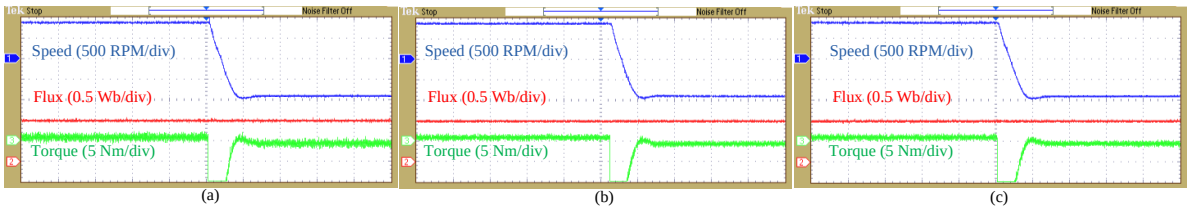

Figure 7.9 Dynamic response of speed, flux and torque with sudden variations in reference speeds from onward (+900 RPM) to backward (-900 RPM) during practical operation. (a) Conventional PTC, (b) Proposed PTC and (c) SFSV objective operated PTC with all 37 VVs (X-axis scale- 1 s/div)

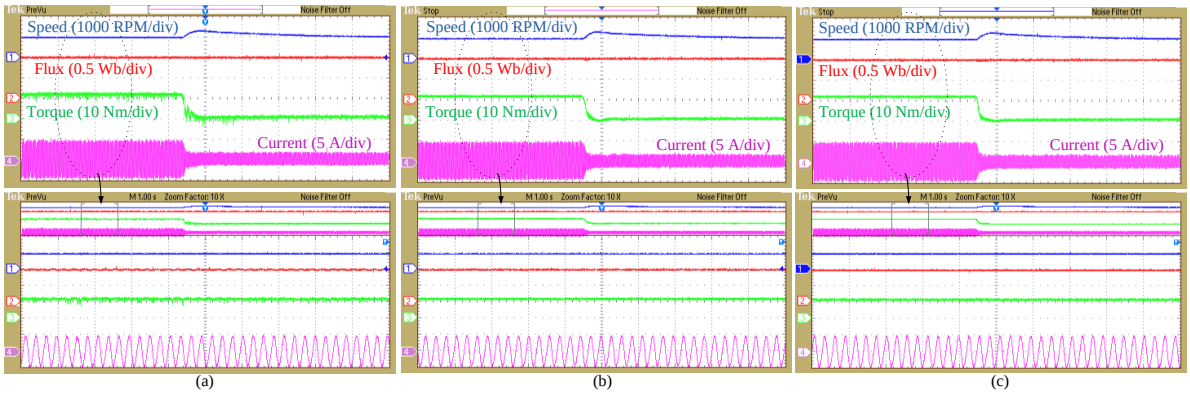

Figure 7.10 Dynamic response of speed, flux, torque and current with sudden variations in load torque during onward rotation (1000 RPM) in practical operation. (a) Conventional PTC, (b) Proposed PTC and (c) SFSV objective operated PTC with all 37 VVs (X-axis scale- 1 s/div)

The tabulation is prepared while comparing average torque and flux ripples when performed with existing and proposed PTC techniques as given in Table 7.1. From these practical results, the following merits of proposed PTC are justified over existing PTC: 1. Enhancement in flux and torque response without weighting factor, 2. The effective limitation of prediction VVs without sacrificing the OEW-IM drive performance that is attained when all the 37 VVs are used in PTC operated with SFSV control objective. Therefore, both the proposed PTC and SFSV objective operated PTC with all 37 VVs attain similar steady state and dynamic response.

The proposed PTC includes the feature of minimum switching state transitions. To justify this, the practical tests are performed at various operating speed conditions. The exhibited average switching frequency response at various speeds are listed when performed with conventional and proposed PTC as presented in Table 7.1. From these results, the reduction in average switching frequency is observed for proposed PTC, thus justified this merit when compared to existing PTC.

Table 7.1 Comparisons of existing and proposed PTC techniques

Speed (RPM)	Conventional PTC			Proposed PTC		
	Torque ripple (Nm)	Flux ripple (Wb)	Switching frequency (Hz)	Torque ripple (Nm)	Flux ripple (Wb)	Switching frequency (Hz)
200	1.401	0.033	2292	1.220	0.020	1244
800	1.260	0.021	2184	1.021	0.015	1826
1000	1.182	0.019	2023	0.810	0.012	1786

As only maximum of 4 limited VVs are involved in prediction and cost-function evaluation of proposed PTC, there is significant reduction in calculations. The computational

times of conventional PTC with 37 prediction VVs and proposed PTC with maximum limited four prediction VVs are observed as 60.93 µs and 28.58 µs. This major reduction in computational time justifies simplicity of proposed PTC when compared to conventional PTC. The average computational times are tabulated for existing and proposed method as given in Table 7.2, when performed real-time experimentations for OEW-IM drive.

Table 7.2 Computational performance evaluation

Terms	**Computational time (µs)**	
	Conventional PTC	**Proposed PTC**
Measurement and estimation	9.95	9.95
Reference SFSV calculation	Nil	10.8
Reference voltage space vector calculation	Nil	1.2
Selection of limited prediction VVs	Nil	1.6
Prediction and Cost-function evaluation	50.98	5.03
Total	60.93	28.58

These overall practical results prove the effectiveness of proposed PTC having the benefits of reduction in prediction VVs number and switching frequency reduction for four-level dual inverter supplied OEW-IM drive implementation.

7.4 Summary

In this chapter, a simplified and effective PTC technique for four-level dual inverter supplied OEW-IM drive is proposed. The following achievements in proposed PTC technique for OEW-IM drive implementation are concluded as: 1. A SFSV control objective is used to eliminate the weighting factor and thereby it's tuning issues. Thus, gaining benefit of optimal flux and torque response with less ripples for OEW-IM drive operation using proposed PTC, 2. The effective reduction in prediction VVs number to maximum of 4 out of 37 is accomplished using reference voltage space vector location. Therefore, simplified proposed PTC with significant reduction in computations is achieved, 3. A reduced switching state transitions by utilizing VV redundant switching states has been developed in proposed PTC

to lessen the switching frequency. Thus, the merit of switching frequency reduction is attained without extra control objective and its weighting factor in main cost-function.

The conducted tests on OEW-IM drive and their results for proposed PTC technique shows overall benefits in terms of enhanced OEW-IM drive steady state torque and flux response, reduced switching frequency and simplicity with reduced computations using effective limited VVs when compared to existing PTC. At the end, it can be stated that the proposed PTC technique is well suitable for four-level dual inverter supplied OEW-IM drive application owing to its attractive benefits.

Chapter 8

Conclusion and Future Scope

Chapter 8
Conclusion and Future Scope

8.1 Introduction

In this thesis, modified Direct Torque Control (DTC) and Predictive Torque Control (PTC) methodologies are implemented for IM drive supplied from two-level and multi-level VSIs. The multi-level VSI operation is exhibited with dual VSI model in three and four level mode. The overall contributions of research works presented in this thesis are designing modified direct torque and predictive torque control strategies, which improves IM drive response in terms of attaining optimal torque and flux response, reduction in switching frequency and simplicity in control operation. In this chapter, the detailed conclusions are presented for this thesis work in section 8.2. The subsequent future scope of these exhibited works is discussed in section 8.3.

8.2 Conclusions

The various control methods for IM drive operation are discussed in Chapter-1. The DTC and PTC schemes are well known for high dynamic performance and simple structure. In addition to this, the motivation for motor drive operation supplied from multi-level VSI is provided. Among the known multi-level VSI structures, the dual VSI configuration tends to have several merits. In this thesis, dual VSI is conducted in three and four level mode for OEWIM drive operation. This is possible by suitable setting of DC link voltage proportion supplied to dual VSI.

To investigate motor drive operations for various control schemes, Chapter-2 presents modelling of motor drive. This includes a discussion on: modelling of two-level VSI and multi-level VSI with dual VSI topology, coordinate frame transformations and dynamic modelling of IM in stationary reference frame.

The OEWIM drive in three-level mode is operated with DTC scheme in Chapter-3, in which equal DC link voltages are fed to dual VSI. The DTC operation for motor drive is explained, where the selection of VV is having direct influence on torque and flux control. The effective possible VVs of total 19 in three-level dual VSI operation are presented. Their participation in DTC operation during low and high speed conditions are given in basic heuristic look-up tables. With these basic look-up tables operated DTC scheme, the following

problems are observed in OEWIM drive operation: high ripple content in torque response, high switching frequency and instability in flux during start-up of motor drive which demands inrush current. To alleviate these pointed issues, a modified look-up tables are generated in proposed DTC operation. These modified look-up tables formation ensures suitable VV selection and avoiding the issues stated in basic DTC operation. This discussion is verified by conducting various tests on three level OEWIM drive and it is justified that the proposed DTC exhibits major improvements in comparison with existing DTC operation.

In Chapter-4, PTC which is one of the modern control methods is exhibited for two-level VSI operated IM drive. The detailed PTC operation with key steps is explained for motor drive supplying from two-level VSI. The discrete mathematical equations of motor drive involved in every step of PTC operation are also presented. From basic PTC operation, it is observed that the weighting factor choice in cost function influence the final voltage vector selection. Therefore, the manual selection of weighting factor needed for effective operation of motor drive is tedious and time taking process. In this chapter, proposed PTC is designed for auto tuning of weighting factor value. The auto tuning of optimal weighting factor is based on minimization of control objective function. This auto tuned weighting factor placed in cost function ensures optimal torque and flux response of motor drive by suitable selection of voltage vector from cost function minimization. The various test results conducted for two-level VSI supplied IM drive verifies the proposed PTC having improved torque and flux performance without any manual tuning as in the case of conventional PTC. Thus, an enhanced PTC with auto tuning feature is designed for two-level VSI supplied IM drive.

In Chapter-5, PTC for four-level dual VSI supplied OEWIM drive is introduced. The dual VSI is functioned with 2:1 DC link voltage proportion, which results in four-level operation. The 37 effective VVs which are the outcome of four-level dual VSI operation are presented. Considering these as prediction VVs, the PTC operation of four-level dual VSI supplied OEWIM drive with main steps involved is explained. Unlike conventional PTC with weighting factor dependent operation, a flux space vector control objective is introduced in proposed PTC for combined flux and torque control of OEWIM drive. Using ranking method, switching frequency objective is also involved without weighting factor in proposed PTC operation. To simplify proposed PTC operation, four-level dual VSI prediction VVs are limited to 20 out of 37 based on stator flux error. From the demonstrated results of proposed PTC in comparison with conventional PTC, it is verified that proposed PTC shows optimal torque and flux control, along with switching frequency limitation.

In Chapter 6, a different approach is introduced for PTC of four-level OEWIM drive operation. The concept of reactive torque is used to replace the flux control objective with reactive torque control. Therefore, cost function is formulated with same units, excluding the necessity of flux weighting factor in cost function. To avail simplicity in proposed PTC operation and further limiting switching frequency, the nearest VV selection strategy is introduced. Thus, its operation requires only limited 12 out of 37 prediction VVs. The various test results are presented for proposed PTC to examine its credibility over conventional PTC such as flux, torque response improvement and switching frequency limitation for four-level OEWIM drive operation.

Finally, in Chapter 7 an effective PTC technique for four-level OEWIM drive is proposed, where the proposed PTC scheme is executed with effective limited prediction VVs of maximum 4 out of 37. The determined limited prediction VVs in every sample interval participates in cost function in which stator flux objective is used, to identify optimal one. Hence, combined flux and torque control without weighting factor is gained along with significant reduction in prediction VVs for proposed PTC operation of four-level OEWIM drive. The redundancy in dual VSI switching states is used to derive the benefit of switching frequency limitation. By observing overall test results it can be justified that the exhibited OEWIM drive response for proposed PTC with less computations gain superior nature in terms of reduction in flux and torque ripples, switching frequency reduction without weighting factors when related to conventional PTC.

At the end, it can be stated that the thesis presents a modified DTC and PTC strategies for IM drive supplied from two-level and multi-level VSIs.

8.3 Future scope

From the presented modified DTC and PTC schemes for IM drive in this thesis, the scope for future work is identified. They are as follows:

1. The proposed DTC and PTC schemes are exhibited with speed sensor i.e. Incremental Encoder. By incorporating Model Reference Adaptive Systems (MRAS) or full order based observers, the proposed control schemes can be extended for speed sensorless applications as future work.

2. The DTC operation is less parameter sensitive than PTC. In PTC operation, the entire system is mathematically modelled as such it is high parameter sensitive, because it is model based control. Therefore, the proposed control schemes can be extended to make the operation less sensitive to parameter variations. This can be considered as another area for research.
3. The proposed control schemes for IM drive are functioned at variable switching frequency. The research can be extended for achieving constant switching frequency IM drive.

Appendix-A
Experimental Test Setup

In this section, a detailed description of experimental test setup used for execution of control schemes (i.e. DTC and PTC) for IM drive is presented. As this thesis deals with two-level and multi-level inverter supplied IM drives, their real time operational block diagrams are presented in Figure A.1 and Figure A.2 respectively. In the case of two-level IM drive configuration, a single VSI is used for supplying to IM. On the other hand, the multi-level IM drive constitutes the dual VSI supplied to OEWIM model.

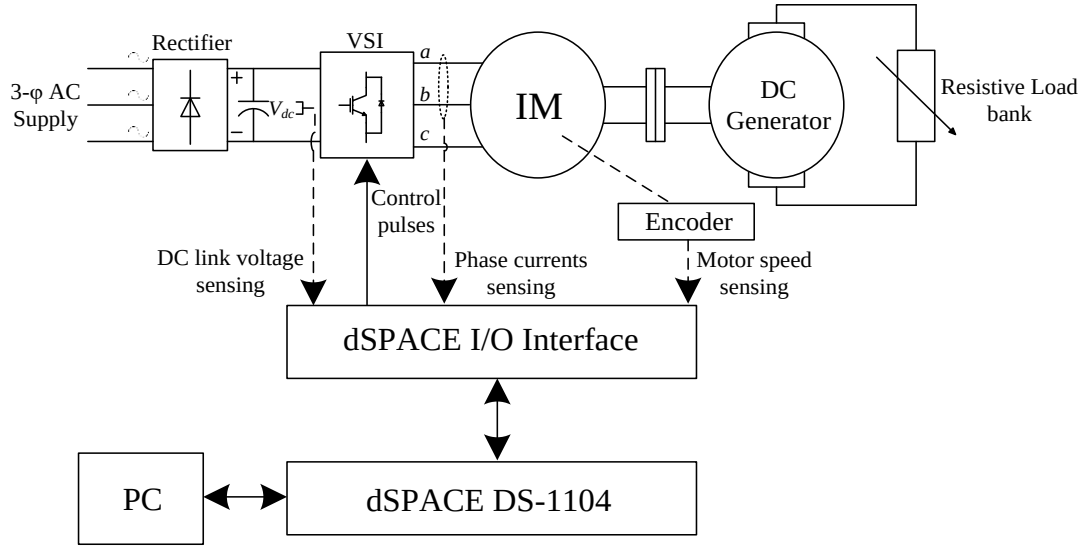

Figure A.1 Block diagram of two-level VSI supplied IM drive

Figure A.2 indicates generalized block diagram of dual VSI supplied OEWIM drive, through which either three or four level inverter drive operation is attained. The DC link voltages of dual two-level VSIs (i.e. VSI-1 and VSI-2) are supplied from two individual three phase full bridge diode rectifiers. From secondary side of three phase isolation transformers, the AC input supply is provided to full bridge diode rectifiers. To achieve three-level dual inverter fed OEWIM drive operation, the three phase diode bridge rectifies are supplied with equal AC voltage tapings. With this arrangement, equal DC link voltages are maintained for both VSIs, which facilitates three-level dual inverter operation. Whereas, to attain four-level dual inverter fed OEWIM drive operation, the AC input supply provided to full bridge diode rectifier of VSI-1 is tapped two times that of AC input supply provided to full bridge diode rectifier of VSI-2. Therefore, DC supply input to VSI-1 is two times of DC supply input to VSI-2, which facilitates four-level dual inverter operation.

The experimental setup photographs for two-level VSI fed IM drive and dual VSI fed OEWIM drive (for multi-level operation) are shown in Figure A.3 and Figure A.4 respectively, in which the hardware requirements for experimentation are presented.

The existing IM specifications are listed in Table A.1. The IM shaft is coupled with DC machine and its ratings are listed in Table A.1. The DC machine as generator acts in the form of load for IM, when its armature winding is connected to resistive load bank. By varying resistive load tapings, the different load torques on IM shaft can be applied. The IM is supplied from VSI. The three-phase VSI specifications with IGBT module are listed in Table A.2.

Using digital signal processing and control engineering (dSPACE-DS1104) platform, all the experimentations are conducted. For this, the Peripheral Component Interconnect (PCI) slot in host Personal Computer (PC) is interfaced with DS1104. While installing dSPACE software, the existing MATLAB can be associated to it. Every time, when MATLAB starts, the dSPACE software gets configure and displays Real Time Interface (RTI) DS1104 platform activation in MATLAB command window. The control schemes for IM drive are implemented in MATLAB/Simulink and built in dSPACE-1104 model which is interfaced to host PC.

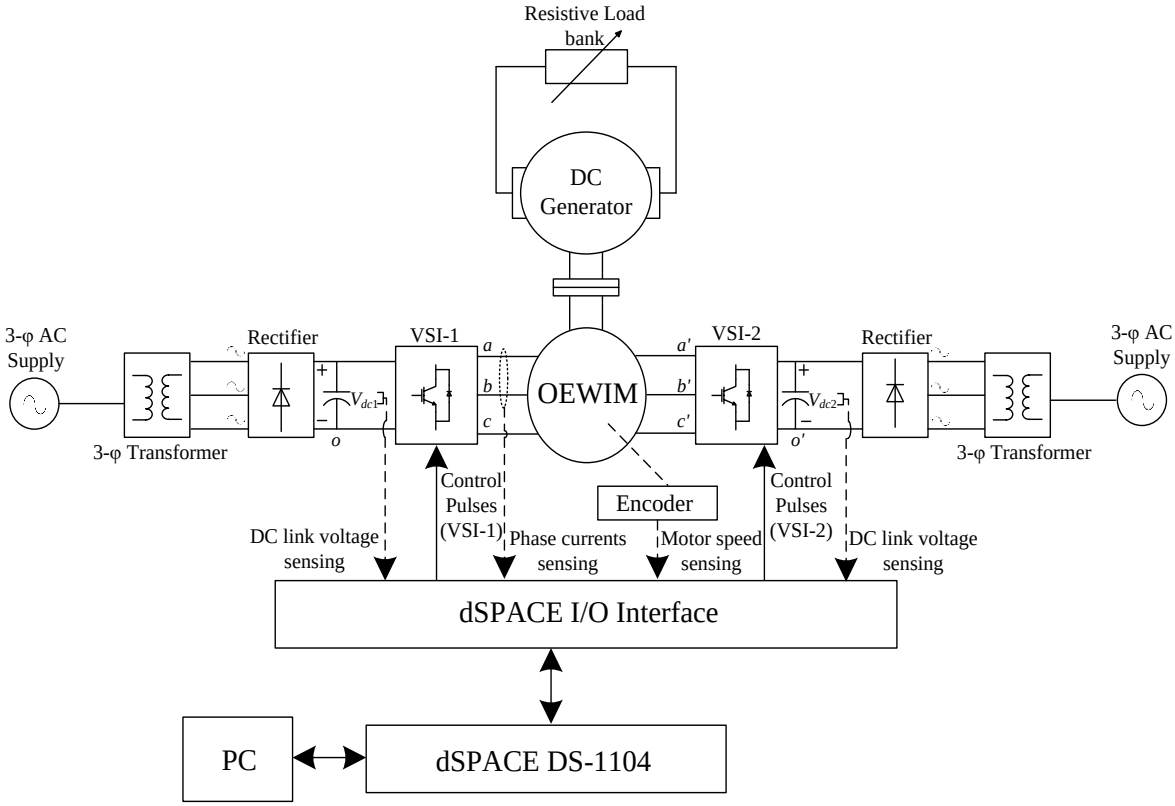

Figure A.2 Block diagram of dual VSI supplied OEWIM drive

The dSPACE Input Output (I/O) interface facilitates the required inputs for execution of control schemes and the control outputs from control schemes to drive IM. The essential input variables for the control operation are IM speed, phase currents and DC link voltage of VSI. The incremental encoder having Pulses per Revolution (PPR)- 1024 is used for sensing actual speed of IM. The output signals (A, B and Z-index) from this encoder are interfaced to dSPACE Incremental Encoder channel 1. From DS1104 library, the Encoder block (DS1104ENC_POS_C1, ENC_SETUP) is accessed. With this, the actual IM speed is gained to provide for control operation. To sense IM phase currents (i_a & i_b) and VSI's DC link voltage, the LEM sensors are used. For sensing currents, the sensor model LA 25-NP (as presented in Figure A.5) is used. The voltage sensor of model LV 25-P (as presented in Figure A.5) is used for sensing DC link voltage of VSI. These current and voltage sensor specifications are mentioned in Table A.3. Through dSPACE RTI blocks such as ADCs, the sensed signals from these sensors can be gained and given for control operation. Finally, with these inputs provided for control operation, the control outputs such as switching states for VSI fed IM drive are derived. These are interfaced with dSPACE RTI blocks named as Master Bit Out pins for accessing in real time and connecting to hardware setup.

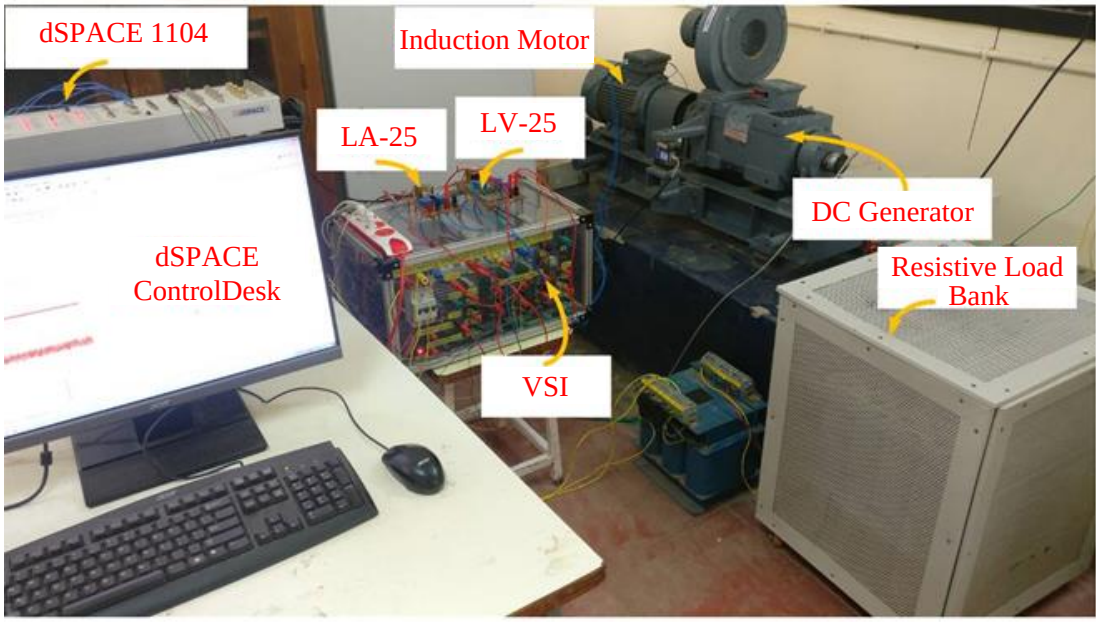

Figure A.3 Test bench setup of IM drive supplied from two-level VSI

After the successful setting up of control algorithm and dSPACE interfacing in Simulink, the entire model is build. With this, the code generation and compilation starts for the build model. Finally, the file name with .sdf extension (system description file) is loaded to DS1104 platform. This completes building process. The other software linked with

dSPACE experiment is ControlDesk, which facilitates measurement and adjusting variables in real time. For this, the generated variable description file (.sdf) is imported to ControlDesk. Therefore, the entire control operation of VSI fed IM drive can be monitored. Additionally, the reference speed variable can be altered in real time to check the speed dynamics for control operation. The experimental illustrations for all discussed control schemes are delivered in above chapters. This is about hardware information for the provided experimentations.

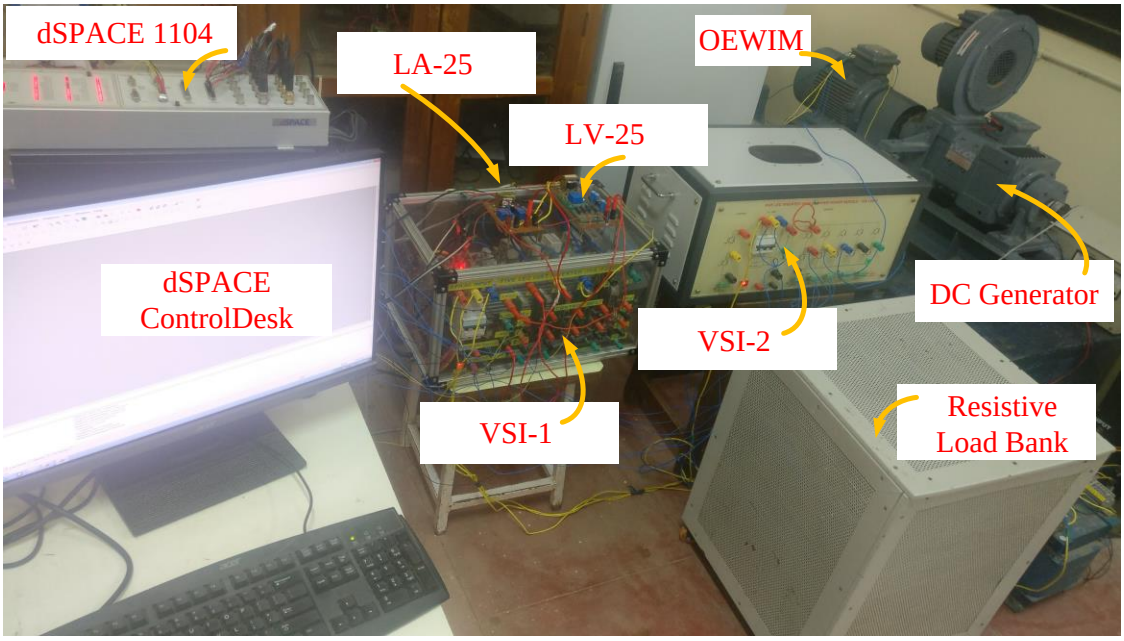

Figure A.4 Test bench setup of OEWIM drive supplied from dual VSI

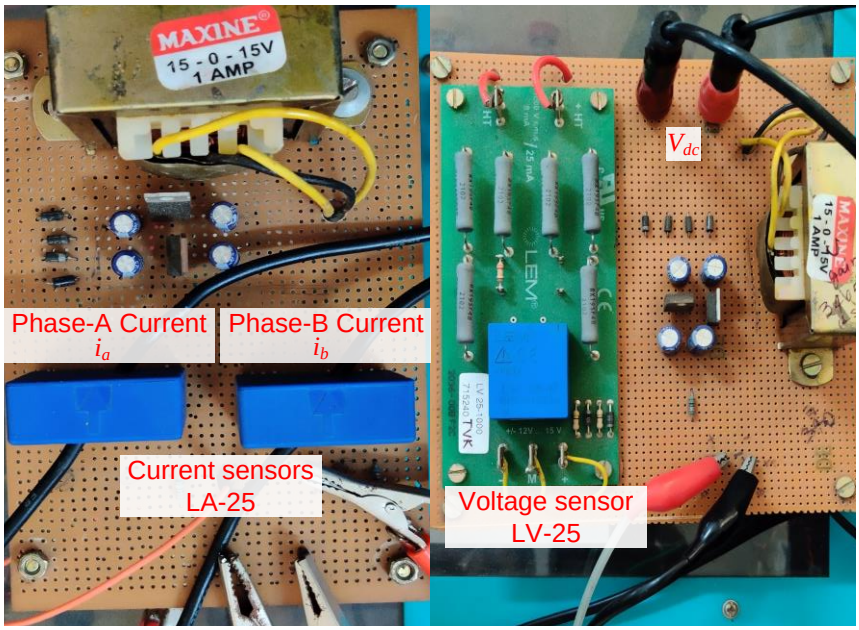

Figure A.5 Current and voltage sensors

Table A.1 Experimental setup specifications

IM specifications	
Parameter	**Value**
Stator Resistance (R_s)	1.8 Ω
Rotor Resistance (R_r)	0.8 Ω
Stator Inductance (L_s)	0.54 H
Rotor Inductance (L_r)	0.54 H
Mutual Inductance (L_m)	0.512 H
Rated speed (N_{rated})	1440 RPM
Rated power	3.7 kW
Poles (P)	4
Rated voltage (Line-Line)	415 V
Rated current (Line)	7.54 A
Inertia (J)	0.031 kg-m^2
Rated flux	1 Wb
Load (DC machine) specifications	
Rated power	3.7 kW
Rated speed	1440 RPM
Rated torque	24.5 Nm

Table A.2 VSI specifications

Switch model	IGBT- SKM75gb12t4
Voltage rating	1200 V
Current rating	75 A
DC link capacitor	4700 µF/ 2 × 450 V

Table A.3 Voltage and current sensor specifications

LV-25 Voltage sensing board	
Supply voltage	± 15 V
Maximum voltage	1000 V
LA-25 Current sensing board	
Supply voltage	± 15 V
Maximum current	25 A

References

[1] Hughes A and Drury W, *Electric motors and drives: fundamentals, types and applications.* Newnes, 2013.

[2] Kirtley JL and Beaty HW, *Electric motor handbook*. McGraw-Hill Professional Publishing, 1998.

[3] Krishnan R, *Electric motor drives: modeling, analysis, and control*. Prentice Hall, 2001.

[4] Rashid MH, *Power electronics handbook*. Butterworth-Heinemann, 2017.

[5] Hudgins J. L and De Doncker R. W, "Power Semiconductor Devices: For Variable Speed Drives," in *IEEE Industry Applications Magazine*, vol. 18, no. 4, pp. 18-25, Jul.-Aug. 2012.

[6] Chau KT, *Electric vehicle machines and drives: design, analysis and application*. John Wiley & Sons, 2015.

[7] Sen P. C, *Principles of Electric Machines and Power Electronics*. Wiley, 1988.

[8] Sen P. C, *Thyristor DC Drives*. Wiley Interscience, 1981.

[9] Bose BK, "Power electronics and motor drives recent progress and perspective," in *IEEE Transactions on Industrial Electronics*, vol. 56, no. 2, pp. 581-588, Feb. 2009.

[10] Yano M, Abe S and Ohno E, *Historical review of power electronics for motor drives in Japan.* IPEC-Niigata, Special Talks, 2005.

[11] Bose Bimal K, *Modern power electronics and AC drives*. Prentice Hall, 2002.

[12] Sen P. C, "Electric motor drives and control-past, present, and future," in *IEEE Transactions on Industrial Electronics*, vol. 37, no. 6, pp. 562-575, Dec. 1990.

[13] Abu-Rub H, Iqbal A, Guzinski J, *High performance control of AC drives with MATLAB/Simulink models*. John Wiley & Sons, 2012.

[14] Patil MB, Ramanarayanan V, Ranganathan VT, *Simulation of power electronic circuits*. Narosa, 2009.

[15] Peter Vas, *Sensorless vector and direct torque control*. Oxford University Press, 1998.

[16] Marino R, Peresada S and Valigi P, "Adaptive input-output linearizing control of induction motors," in *IEEE Transactions on Automatic Control*, vol. 38, no. 2, pp. 208-221, Feb. 1993.

[17] Cruz P, Gallegos M. A, Alvarez R and Pazos F, “Comparison of several nonlinear controllers for induction motors,” in *9th IEEE International Power Electronics Congress*, Mexico, pp. 134-139, 2004.

[18] Blaschke F, “The principle of field-orientation as applied to the transvector closed-loop control system for rotating-field machines,” in *Siemens Review*, vol. 34, no. 3, pp. 217- 220, 1972.

[19] Sathikumar S and Vithayathil J, “Digital simulation of field-oriented control of induction motor,” in *IEEE Transactions on Industrial Electronics*, vol. IE-31, no. 2, pp. 141-148, May 1984.

[20] Takahashi I and Noguchi T, “A new quick-response and high-efficiency control strategy of an induction motor,” in *IEEE Transactions on Industry Applications*, vol. IA-22, no. 5, pp. 820-827, Sep. 1986.

[21] Casadei D, Profumo F, Serra G and Tani A, “FOC and DTC: two viable schemes for induction motors torque control,” in *IEEE Transactions on Power Electronics*, vol. 17, no. 5, pp. 779-787, Sep. 2002.

[22] Korkmaz F, Topaloğlu İ, Çakir M. F and Gürbüz R, “Comparative performance evaluation of FOC and DTC controlled PMSM drives,” in *4th International Conference on Power Engineering, Energy and Electrical Drives*, pp. 705-708, Istanbul, May 2013.

[23] Niu F, Wang B, Babel A. S, Li K and Strangas E. G, “Comparative Evaluation of Direct Torque Control Strategies for Permanent Magnet Synchronous Machines,” in *IEEE Transactions on Power Electronics*, vol. 31, no. 2, pp. 1408-1424, Feb. 2016.

[24] Camacho E. F and Bordons C, *Model predictive control*. Springer, 2004.

[25] Maciejowski J. M, *Predictive control with constraints*. Prentice Hall, 2002.

[26] Rodriguez J and Cortes P, *Predictive control of power converters and electrical drives*. Wiley, 2012.

[27] Wang F, Zhang Z, Mei X, Rodríguez J, Kennel R, “Advanced control strategies of induction machine: Field oriented control, direct torque control and model predictive control,” in *Energies*. vol. 11, no. 1, pp. 1-13, Jan. 2018.

[28] Kouro S et al., “Recent Advances and Industrial Applications of Multilevel Converters,” in *IEEE Transactions on Industrial Electronics*, vol. 57, no. 8, pp. 2553-2580, Aug. 2010.

[29] Kouro S, Rodriguez J, Wu B, Bernet S and Perez M, “Powering the Future of Industry: High-Power Adjustable Speed Drive Topologies,” in *IEEE Industry Applications Magazine*, vol. 18, no. 4, pp. 26-39, Jul.-Aug. 2012.

[30] Rodriguez J, Jih-Sheng Lai and Fang Zheng Peng, "Multilevel inverters: a survey of topologies, controls, and applications," in *IEEE Transactions on Industrial Electronics*, vol. 49, no. 4, pp. 724-738, Aug. 2002.

[31] Gupta K. K, Ranjan A, Bhatnagar P, Sahu L. K and Jain S, "Multilevel Inverter Topologies with Reduced Device Count: A Review," in *IEEE Transactions on Power Electronics*, vol. 31, no. 1, pp. 135-151, Jan. 2016.

[32] Mittal N, Singh B, Singh S. P, Dixit R and Kumar D, "Multilevel inverters: A literature survey on topologies and control strategies," in *2nd International Conference on Power, Control and Embedded Systems*, Allahabad, pp. 1-11, Dec. 2012.

[33] Lakhimsetty S and Somasekhar V. T, "A Four-Level Open-End Winding Induction Motor Drive with a Nested Rectifier-Inverter Combination with Two DC Power Supplies," in *IEEE Transactions on Power Electronics*, vol. 34, no. 9, pp. 8894-8904, Sep. 2019.

[34] Reddy B. V and Somasekhar V. T, "A Dual Inverter Fed Four-Level Open-End Winding Induction Motor Drive with a Nested Rectifier-Inverter," in *IEEE Transactions on Industrial Informatics*, vol. 9, no. 2, pp. 938-946, May 2013.

[35] Lakhimsetty S, Surulivel N and Somasekhar V. T, "Improvised SVPWM Strategies for an Enhanced Performance for a Four-Level Open-End Winding Induction Motor Drive," in *IEEE Transactions on Industrial Electronics*, vol. 64, no. 4, pp. 2750-2759, Apr. 2017.

[36] Telford D, Dunnigan M. W and Williams B. W, "A comparison of vector control and direct torque control of an induction machine," in *IEEE 31st Annual Power Electronics Specialists Conference*. Ireland, vol. 1, pp. 421-426, 2000.

[37] Zhong L, Rahman M. F, Hu W. Y and Lim K. W, "Analysis of direct torque control in permanent magnet synchronous motor drives," in *IEEE Transactions on Power Electronics*, vol. 12, no. 3, pp. 528-536, May 1997.

[38] Habetler T. G, Profumo F, Pastorelli M and Tolbert L. M, "Direct torque control of induction machines using space vector modulation," in *IEEE Transactions on Industry Applications*, vol. 28, no. 5, pp. 1045-1053, Sep.-Oct. 1992.

[39] Vinay Kumar Thippiripati and Srinivasa Rao Sandepudi, "Hardware Implementation of Direct Load Angle Controlled Induction Motor Drive," in *Electric Power Components and Systems*, vol. 42, no. 14, pp. 1505-1516, Oct. 2014.

[40] Abosh A. H, Zhu Z. Q and Ren Y, "Reduction of Torque and Flux Ripples in Space Vector Modulation-Based Direct Torque Control of Asymmetric Permanent Magnet Synchronous Machine," in *IEEE Transactions on Power Electronics*, vol. 32, no. 4, pp. 2976-2986, Apr. 2017.

[41] Lee K and Blaabjerg F, “Sensorless DTC-SVM for Induction Motor Driven by a Matrix Converter Using a Parameter Estimation Strategy,” in *IEEE Transactions on Industrial Electronics*, vol. 55, no. 2, pp. 512-521, Feb. 2008.

[42] D. Casadei, G. Serra and K. Tani, “Implementation of a direct control algorithm for induction motors based on discrete space vector modulation,” in *IEEE Transactions on Power Electronics*, vol. 15, no. 4, pp. 769-777, Jul. 2000.

[43] Kumar V and Rao S, “Modified direct torque control of three phase induction motor drives with low ripple in flux and torque,” in *Leonardo Journal of Sciences*. Vol. 10, no. 18, pp. 27-44, Jan. 2011.

[44] Kang J. K and Sul S. K, “New direct torque control of induction motor for minimum torque ripple and constant switching frequency,” in *IEEE Transactions on Industry Applications*, vol. 35, no. 5, pp. 1076-1082, Sep. 1999.

[45] Adamidis G, Koutsogiannis Z and Vagdatis P, “Investigation of the Performance of a Variable-speed Drive Using Direct Torque Control with Space Vector Modulation,” in *Electric Power Components and Systems*, vol. 39, no. 12, pp. 1227-1243, Aug. 2011.

[46] Shyu K. K, Lin J. K, Pham V. T, Yang M. J and Wang T. W, “Global minimum torque ripple design for direct torque control of induction motor drives,” in *IEEE Transactions on Industrial Electronics*, vol. 57, no. 9, pp. 3148-3156, Sep. 2010.

[47] Abdalla T. Y, Hairik H. A and Dakhil A. M, “Minimization of torque ripple in DTC of induction motor using fuzzy mode duty cycle controller,” in *1st International Conference on Energy, Power and Control (EPC-IQ)*, Basrah, pp. 237-244, Nov. 2010.

[48] Niu F et al., “A Simple and Practical Duty Cycle Modulated Direct Torque Control for Permanent Magnet Synchronous Motors,” in *IEEE Transactions on Power Electronics*, vol. 34, no. 2, pp. 1572-1579, Feb. 2019.

[49] Venkataramana Naik N and Singh S. P, “Improved Torque and Flux Performance of Type-2 Fuzzy-based Direct Torque Control Induction Motor Using Space Vector Pulse-width Modulation,” in *Electric Power Components and Systems*, vol. 42, no. 6, pp. 658-669, Apr. 2014.

[50] Okumus H. I and Aktas M, “Direct torque control of induction machine drives using adaptive hysteresis band for constant switching frequency,” in *IEEE International Electric Machines and Drives Conference*, vol. 2, pp. 1762–1767, May 2007.

[51] Kang J. K, Chung D. W and Sul S. K, “Direct torque control of induction machine with variable amplitude control of flux and torque hysteresis bands,” in *International Electric Machines and Drives Conference*, pp. 640–642, May 1999.

[52] Hafeez M, Uddin M. N, Rahim N. A and Ping H. W, "Self-Tuned NFC and Adaptive Torque Hysteresis-Based DTC Scheme for IM Drive," in *IEEE Transactions on Industry Applications*, vol. 50, no. 2, pp. 1410-1420, Mar.-Apr. 2014.

[53] Noguchi T, Yamamoto M, Kondo S and Takahashi I, "Enlarging switching frequency in direct torque-controlled inverter by means of dithering," in *IEEE Transactions on Industry Applications*, vol. 35, no. 6, pp. 1358-1366, Nov.-Dec. 1999.

[54] Noguchi T, Yamamoto M, Kondo S and Takahashi I, "High frequency switching operation of PWM inverter for direct torque control of induction motor," in *IEEE Industry Applications Conference Thirty-Second IAS Annual Meeting*, vol. 1, pp. 775-780, Oct. 1997.

[55] Ambrozic V, Buja G. S and Menis R, "Band-constrained technique for direct torque control of induction motor," in *IEEE Transactions on Industrial Electronics*, vol. 51, no. 4, pp. 776-784, Aug. 2004.

[56] Metidji B, Taib N, Baghli L, Rekioua T and Bacha S, "Low-Cost Direct Torque Control Algorithm for Induction Motor Without AC Phase Current Sensors," in *IEEE Transactions on Power Electronics*, vol. 27, no. 9, pp. 4132-4139, Sep. 2012.

[57] Cirrincione M, Pucci M, Vitale G and Cirrincione G, "A new direct torque control strategy for the minimization of common-mode emissions," in *IEEE Transactions on Industry Applications*, vol. 42, no. 2, pp. 504-517, Mar.-Apr. 2006.

[58] Fatma Ben Salem and Nabil Derbel, "Direct Torque Control of Induction Motors Based on Discrete Space Vector Modulation Using Adaptive Sliding Mode Control," in *Electric Power Components and Systems*, vol. 42, no. 14, pp. 1598-1610, Oct. 2014.

[59] Alsofyani I. M and Idris N. R. N, "Simple flux regulation for improving state estimation at very low and zero speed of a speed sensorless direct torque control of an induction motor," in *IEEE Transactions on Power Electronics*, vol. 31, no. 4, pp. 3027–3035, Jun. 2016.

[60] Idris N. R. N and Yatim A. H. M, "Direct torque control of induction machines with constant switching frequency and reduced torque ripple," in *IEEE Transactions on Industrial Electronics*, vol. 51, no. 4, pp. 758-767, Aug. 2004.

[61] Alsofyani I. M, Idris N. R. N, Alamri Y. A, Anbaran S. A, Wangsupphaphol A and Low W. Y, "Improved EKF-based direct torque control at the start-up using constant switching frequency," in *IEEE Conference on Energy Conversion (CENCON)*, Johor Bahru, pp. 237-242, 2014.

[62] Alsofyani I. M, Idris N. R. N and Lee K, "Dynamic Hysteresis Torque Band for Improving the Performance of Lookup-Table-Based DTC of Induction Machines," in *IEEE Transactions on Power Electronics*, vol. 33, no. 9, pp. 7959-7970, Sep. 2018.

[63] Buja G. S and Kazmierkowski M. P, “Direct torque control of PWM inverter-fed AC motors - a survey,” in *IEEE Transactions on Industrial Electronics*, vol. 51, no. 4, pp. 744-757, Aug. 2004.

[64] Sutikno T, Idris N. R. N and Jidin A, “A review of direct torque control of induction motors for sustainable reliability and energy efficient drives,” in *Elsevier publications, Renewable and Sustainable Energy Reviews*, vol. 32, pp. 548-558, Apr. 2014.

[65] Sadeghi A, Mohamadian M, Shahparasti M and Fatemi A, “A new switching algorithm for voltage balancing of a three-level NPC in DTC drive of a three-phase IM,” in *Twenty-Eighth Annual IEEE Applied Power Electronics Conference and Exposition (APEC)*, Long Beach, CA, pp. 489-495, Mar. 2013.

[66] Payami S, Behera R. K and Iqbal A, “DTC of Three-Level NPC Inverter Fed Five-Phase Induction Motor Drive with Novel Neutral Point Voltage Balancing Scheme,” in *IEEE Transactions on Power Electronics*, vol. 33, no. 2, pp. 1487-1500, Feb. 2018.

[67] Ismail H et al., “Direct Torque Control of induction machine using 3-level neutral point clamped inverter,” in *IEEE Student Conference on Research and Development (SCOReD)*, Kuala Lumpur, pp. 571-576, Dec. 2015.

[68] Naik V, Panda A and Singh SP, “A three-level fuzzy-2 DTC of induction motor drive using SVPWM,” in *IEEE Transactions on Industrial Electronics*, vol. 63, no. 3, pp. 1467-1479, Mar. 2016.

[69] Nair R, Jidin A, Othman M. N, Jopri M. H and Manap M, “Comparison performance of 3-Level and 5-Level Cascaded H-Bridge multilevel inverter of DTC of Induction Machine,” in *International Conference on Electrical Machines and Systems (ICEMS)*, Busan, pp. 2100-2104, Oct. 2013.

[70] Kumar T. V, and Rao S. S, “Direct torque controlled induction motor drive based on cascaded three two-level inverters,” in *International Journal of Modelling and Simulation*, vol. 34, no. 2, pp. 70–82, Jan. 2014.

[71] Kirankumar B, Siva Reddy Y. V and Vijayakumar M, “Multilevel inverter with space vector modulation: intelligence direct torque control of induction motor,” in *IET Power Electronics*, vol. 10, no. 10, pp. 1129-1137, Apr. 2017.

[72] Escalante M. F, Vannier J and Arzande A, “Flying capacitor multilevel inverters and DTC motor drive applications,” in *IEEE Transactions on Industrial Electronics*, vol. 49, no. 4, pp. 809-815, Aug. 2002.

[73] Ortega C, Arias A, Caruana C, Balcells J and Asher G, “Improved waveform quality in the direct torque control of matrix-converter-fed PMSM drives,” in *IEEE Transactions on Industrial Electronics*, vol. 57, no. 6, pp. 2101–2110, Jun. 2010.

[74] Yan Y, Zhao J, Xia C and Shi T, "Direct torque control of matrix converter-fed permanent magnet synchronous motor drives based on master and slave vectors," in *IET Power Electronics*, vol. 8, no. 2, pp. 288-296, Feb. 2015.

[75] Lara J, Guzman V, Restrepo J, Gimenez M. I and Cabello A, "Matrix converter induction motor drive with DTC-based fuzzy control," in *42nd International Universities Power Engineering Conference*, Brighton, pp. 1115-1121, Sep. 2007.

[76] Lakhimsetty S, Satelli V. S. P, Rathore R. S and Somasekhar V. T, "Multilevel Torque Hysteresis-Band based Direct-Torque Control Strategy for a Three-Level Open-End Winding Induction Motor Drive for Electric Vehicle Applications," in *IEEE Journal of Emerging and Selected Topics in Power Electronics*, vol. 7, no. 3, pp. 1969-1981, Sep. 2019.

[77] Rahim K, Jidin A, Patkar F, Jamil M. L. M, Ahmadi M. Z. R. Z and Karim K. A, "A dual mode DTC of open-end winding induction motor drive with reduced torque ripple," in *IEEE Conference on Energy Conversion (CENCON)*, Johor Bahru, pp. 106-111, Oct. 2014.

[78] Kunisetti VP and Thippiripati VK, "An Enhanced Three-Level Voltage Switching State Scheme for Direct Torque Controlled Open End Winding Induction Motor," in *Journal of the Institution of Engineers (India): Series B*, vol. 99, no. 3, pp. 235-43, Jun. 2018.

[79] Patel C, Rajeevan PP, Dey A, Ramchand R, Gopakumar K, Kazmierkowski MP, "Fast direct torque control of an open-end induction motor drive using 12-sided polygonal voltage space vectors," in *IEEE Transactions on Power Electronics*, vol. 27, no. 1, pp. 400-10, Jun. 2011.

[80] Rahim M. K et al., "Reduced torque ripple and switching frequency using optimal DTC switching strategy for open-end winding of induction machines," in *IEEE 11th International Conference on Power Electronics and Drive Systems*, Sydney, NSW, pp. 767-772, Jun. 2015.

[81] Kunisetti V Praveen Kumar and Thippiripati Vinay Kumar, "An Effective Four-Level Voltage Switching State Algorithm for Direct Torque Controlled Open End Winding Induction Motor Drive by Using Two Two-Level Inverters," in *Electric Power Components and Systems*, vol. 45, no. 19, pp. 2175-2187, Nov. 2017.

[82] Kumar K. V. P and Kumar T. V, "Experimental implementation of direct torque control of open end winding induction motor," in *IEEE Region 10 Conference (TENCON)*, Singapore, pp. 3318-3323, 2016.

[83] Arbind Kumar, Fernandes B. G and Chatterjee K, "DTC of open-end winding induction motor drive using space vector modulation with reduced switching frequency," in *IEEE 35th Annual Power Electronics Specialists Conference (IEEE Cat. No.04CH37551)*, Aachen, Germany, vol. 2, pp. 1214-1219, Jun. 2004.

[84] Arbind Kumar, Fernandes B. G and Chatterjee K, “Direct torque control of open-end winding induction motor drive using the concept of imaginary switching times for marine propulsion systems,” in *31st Annual Conference of IEEE Industrial Electronics Society*, pp. 1-6, Nov. 2005.

[85] Levi E, Satiawan I. N. W, Bodo N and Jones M, “A space-vector modulation scheme for multi-level open-end winding five-phase drives,” in *IEEE Power and Energy Society General Meeting*, San Diego, CA, pp. 1-1, Dec. 2012.

[86] Vinod B. R. and Baiju M. R, “Direct torque control implemented on a three-level open-end winding induction motor drive,” in *IEEE International Conference on Power Electronics, Drives and Energy Systems (PEDES)*, Trivandrum, pp. 1-6, 2016.

[87] Vinod B. R, Baiju M. R and Shiny G, “Five-Level Inverter-Fed Space Vector Based Direct Torque Control of Open-End Winding Induction Motor Drive,” in *IEEE Transactions on Energy Conversion*, vol. 33, no. 3, pp. 1392-1401, Sep. 2018.

[88] Preindl M and Bolognani S, “Comparison of direct and PWM model predictive control for power electronic and drive systems,” in *Twenty-Eighth Annual IEEE Applied Power Electronics Conference and Exposition (APEC)*, pp. 2526-2533, Long Beach, CA, USA, 2013.

[89] Ahmed Abdelsalam A, Jung-Su Kim and Young Il Lee, “Model predictive torque control of PMSM for EV drives: A comparative study of finite control set and predictive dead-beat control schemes,” in *Power Systems Conference (MEPCON)*, Middle East, pp. 156-163, 2016.

[90] Rodriguez J *et al*., “State of the Art of Finite Control Set Model Predictive Control in Power Electronics,” in *IEEE Transactions on Industrial Informatics*, vol. 9, no. 2, pp. 1003-1016, May 2013.

[91] Wang F, Chen Z, Stolze P, Kennel R, Trincado M and Rodriguez J, “A Comprehensive Study of Direct Torque Control (DTC) and Predictive Torque Control (PTC) for High Performance Electrical Drives,” in *EPE Journal*, vol. 25, no. 1, pp. 12-21, Mar. 2015.

[92] Ammar A, Kheldoun A, Metidji B, Talbi B, Ameid T and Azzoug Y, “An Experimental Assessment of Direct Torque Control and Model Predictive Control Methods for Induction Machine Drive,” in *International Conference on Electrical Sciences and Technologies in Maghreb (CISTEM)*, Algeria, pp. 1-6, 2018.

[93] Wang F, Li S, Mei X, Xie W, Rodríguez J and Kennel R. M, “Model-Based Predictive Direct Control Strategies for Electrical Drives: An Experimental Evaluation of PTC and PCC Methods,” in *IEEE Transactions on Industrial Informatics*, vol. 11, no. 3, pp. 671-681, Jun. 2015.

[94] Lunardi A. S, Sguarezi A. J and Filho, “Experimental results for predictive direct torque control for a squirrel cage induction motor,” in *Brazilian Power Electronics Conference (COBEP)*, Juiz de Fora, pp. 1-5, 2017.

[95] Habibullah M, Lu DD, Xiao D, Rahman MF, “A simplified finite-state predictive direct torque control for induction motor drive,” in *IEEE Transactions on Industrial Electronics*, vol. 63, no. 6, pp. 3964-75, Jun. 2016.

[96] Wang F, Zhang Z, Kennel R, Rodríguez J, “Model predictive torque control with an extended prediction horizon for electrical drive systems,” in *International Journal of Control*, vol. 88, no. 7, pp. 1379-88, Jul. 2015.

[97] Zhou D, Zhao J, Liu Y, “Predictive torque control scheme for three-phase four-switch inverter-fed induction motor drives with DC-link voltages offset suppression,” in *IEEE Transactions on Power Electronics*, vol. 30, no. 6, pp. 3309–3318, Jun. 2015.

[98] Zhou D, Zhao J, Li Y, “Model predictive control scheme of five-leg AC-DC-AC converter-fed induction motor drive,” in *IEEE Transactions on Industrial Electronics*, vol. 63, no. 7, pp. 4517–4526, Mar. 2016.

[99] Himabindu T, Teja A. V. R, Bhuvaneswari G and Singh B, “Predictive torque control of a three-level reduced switch inverter fed induction motor drive,” in *IEEE 26th International Symposium on Industrial Electronics (ISIE)*, Edinburgh, pp. 348-353, 2017.

[100] Kashyap N and Patidar S, “Model predictive direct torque control of neutral point clamped induction drive,” in *International Conference on Power and Embedded Drive Control (ICPEDC)*, pp. 202-207, 2017.

[101] Habibullah M, Lu D. D, Xiao D and Rahman M. F, “Finite-State Predictive Torque Control of Induction Motor Supplied from a Three-Level NPC Voltage Source Inverter,” in *IEEE Transactions on Power Electronics*, vol. 32, no. 1, pp. 479-489, Jan. 2017.

[102] Stolze P, Du Toit D, Tomlinson M, Kennel R and Mouton T, “Predictive torque control of an induction machine fed by a flying capacitor converter,” in *IEEE Africon '11*, Livingstone, pp. 1-6, Sep. 2011.

[103] Abdel-Rahim O, Ellabban O and Abu-Rub H, “Predictive Torque Control of an induction motor fed by five-to-three direct matrix converter,” in *40th Annual Conference of the IEEE Industrial Electronics Society*, Dallas, TX, pp. 800-804, 2014.

[104] Rodriguez J et al., “Predictive direct torque control of an induction motor fed by a matrix converter,” in *European Conference on Power Electronics and Applications*, Aalborg, pp. 1-10, 2007.

[105] Vargas R, Ammann U, Hudoffsky B, Rodriguez J and Wheeler P, "Predictive Torque Control of an Induction Machine Fed by a Matrix Converter with Reactive Input Power Control," in *IEEE Transactions on Power Electronics,* vol. 25, no. 6, pp. 1426-1438, Jun. 2010.

[106] Zhu B, Rajashekara K and Kubo H, "Predictive torque control with zero-sequence current suppression for open-end winding induction machine," in *IEEE Industry Applications Society Annual Meeting,* Addison, TX, pp. 1-7, 2015.

[107] Praveen Kumar K. V and Vinay Kumar T, "Predictive torque control of open-end winding induction motor drive fed with multilevel inversion using two two-level inverters," in *IET Electric Power Applications,* vol. 12, no. 1, pp. 54-62, Jan. 2018.

[108] Davari S. A, Khaburi D. A and Kennel R, "An Improved FCS–MPC Algorithm for an Induction Motor with an Imposed Optimized Weighting Factor," in *IEEE Transactions on Power Electronics,* vol. 27, no. 3, pp. 1540-1551, Mar. 2012.

[109] Zhang Y and Yang H, "Torque ripple reduction of model predictive torque control of induction motor drives," in *IEEE Energy Conversion Congress and Exposition,* Denver, CO, pp. 1176-1183, 2013.

[110] Zhang Y and Yang H, "Model Predictive Torque Control of Induction Motor Drives with Optimal Duty Cycle Control," in *IEEE Transactions on Power Electronics,* vol. 29, no. 12, pp. 6593-6603, Dec. 2014.

[111] Zhang Y and Yang H, "Generalized Two-Vector-Based Model-Predictive Torque Control of Induction Motor Drives," in *IEEE Transactions on Power Electronics,* vol. 30, no. 7, pp. 3818-3829, Jul. 2015.

[112] Cortes P et al., "Guidelines for weighting factors design in Model Predictive Control of power converters and drives," in *IEEE International Conference on Industrial Technology,* Gippsland, VIC, pp. 1-7, 2009.

[113] Uddin M, Mekhilef S, Mubin M, et al, "Model predictive torque ripple reduction with weighting factor optimization fed by an indirect matrix converter," in *Electric Power Components and Systems,* vol. 42, no. 10, pp. 1059–1069, Jul. 2014.

[114] Muddineni V.P, Sandepudi S.R, Bonala A.K, "Finite control set predictive torque control for induction motor drive with simplified weighting factor selection using TOPSIS method," in *IET Electric Power Applications,* vol. 11, no. 5, pp. 749–760, May 2017.

[115] Muddineni V.P, Bonala A.K, Sandepudi S.R, "Enhanced weighting factor selection for predictive torque control of induction motor drive based on VIKOR method," in *IET Electric Power Applications,* vol. 10, no. 9, pp. 877–888, Nov. 2016.

[116] Zanchetta P, "Heuristic multi-objective optimization for cost function weights selection in finite states model predictive control," in *workshop on Predictive Control of Electrical Drives and Power Electronics*, Munich, pp. 70-75, 2011.

[117] Guazzelli P. R. U, Pereira W. C. A, Oliveira C. M. R, Castro A. G and Aguiar M. L, "Weighting Factors Optimization of Predictive Torque Control of Induction Motor by Multi-objective Genetic Algorithm," in *IEEE Transactions on Power Electronics*. vol. 34, no. 7, pp. 6628-6638, Jul. 2019.

[118] Rojas C. A, Rodriguez J, Villarroel F, Espinoza J and Khaburi D. A, "Multiobjective Fuzzy Predictive Torque Control of an induction motor drive," in *The 6th Power Electronics, Drive Systems & Technologies Conference (PEDSTC2015)*, Tehran, pp. 201-206, Feb. 2015.

[119] Zhou D, Zhao J and Liu Y, "Online tuning of weighting factors based on sugeno fuzzy method in predictive torque control of four-switch three-phase inverter-fed IM," in *International Symposium on Power Electronics, Electrical Drives, Automation and Motion (SPEEDAM)*, Anacapri, pp. 734-739, Jun. 2016.

[120] Rojas C. A, Kouro S, Perez M and Villarroel F, "Multiobjective Fuzzy Predictive Torque Control of an induction machine fed by a 3L-NPC inverter," in *IEEE International Symposium on Predictive Control of Electrical Drives and Power Electronics (PRECEDE)*, Valparaiso, pp. 21-26, 2015.

[121] Norambuena M, Rodriguez J, Zhang Z, Wang F, Garcia C and Kennel R, "A Very Simple Strategy for High-Quality Performance of AC Machines Using Model Predictive Control," in *IEEE Transactions on Power Electronics*, vol. 34, no. 1, pp. 794-800, Jan. 2019.

[122] Norambuena M, Garcia C, Rodriguez J, "A very simple high performance torque and flux control of AC machines using predictive control," in *IEEE 19th Workshop on Control and Modeling for Power Electronics (COMPEL)*, pp. 1-5, 2018.

[123] Zhang Y and Bai Y, "Model predictive flux control of three-level inverter-fed induction motor drives based on space vector modulation," in *IEEE 3rd International Future Energy Electronics Conference and ECCE Asia*, pp. 986- 991, Jun. 2017.

[124] Zhang Y, Yang H and Xia B, "Model-Predictive Control of Induction Motor Drives: Torque Control Versus Flux Control," in *IEEE Transactions on Industry Applications*, vol. 52, no. 5, pp. 4050-4060, Sep.-Oct. 2016.

[125] Zhang Y and Yang H, "Model-Predictive Flux Control of Induction Motor Drives with Switching Instant Optimization," in *IEEE Transactions on Energy Conversion*, vol. 30, no. 3, pp. 1113-1122, Sep. 2015.

[126] Davari S. A, Khaburi D. A, Wang F and Kennel R. M, "Using Full Order and Reduced Order Observers for Robust Sensorless Predictive Torque Control of Induction Motors," in *IEEE Transactions on Power Electronics*, vol. 27, no. 7, pp. 3424-3433, Jul. 2012.

[127] Habibullah M and Lu D. D, "A Speed-Sensorless FS-PTC of Induction Motors Using Extended Kalman Filters," in *IEEE Transactions on Industrial Electronics*, vol. 62, no. 11, pp. 6765-6778, Nov. 2015.

[128] Zhu K. Rajashekara and Kubo H, "A novel predictive current control for open-end winding induction motor drive with reduced calculation burden and enhanced zero sequence current suppression," in *IEEE Applied Power Electronics Conference and Exposition (APEC)*, Tampa, pp. 552-557, 2017.

[129] Wang F, Zhang Z, Davari A, Rodríguez J, and Kennel R, "An experimental assessment of finite-state Predictive Torque Control for electrical drives by considering different online-optimization methods," in *Control Engineering Practice*, vol. 31, pp. 1–8, 2014.

[130] Hu J, Zhu J, Lei G, Platt G and Dorrell D. G, "Multi-Objective Model-Predictive Control for High-Power Converters," in *IEEE Transactions on Energy Conversion*, vol. 28, no. 3, pp. 652-663, Sep. 2013.

[131] Zhang Y and Xie W, "Low Complexity Model Predictive Control—Single Vector-Based Approach," in *IEEE Transactions on Power Electronics*, vol. 29, no. 10, pp. 5532-5541, Oct. 2014.

[132] Parvez Akter M, Mekhilef S, Mei Lin Tan N and Akagi H, "Modified Model Predictive Control of a Bidirectional AC–DC Converter Based on Lyapunov Function for Energy Storage Systems," in *IEEE Transactions on Industrial Electronics*, vol. 63, no. 2, pp. 704-715, Feb. 2016.

[133] Miranda H, Cortes P, Yuz J. I and Rodriguez J, "Predictive Torque Control of Induction Machines Based on State-Space Models," in *IEEE Transactions on Industrial Electronics*, vol. 56, no. 6, pp. 1916-1924, Jun. 2009.

[134] Cortes P, Rodriguez J, Silva C and Flores A, "Delay Compensation in Model Predictive Current Control of a Three-Phase Inverter," in *IEEE Transactions on Industrial Electronics*, vol. 59, no. 2, pp. 1323-1325, Feb. 2012.

[135] Yaramasu V, Rivera M, Narimani M, Wu B and Rodriguez J, "Finite State Model-based Predictive Current Control with Two-step Horizon for Four-leg NPC Converters," in *Journal of Power Electronics*, vol. 14, no. 6, pp. 1178–1188, Nov. 2014.

Publications

Journals Published:

1. R. E. Kodumur Meesala and V. K. Thippiripati, “An Improved Direct Torque Control of Three-Level Dual Inverter fed Open-Ended Winding Induction Motor Drive Based on Modified Look-Up Table,” in *IEEE Transactions on Power Electronics*, vol. 35, no. 4, pp. 3906-3917, Apr. 2020.

2. Ravi Eswar KM, Venkata Praveen Kumar K, Vinay Kumar T, “Enhanced Predictive Torque Control with Auto-Tuning Feature for Induction Motor Drive,” in *Electric Power Components and Systems*, vol. 46, no. 7, pp. 825-36, Oct. 2018.

3. R. E. Kodumur Meesala, V. P. K. Kunisetti and V. Kumar Thippiripati, “Enhanced Predictive Torque Control for Open End Winding Induction Motor Drive Without Weighting Factor Assignment,” in *IEEE Transactions on Power Electronics*, vol. 34, no. 1, pp. 503-513, Jan. 2019.

4. K. M. R. Eswar, K. V. P. Kumar and T. V. Kumar, “A Simplified Predictive Torque Control Scheme for Open-End Winding Induction Motor Drive,” in *IEEE Journal of Emerging and Selected Topics in Power Electronics*, vol. 7, no. 2, pp. 1162-1172, Jun. 2019.

Curriculum-Vitae

Name	:	K.M. Ravi Eswar
Date of Birth	:	11th September 1993
Gender	:	Male
Contact Number	:	+91-9494709710
Email Id	:	nit.ravieswar@gmail.com

Academic Qualifications

Program	University	%/CGPA	Year of completion
M. Tech (Power Electronics and Drives)	VIT, Vellore	9.61 (CGPA)	2016
B. Tech (Electrical and Electronics Engineering)	JNTU Anantapur	81.58 %	2014